MODE-LOCKED BREWSTER-ANGLED GaAlAs DIODE LASERS

Thesis submitted for the degree of Doctor of Philosophy of the University of London and for the Diploma of Membership of Imperial College

by

CHEN JIANGUO

April, 1984

The Blackett Laboratory,
Imperial College of Science
and Technology,
London SW7 2BZ, U.K.

ABSTRACT

The oxide-defined stripe of a GaAlAs double heterostructure semiconductor diode has been tilted at the Brewster angle to the diode cleaved facets. When placed within an external cavity, it has been observed that the sub-cavity diode resonances have been suppressed, so that the diode behaves solely as an amplifying medium. To ensure reliable performance a special mounting pillar has been designed to provide good thermal conductivity and appropriate accessibility for various cavity configurations. The general performance characteristics of the Brewster-angled diode laser are described and its relative merits outlined.

Mode-locking of the laser has been undertaken by supplementing a subthreshold dc bias current with an ac injection current whose frequency is matched to the longitudinal mode spacing (or its harmonics) of the external cavity. The intensity profile and durations (FWHM) of the output pulses were monitored with a repetitively-operating (Synchroscan) streak camera and pulsewidths less than 7ps have been inferred. The usefulness of this diagnostic technique has been demonstrated in the investigation of the effects of frequency mismatch between the injected current modulation and the cavity round-trip frequency. An important observation has been that the variation of the

pulsewidth with this mismatch is clearly asymmetric about the optimum modulation frequency.

The wavelength of the laser output has been tuned by employing cavity configurations that included either an intracavity Fabry-Perot etalon or a grating cavity reflector. A tunability $\sim$14nm has been achieved under both unmode-locked and mode-locked conditions. It has been noticed that the output power/oscillating wavelength characteristic of the frequency-tunable laser is modulated, and a possible explanation has been advanced.

Preliminary studies of a GaAlAs amplifier have also been carried out. The gain medium is again a Brewster-angled diode and gains of over one hundred have been achieved for both continuous and pulsed inputs.

CONTENTS

Chapter 1

GENERAL INTRODUCTION

Ultrashort laser pulses are finding increasing applications in numerous branches of science and technology. Most notably subject areas of current research activity include molecular dynamics in photochemistry [1], photobiology [2], and carrier kinetics in semiconductors [3], etc. To date, the most common method of generating pulses in the picosecond/subpicosecond regime is the technique known as "mode-locking" which refers to maintaining the relative values of the phases of the oscillating axial modes in the laser cavity and results in the production of trains of discrete optical pulses [4]. The first experimental demonstration of mode-locking was reported by Hargrove and his co-workers [5], where "active" loss modulation was applied at a frequency equal to that of the laser longitudinal mode spacing. Then came the reports by DeMaria et al and Mocker et al [6,7] who used saturable absorbers as a means to "passively" phase-lock the laser modes. In their report, DeMaria et al suggested that subpicosecond pulses might be obtained from the Nd:glass laser. Later, Ruddock et al succeeded in generating bandwidth limited pulses of 0.3ps in duration from a passively mode-locked CW dye laser [8] and more recently, Halbout and Tang reported 55fs duration pulses from a so-called "colliding pulse" mode-locked ring cavity CW dye laser [9]. Also Mourou et al obtained 70fs pulses from a synchronously-pumped CW dye laser [10].

It is now possible to reliably produce pulses with bandwidth limited duration of the order of picosecond from pulsed lasers and subpicosecond from CW lasers. In addition, theoretical models have been refined to the stage that there is excellent agreement even with details of the experimental results, and there is a very good understanding of the mechanism by which ultrashort pulses evolve from the initial flourescence intensity fluctuation patterns. Meanwhile, various methods have been developed to directly or indirectly measure mode-locked pulsewidths. As a result, the methods of picosecond and subpicosecond pulse generation and measurement are now sufficiently refined and catalogued for them to be used with confidence for the investigation on a picosecond/subpicosecond time scale of the interaction of coherent light with matter.

While quantum electronics was developing rapidly, the operating characteristics of semiconductor lasers were being progressively improved. Now, after more than two decades of research and development, the semiconductor laser has emerged as an important device in quantum electronics.

During the years from 1957 to 1961, Nishizawa et al [11], Basov and co-workers [12], and Aigrain [13] independently proposed the p-n junction laser. In 1962, Dumke [14] showed theoretically that laser action was possible in direct bandgap semiconductors. The theoretical calculations of Burnard and Duraffourg [15] in 1961 quantified the necessary condition for lasing, using the concept of quasi-Fermi levels.

With many groups actively investigating lasing possibilities in semiconductor material, it was not surprising that almost simultaneously three groups, headed by Hall [16], Nathan [17], and Quist [18], respectively, announced at the end of 1962 the achievement of laser action from GaAs p-n junctions. Shortly afterwards, Holonyak et al observed laser action in the junctions of $Ga\ As_{1-x}P_x$ at 710nm. This discovery demonstrated that the laser wavelength could be varied by altering the relative amount of arsenic and phosphorus [19]. Nowadays, the wavelength of the coherent radiation from semiconductor lasers has been extended through the visible into the infrared.

Holonyak realized that a better approach to the fabrication of the Fabry-Perot cavity might be to obtain plane-parallel mirrors by cleaving along parallel crystal planes [20]. The earliest reported use of cleaving to form the injection laser mirrors was by Bond et al [21]. Furnanage and Wilson [22] first suggested the employment of the active region in the shape of a long, narrow rectangle in order to control the modes along the junction plane.

Dyment succeeded in making a contact of 50μm wide stripes etched in a SiO_2 layer [23], and later he and his co-worker further reduced the stripe width to 12.5μm for which CW operation of homostructure GaAs lasers was demonstrated at temperature up to 202.5K [24]. However, all these homojunction lasers had very high threshold current densities and operated at low temperatures. These drawbacks were overcome by the construction of heterojunction lasers which drastically reduced the threshold current density.

In 1963, Kroemer suggested that the heterojunction could be manufactured by sandwiching a relatively narrow energy gap semiconductor layer into two layers of a wider energy gap semiconductor [25]. By 1968, single heterojunction semiconductor lasers were produced [26,27,28]. In 1969, Alferov et al completed the first double heterojunction semiconductor injection laser with a CW threshold current density of $4 \times 10^3 A/cm^2$ at room temperature [29]. Extending the idea of confining the carriers and photons along the direction perpendicular to the junction plane to include also the direction parallel to the junction led to the creation of the stripe geometry lasers. This type of laser provided yet lower threshold current, better mode control, desirable choice of the light source dimension and effective protection of the active layer from the ambient [30].

A significant event that intensified the research activities on the semiconductor lasers is attributed to the advent of optical fibre in 1970 [31], which ushered in the dawn of the fibre-optic telecommunciation age, and in turn gave birth to the field of integrated optics in the same year [32]. By 1979, the loss of the optical fibre had been decreased to as low as 0.2dB/Km [33]. In the meantime, Bloom et al demonstrated nearly distortionless propagation of 5ps pulses through kilometer lengths of optical fibre [34]. The ideal light source for the optical fibre communication is the injection heterostructure diode laser which possesses the highest power efficiency of all the laser types and has the unique features of low power electrical excitation, small size and compatibility for interfacing with semiconductor electronic devices and optical fibres and other waveguide configurations that are entering optical technology [35].

To meet the demands for high bit rates in optical fibre communication, frequency multiplexing and/or time multiplexing transmitters seem to be the most promising candidates. These transmitters require that the injection lasers be operated in frequency ordered and time ordered regimes [36]. Experiments have shown that the frequency-tunable external cavity diode lasers have very narrow bandwidths [37] and can be tuned over 14nm for GaAlAs [38] and 55nm for InGaAsP [37]. Mode-locked injection lasers appear to be promising as well. Pulse durations below 20ps have become commonplace [39-43] from actively mode-locked injection lasers. The fundamental limits on the minimum pulse width are expected to be 1ps (10^{-12}s) beyond which the dispersion of the laser medium may become important [44]. Combining frequency-tuning and mode-locking techniques into one diode laser system [38,45], Lundquist et al predicted that a wavelength multiplexing and time multiplexing system, which uses this type of laser as the light source, would offer a potential in excess of 1 Tbit/s.

In this thesis the development and characterisation of an actively mode-locked frequency-tunable semiconductor diode laser system is described. The amplifying medium has been a Brewster-angled GaAlAs double heterostructure diode with its oxide defined stripe being tilted with respect to the normal to the cleaved facets so that the guided wave was incident onto the facets at the Brewster angle. The evolution of the laser mode-locking has been made possible to observe by the employment of an electron-optical streak camera. However, throughout this work the emphasis has been on the treatment of the injection laser using similar methods to those applied for other laser systems. The establishment of mode-locking and frequency-tuning has been appropriately adopted for the particular operational constraints of a diode laser operating in an external configuration.

References

[1] W. Sibbett, J. R. Taylor and D. Welford, IEEE J. Quantum Electron., Vol. QE-17, 500 (1981).

[2] P. G. May, W. Sibbett, J. R. Taylor, FEBS Lett., Vol. 134, No. 2, 240 (1981).

[3] C. V. Shank et al, Solid State Commun., Vol. 47, 981 (1983).

[4] G. H. C. New, Rep.Prog.Phys., Vol. 46, 877 (1983).

[5] L. E. Hargrove, R. E. Fork, and M. A. Pollack, Appl.Phys.Lett., Vol. 5, 4 (1961).

[6] A. J. DeMaria, D. A. Stetser and H. Heynau, Ibid, Vol. 8, 174 (1966).

[7] H. Mocker, R. J. Collins, Ibid, Vol. 7, 270 (1965).

[8] I. S. Ruddock, D. J. Bradley, Ibid, Vol. 29, 296 (1976).

[9] J. M. Halbout, C. L. Tang, IEEE J. Quantum Electron., Vol. QE-19, 487 (1983).

[10] G. A. Mourou and T. Sizer, Opt. Commun. Vol. 41, 47 (1982).

[11] J. N. Nishizawa, Y. Watanabe, Electronics, 117 (Dec. 11, 1967).

[12] N. G. Basov et al., Sov. Phys., JETP, Vol. 10, 416 (1960).

[13] P. Aigrain, as reported in Proc.Conf.Quantum Electron., Paris, 1762 (1963).

[14] P. W. Dumke, Phys.Rev., Vol. 127, 1559 (1962).

[15] M. G. A. Bernard and G. Duraffourg, Phys.Stat.Solidi, Vol. 1, 699 (1961).

[16] R. N. Hall et al., Phys.Rev.Lett., Vol. 9, 366 (1962).

[17] M. I. Nathan et al., Appl.Phys.Lett., Vol. 1, 62 (1962).

[18] T. M. Quist et al., Ibid, Vol. 1, 91 (1962).

[19] N. Holonyak, Jr., and S. F. Bevacqua, Ibid, Vol. 1, 82 (1962).

[20] N. Holonyak, Jr., Private communication, see reference 30.

[21] W. L. Bond et al., Appl.Phys.Lett., Vol. 2, 57 (1963).

[22] R. A. Furnanage and D. K. Wilson, U.S. Patent No. 3363195 Jan. 1968.

[23] J. C. Dyment, Appl.Phys.Lett., Vol. 10, 84 (1967).

[24] J. C. Dyment and L. A. D'Asaro, Ibid, Vol. 11, 292 (1967).

[25] H. Kroemer, Proc. IEEE, Vol. 51, 1782 (1962).

[26] H. Kressel and H. Nelson, RCA Rev., Vol. 30, 106 (1969).

[27] I. Hayashi, M. B. Panish and P. W. Fog, IEEE J. Quantum Electron., Vol. QE-5, 211 (1969).

[28] M. B. Panish, I. Hayashi and S. Sumski, Ibid, 210 (1969).

[29] Zh.I. Alferov et al., Sov.Phys.Semicond., Vol. 3, 1107 (1970).

[30] H. C. Casey, Jr., M. B. Panish, "Heterostructure Lasers", Academic Press, (1978).

[31] F. P. Kapron, D. B. Keck and R. D. Maurer, Appl.Phys.Lett., Vol. 17, 423 (1970).

[32] N. A. Passino, G. E. Eberhart, H. D. Holt, SPIE, Vol. 258, 2 (1980).

[33] T. Miya, T. Hosake, T. Miyashita, Electron. Lett., Vol. 15, 106 (1979).

[34] D. M. Bloom et al., Opt.Lett., Vol. 4, 297 (1979).

[35] A. Yariv, "Introduction to Optical Electronics", Holt, Rinehart and Winston, (1976).

[36] M. B. Holbrook, Ph.D. Thesis, University of London, (1980).

[37] R. Wyatt, W. J. Devlin, Electron.Lett., Vol. 19, 110 (1983).

[38] J. Chen, W. Sibbett, J. I. Vukusic. Opt.Commun., Vol. 48, 427 (1984).

[39] P. T. Ho et al., Appl.Phys.Lett., Vol. 33, 241 (1978).

[40] M. B. Holbrook, W. E. Sleat and D. J. Bradley, Ibid, Vol. 37, 59 (1980).

[41] A. Olsson and C. T. Tang, IEEE J. Quantum Electron., Vol. QE-17, 1977 (1981).

[42] J. C. AuYueng and A. R. Johnston, Appl.Phys.Lett., Vol. 40, 112 (1982).

[43] J. Chen, W. Sibbett, J. I. Vukusic, Electron.Lett., Vol.18, 426 (1982).

[44] H. A. Haus, J.Appl.Phys., Vol. 51, 4042 (1980).

[45] S. Lundquist, T. Anderson, and S. T. Eng, Appl.Phys.Lett., Vol. 43, 715 (1983).

Chapter 2

GENERATION AND MEASUREMENT OF SHORT OPTICAL PULSES FROM MODE-LOCKED DIODE LASERS

2.1. Introduction

Since the invention of the laser, many methods have been developed by which short optical pulses with wavelengths covering the parts of the electromagnetic spectrum from the X-ray to the near infra-red are produced. For general background material the reader is referred to a review paper on the generation of short optical pulses ($<$ 50ns) [1], but the specific subject matter of this thesis is concerned principally with the generation of picosecond optical pulses from actively mode-locked semiconductor diode lasers. As for the measurement technique, only the real-time measurement involving an electron-optical streak camera, has been employed in this work, so it will be described in some detail.

The broadening of discrete electron states into bands gives the semiconductor laser a wide amplification bandwidth ($\sim$14nm for GaAlAs), which offers the possibility of generating ultrashort pulses from diode lasers by means of the so-called mode-locking technique. In this chapter, a sequential treatment is given starting with the theoretical aspects and culminating in the practical realization of mode-locking.

2.2. General Concepts of Mode-Locking

By forcing the oscillating axial modes of a laser into phase with each other, ultrashort optical pulses can be obtained as a result of the phase-locking or mode-locking influence which has led to a reliable and powerful method of generating picosecond and femtosecond optical pulses [2]. Generally, there are two principal means of achieving this mode-locked laser operation, namely active and passive. In the passive case, mode-locking is achieved through the action of an intra-cavity saturable absorber without external intervention [3]. This is a very simple and effective way of generating ultrashort optical pulses. Pulses of 55fs have been claimed from the passively mode-locked dye laser in a ring cavity [4].

For the active regime, a modulator driven by an external high frequency generator is inserted into the cavity. The applied frequency is equal to, or a multiple/submultiple of, the axial mode separation of the external cavity. This method provides the possibility of synchronizing the pulses with external events.

Of course, passive and active methods can be combined together. For example, May et al have obtained 0.3 ps pulses from their synchronously pumped dye laser incorporating a saturable absorber in a so-called hybrid configuration [6]. Mourou et al have described a synchronously pumped dye laser which combined gain and absorber dyes in a single jet and pulses as short as 70fs were generated [7]. Subpicosecond pulses have been claimed from an actively mode-locked GaAs diode laser with one side exhibiting saturable absorption introduced by proton bombardment [8].

2.2.1. Mode-locking in inhomogeneously broadened lasers

It is relatively easy to understand the mode-locking phenomenon in an inhomogeneously broadened laser system. Mode-locking will therefore be considered for the case of an inhomogeneously broadened medium before dealing with the phenomenon for the homogeneously broadened counterpart.

For the inhomogeneously broadened laser system, atoms with different transition energies are independent of each other and consequently a strong incident optical field can lead to local saturation effects which are manifested as a "hole" in the gain curve. Once threshold at frequency ν_q of the laser mode q is reached, the gain at this frequency remains clamped at the threshold value. Because of the independence of the atoms, the gain at other frequencies which is mainly contributed by other groups of atoms with transition frequencies different from ν_q, will increase with further pumping, leading to an additional longitudinal mode frequency, which are separated, according to the regenerative condition by

$$\nu_{q+1} - \nu_q = c/(2L) \equiv \nu_m \qquad (2\text{-}1)$$

where L is the optical length of the resonator and c is the speed of light in free space. According to the regenerative condition, we also have

$$\nu_q = qc/(2L) \qquad (2\text{-}2)$$

where q is an integer. Suppose the total optical field in the cavity resulting from multimode oscillation is

$$\underline{E}(\underline{r},t) = \sum_k \underline{E}_k(\underline{r})\exp\{i[(\omega_o+k\omega_m)t + \phi_k]\} \qquad (2\text{-}3)$$

where the summation is extended over the oscillating modes and ω_o is chosen arbitrarily as a reference frequency, ϕ_k is the phase of the kth mode. From equations (2-1) and (2-2), it can been seen that, if the ϕ_ks are fixed in equation (2-3), $\underline{E}(\underline{r},t)$ is periodic in

$$t = T = 2\pi/\omega_m = 2L/c \qquad (2\text{-}4)$$

where T is the cavity round-trip time. However, in a typical laser, the phases ϕ_ks are likely to vary randomly with time [9] so this causes the intensity of the laser output to fluctuate randomly and greatly reduces its usefulness for many applications. There are two ways in which this problem can be solved. The first is to make the laser oscillate in a single longitudinal mode in which case the laser has a narrow spectral output. The alternative is to force the mode phases ϕ_ks to maintain their relative values. With this mode-locking technique, the output intensity consists of a periodic train of pulses with each pulse being separated by T = 2L/c from its nearest neighbour. In order to get some important features of the mode-locked output, it can be supposed that, in equation (2-3), there are n modes oscillating in the cavity and for simplicity it is assumed that ϕ_k is zero and $\underline{E}_k(\underline{r})$s' are the same in magnitude and along the same direction, for all modes, so that

$$E \propto \sum_{-(n-1)/2}^{(n-1)/2} \exp[i(\omega_o + k\omega_m)t]$$

$$= \exp(i\omega_o t)\ \{\mathrm{Sin}(n\omega_m t/2)/\mathrm{Sin}(\omega_m t/2)\} \qquad (2\text{-}5)$$

The averaged laser output is proportional to $\underline{E}^*.\underline{E}$,

$$P(t) \propto \mathrm{Sin}^2(n\omega_m t/2)/\mathrm{Sin}^2(\omega_m t/2) \qquad (2\text{-}6)$$

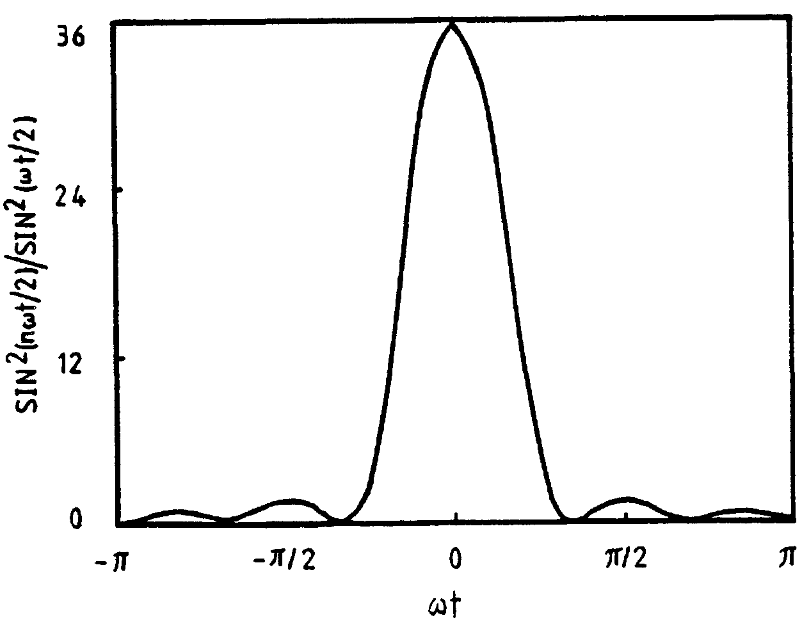

Fig. (2-1) Theoretical plot of the optical power output $P(t) \propto \mathrm{Sin}^2(n\omega_m t/2)/\mathrm{Sin}^2(\omega_m t/2)$ resulting from phase locking of 6(n=6) equal amplitude modes separated from each other by a frequency interval of $\nu_m = 1/T$.

The theoretical plot of the intensity of the optical field corresponding to equation (2-6) is shown in Fig. (2-1), and the following defining parameters can be deduced.

(1) The power is emitted in a form of a train of pulses with a period of $T=2L/c$.

(2) The peak power (when $t=sT$, $s=0, 1, 2, \ldots$) is equal to n times the average power, where n is the number of modes locked together.

(3) The peak field amplitude is equal to n times the amplitude of a single mode.

(4) The individual pulse width, defined as the time from the peak to the first zero, is $\tau_p = T/n$. The number of the oscillating modes can be estimated by $n \sim \Delta\nu/\nu_m$, which is the ratio of the transition lineshape width $\Delta\nu$ to the frequency spacing between neighbouring axial modes. Therefore,

$$\tau_p = T/n \sim 1/\Delta\nu \qquad (2\text{-}7)$$

Thus, the width of the mode-locked pulse is approximately equal to the inverse of the gain linewidth.

Because of the travelling feature of the solutions to Maxwell's equations in a laser cavity (a standing wave can be regarded as the sum of two equal amplitude waves travelling in the opposite directions), mode-locking causes the oscillating energy of the laser to be condensed into a discrete packet that travels back and forth between the mirrors with the velocity of light. The spatial length of the pulse, Lp, must correspond to its time multiplied by its velocity, ie,

$$Lp = \tau_p c = 2L/n \qquad (2-8)$$

as shown in Fig. (2-2).

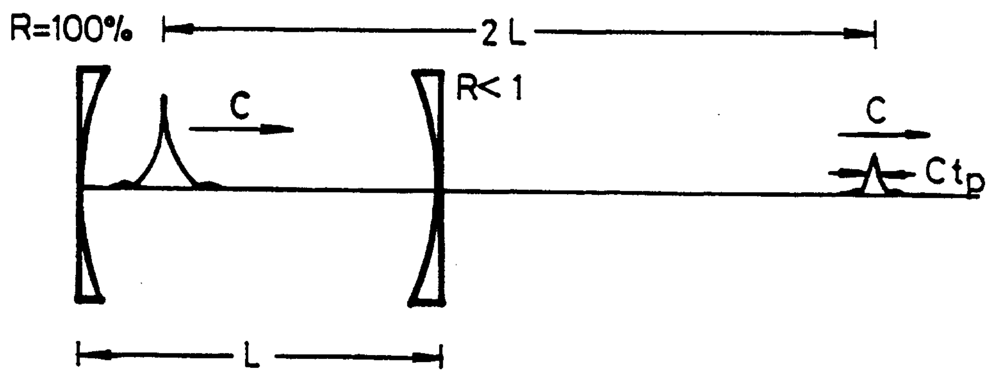

Fig. (2-2) Travelling pulses of energy resulting from the mode-locking of n laser modes.

Mode-locking can be achieved by modulating the loss (or gain) of the laser at a frequency $\nu_m = c/(2L)$. A plausible argument can be made as follows. As a form of loss modulation, consider a thin shutter inserted inside the laser resonator and let the shutter be closed (corresponding to high optical loss) most of the time except for brief periodic openings for a duration τ_{open} every $T = 1/\nu_m$ second. A single mode laser will not oscillate in this case because of the high loss (assuming that τ_{open} is too short to allow single mode oscillation to build up during each opening). The same argument applies to multimode oscillation with arbitrary phases. There is one exception, however, if the phases were locked as in equation (2-6), the energy distribution inside the resonator would consist of a narrow ($\tau_p \sim 2L/n$) travelling pulse as shown in Fig. (2-2). If this pulse should arrive at the shutter position when it is open and if the pulse temporal width τ_p is shorter than the opening time τ_{open}, the mode-locked pulse will be "unaware" of the existence of the shutter and will not be attenuated by it. In reality, the periodic shutter chops off any intensity tails acquired by the mode-locked pulses due to a "wandering" of the phases from their ideal values. This has the effect of continuously restoring the pulses. Alternatively, it may be said that, the saturable absorber shortens the front of the pulse whereas the gain saturation effect of the medium shortens the rear of the pulse [10].

Such shutters can be activated by an external signal as in the case of active mode-locking. The effect of a periodic gate can also be provided by inserting in the cavity a saturable absorber whose absorption at the laser wavelength decreases with increasing intensity. This saturable absorber will clearly "encourage" the laser to oscillate in a pulsed fashion since this mode of oscillation will undergo smaller losses [11].

2.2.2. Mode-locking in homogeneously broadened lasers

It has been suggested that, at least in the vicinity of the threshold, the gain line of the AlGaAs/GaAs laser is homogeneously broadened [12 - 15]. In an ideally homogeneously broadened laser it would be expected that only one mode would oscillate [9]. Experiments, however, revealed that mode-locking led to short pulses in a manner quite similar to the case of inhomogeneously broadened lasers. This could be explained by recognising that in the presence of internal modulation, power is transferred continuously from the high gain modes to low gain modes which would not oscillate under normal conditions. The real physical process could be regarded as a mode generating process. The net result, however, is that a large number of oscillating modes, with equal frequency spacing and fixed phases, are locked together leading to ultrashort pulses as in the inhomogeneous case [9].

Kuizenga et al [16] have derived expressions which could predict the mode-locking results in a homogeneously broadened laser for certain sets of laser parameters. By assuming that there was a short Gaussian pulse inside the cavity, then following this pulse once around the cavity, through the active medium and the modulation, requiring a self-consistent solution, Kuizenga et al arrived at the following results.

(1) In the phase modulation case (FM), if the modulation frequency ν_m equals the ideal modulation frequency, which is slightly different from the cavity round trip frequency, the mode-locked pulse duration and bandwidth are

$$\tau_{po}(FM) = \left[(2\sqrt{2}\ln 2)^{\frac{1}{2}}/\pi\right](g_o/\delta c)^{\frac{1}{4}} \ (\Delta\nu.\nu_m)^{-\frac{1}{2}} \qquad (2\text{-}10)$$

$$\delta\nu_{po}(FM) = (2\sqrt{2}\ln 2)^{\frac{1}{2}}(\delta c/g_o)^{\frac{1}{4}} \ (\Delta\nu.\nu_m)^{\frac{1}{2}} \qquad (2\text{-}11)$$

where, δc is the effective single-pass phase retardation of the modulator and g_o is the central mode gain coefficient. The exact modulation frequency is,

$$\nu_{mo}(FM) = \{2L/c \pm 2(\delta c/\pi)(\lambda a/c) + g_o/(\pi\Delta\nu)\}^{-1} \qquad (2\text{-}12)$$

where λa is the peak wavelength of the medium gain.

(2) In the amplitude modulation case (AM), similar results are obtained

$$\tau_{po}(AM) = \left[(\sqrt{2}\ln 2)^{\frac{1}{2}}/\pi\right)(g_o/\delta e)^{\frac{1}{4}} \ (\Delta\nu.\nu_m)^{-\frac{1}{2}} \qquad (2\text{-}13)$$

$$\delta\nu_{po}(AM) = (2\sqrt{2}\ln 2)^{\frac{1}{2}}(\delta e/g_o)^{\frac{1}{4}} \ (\Delta\nu.\nu_m)^{\frac{1}{2}} \qquad (2\text{-}14)$$

where δe is the modulation coefficient of the amplitude modulator. The exact modulation frequency is

$$\nu_{mo}(AM) = \tfrac{1}{2}\left[2L/c + g_o/(\pi\Delta\nu)\right]^{-1} \qquad (2\text{-}15)$$

From equations (2-10) to (2-15), it can be seen that there are some differences between phase modulation and amplitude modulation. The pulse-bandwidth product for the phase modulation case is

$$\tau_{po}(FM).\delta\nu_{po}(FM) = 2\sqrt{2}\ln 2/\pi = 0.626 \qquad (2\text{-}16)$$

and for the amplitude modulation case is

$$\tau_{po}(AM).\delta\nu_{po}(AM) = 2\ln 2/\pi = 0.440 \qquad (2\text{-}17)$$

Also the modulation frequencies are different as can be seen from equations (2-12) and (2-15).

Some common conclusions can be drawn from these equations. Because the pulse width is inversely proportional to $(\delta c)^{\frac{1}{4}}$ or $(\delta e)^{\frac{1}{4}}$, pulse shortening depends only weakly on increased modulation depth. Since the pulse width is proportional to $(\nu_m)^{-\frac{1}{2}}$, an increase in modulation frequency is a better way of shortening the pulse durations. Another point worth mentioning is that Kuizenga et al predicted that the shortest pulse will not be produced when the modulation frequency equals that expressed in equation (2-12) but rather when ν_m is slightly larger than ν_{mo} [16].

2.3. Active Mode-Locking of Semiconductor Lasers

Active mode-locking of semiconductor injection lasers could not be achieved, at present, with solitary diode lasers which have typical lengths of hundreds of micrometers. For one thing, the axial mode spacing of the diode laser is of the order of 10^{11}Hz, and so the capacitance of the diode junction will prevent the carriers being effectively injected into the active region [18].

Another reason is due to the finite lifetime of the injection carriers which makes it difficult for the diode laser to respond to the high modulation frequency [19]. These two problems will be discussed in Chapter 3.

According to the present state-of-the-art, an extended laser cavity is still needed for the active mode-locking of an injection semiconductor laser. In order to couple the semiconductor diode into an external cavity, the vital thing is to suppress the facet reflectivity of the diode. This is usually realized by either antireflection (AR) coating of the diode facet(s) or tilting the stripe at near Brewster angle to the facet normal (so that the guided wave is incident on the facet at or near the Brewster angle). A detailed description of this latter scheme will be given later. So, assuming that the diode has been coupled to the external cavity, Haus' treatment will be followed to give a mathematical description to the active mode-locking of a semiconductor injection laser [17].

2.3.1. Mode-locking equation

Suppose the system gain has the time dependence

$$\omega_n/(2Q_n)g(n)\{1-2M[1-\mathrm{Cos}(\omega_m t)]\} \qquad (2\text{-}18)$$

where ω_m is the modulation angular frequency, ie, the system is modulated with a sinusoidal signal, $\omega/(2Q)$ is the rate of decay of the amplitude of the excitation in the absence of modulation, and M is the modulation index. It is assumed that there is no modulation frequency mismatch, that is, ω_m is taken to be $(\pi C/L)$. The nth axial mode $V_n \exp(i\omega_n t)$ is modulated by equation (2-18), and will produce the injection signals

$$-2[\omega_n/(2Q_n)]Mg(n)V_n \text{ at frequency } \omega_n \text{ and}$$

$$\omega_n/(2Q_n)Mg(n)V_n \text{ at frequencies } \omega_{n\pm 1} .$$

When there is no noise component, then for the nth mode, in the steady state, the gain and loss equilibrium condition leads to

$$\omega_n/(2Q_n)[g(n)-1]V_n = -M\{[\omega_{n+1}/(2Q_{n+1})]g(n+1)V_{n+1}$$

$$-[2\omega_n/(2Q_n)]g(n)V_n + [\omega_{n-1}/(2Q_{n-1})]g(n-1)V_{n-1}\} \qquad (2-19)$$

If a noise source is present, then a source term Sn is included on the right hand side of equation (2-19), in addition to the injection signal, the physical origin of the practical noise source Sn being spontaneous emission. Normally, Sn is negligible compared to the oscillating field, therefore only the noise free condition is considered here. Neglecting the weak frequency dependence of the factor $\omega_n/(2Q_n)$, equation (2-19) becomes

$$[1-g(n)]V_n - M[g(n+1)V_{n+1}-2g(n)V_n+g(n-1)V_{n-1}]=0 \qquad (2-20)$$

This equation leads to the solutions V_n, that decrease in magnitude to zero with $|n|\to\infty$, only for certain values of peak gain $g(n=o)$. Physically, this implies that the power in the laser settles at a level such that gain saturation selects $g(o)$ at the required level [17].

Suppose the central oscillating angular frequency is ω_o, which coincides with the angular frequency of one cavity mode, then the nth oscillating axial mode has an angular frequency $(\omega_o+n\omega_m)$. Suppose the linewidth is $\Delta\omega_d$ (for the GaAlAs diode used in this work, $\Delta\omega_d$ is $\sim 7.8\times10^{13}$ rad./s), but since ω_m used in this work was smaller than 3×10^9 rad./s, obviously $\omega_m \ll \omega_d$. So for the frequency deviation of the nth mode from ω_o, $n\omega_m$, the following approximation can be made

$$\omega = \lim_{\omega_m \to 0} n\omega_m \tag{2-21}$$

such that ω can be regarded as a continuous variable. $g(n)$ can also be regarded as a function of ω. Then equation (2-20) becomes

$$[1-g(\omega)]V(\omega)-M\omega_m^2 \, d^2/d\omega^2 \, [g(\omega)V(\omega)] = 0 \tag{2-22}$$

Denoting $g(\omega)V(\omega) = U(\omega)$ (2-23)

then, equation (2-22) may be expressed as

$$\{1-1/g(\omega)\}U(\omega)+M\omega_m^2 \, d^2U/d\omega^2 = 0 \tag{2-24}$$

2.3.2. System gain

Suppose the peak gain of the medium, normalized to the system loss, is g_o, the angular frequency of the peak ω_g, then the homogeneously broadened gain takes the form

$$g(\omega) = g_o\{1+[(\omega-\omega_g)/(\Delta\omega_d/2)]^2\}^{-1} \qquad (2\text{-}25)$$

If for some reason, say by the insertion of a frequency tuning element inside the cavity, the system oscillates at some frequency away from ω_g, then the peak gain should be reasonably larger than unity in order that $g(\omega)$ matches the system losses, otherwise the laser will cease to operate at that frequency.

2.3.3. Fabry-Perot

In this work, frequency-tuning elements, such as a Fabry-Perot etalon or a grating, have been used to select the lasing wavelength. Their effects on the system can be regarded as imposing high losses on unwanted modes. Combining this constraint with the system gain, the tuning element leads to selection of the lasing wavelengths. In this section, the effect of an intracavity Fabry-Perot etalon will be discussed. Assuming that there is no insertion loss and that the free spectral range of the etalon is larger than the spectral width of the gain line of the diode then only one pass band of the etalon can be tuned to overlap with part of the gain curve. In this work, the free spectral range was 36nm, which is substantially larger than the bandwidth of the spontaneous emission of the GaAlAs Brewster-angled diode. With the following etalon parameters, reflectivity $R_1=R_2=R$, optical length of the gap ℓ, angular frequency of the peak of the transmission band ω_F, then the transmissivity T is given by [20]

$$T = \{1+[4R/(1-R)^2]\mathrm{Sin}^2[(\omega-\omega_F)\ell/c]\}^{-1} \qquad (2\text{-}26)$$

This may be considered as an extra loss α_{FP} imposed on the oscillation at frequency ω due to the Fabry-Perot etalon, which when normalized to the system quality factor is given by

$$\alpha_{FP} = cQ/(\omega L)\ln\{1+[4R/(1-R)^2]\mathrm{Sin}^2[(\omega-\omega_F)\ell/c]\} \qquad (2\text{-}27)$$

In these experiments, the output linewidth from the mode-locked Brewster-angled diode laser was $\sim$0.5nm so this gives rise to a very small value for $(\omega-\omega_F)\ell/c$, such that

$$\alpha_{FP} \sim \frac{cQ}{\omega L} \cdot \frac{4R}{(1-R)^2} \left(\frac{\omega-\omega_F}{c}\ell\right)^2 \quad \text{for } \omega\to\omega_F \qquad (2\text{-}28)$$

For convenience, we define

$$(\Delta\omega_F/2)^2=\omega Lc(1-R)^2/(4RQ\ell^2) \qquad (2\text{-}29)$$

Finally, the sum of the system gain and the etalon loss at a frequency near the peak of the pass band of the Fabry-Perot etalon (normalized to the system loss (excluding etalon)) is

$$g(\omega)=g_o\{1+(\omega-\omega_g)^2/(\Delta\omega_d/2)^2\}^{-1}-(\omega-\omega_F)^2/(\Delta\omega_F/2)^2 \quad \text{for } \omega\to\omega_F \qquad (2\text{-}30)$$

If ω_o is chosen to be equal to ω_F, and ω is now used to express the deviation of the frequency from ω_o, in accordance with the definition taken earlier, then equation (2-30) becomes:

$$g(\omega)=g_o\{1+[\omega-(\omega_g-\omega_F)]^2/(\Delta\omega_d/2)^2\}^{-1}-\omega^2/(\Delta\omega_F/2)^2 \quad \text{for } \omega\to 0 \qquad (2\text{-}31)$$

2.3.4. Solutions to Haus' equation with Fabry-Perot etalon in the cavity

It has been derived that the mode-locked pulse width is (see Appendix to this chapter equation (A-27))

$$\tau_p \sim \left(\frac{2\ln 2}{\pi^2}\right)^{\frac{1}{2}} \left\{\frac{g_o(\Delta\nu_F/\Delta\nu_d)^2+[1+4(\nu_g-\nu_F)^2/(\Delta\nu_d)^2]^2}{Mg_o^2\nu_m{}^2\Delta\nu_F^2}\right\}^{\frac{1}{4}} \qquad (2\text{-}32)$$

Meanwhile, it can also be seen, from equation (A-23), that when the transmission peak of the etalon is not coincident with the peak wavelength of the medium gain, the peak frequency of the oscillating modes will deviate from the centre of the etalon pass band. The frequency shift towards the centre of the medium gain can be expressed as

$$\delta\omega = \frac{g_o(\omega_g-\omega_F)\Delta\omega_F{}^2\Delta\omega_d{}^2}{g_o\Delta\omega_F{}^2\Delta\omega_d{}^2+[\Delta\omega_d{}^2+4(\omega_g-\omega_F)^2]^2} \qquad (2\text{-}33)$$

This is due to the fact that the product of the gain with loss due to the etalon will have a maximum at a frequency away from the peak of the etalon pass band and towards the peak of the medium gain. The deviation $\delta\omega$ will increase when the pass band of the etalon is set further away from the gain peak. This process, however, can not go on indefinitely. Firstly, this is because when the parameter $2(\omega_g-\omega_F)/\Delta\omega_d$ becomes larger, $\delta\omega$ will become larger and the approximation made in equation (2-28) or (2-31) will become invalid. Secondly, when the pass band of the etalon is tuned further away from the gain peak, the system needs to be pumped harder in order that the gain of the lasing modes can match the loss. As a result, the noise will become stronger, and eventually equation (2-24) will become invalid.

The discussion is now continued in two steps below:

(a) When the peak wavelength of the Fabry-Perot etalon pass band is tuned to overlap precisely with the gain peak, the pulse duration, according to equation (2-32), is

$$\tau_p \sim [(2\ln 2)^{\frac{1}{2}}/\pi][Mg_o^2\nu_m^2]^{-\frac{1}{4}}\{g_o/\Delta\nu_d^2+1/\Delta\nu_F^2\}^{\frac{1}{4}} \qquad (2\text{-}34)$$

From the above expression, it can be concluded that the insertion of the etalon will increase the pulse width, and this has been confirmed by Kuizenga et al [16]. In this work, however, $\Delta\nu_F$ was about one third of the spectral width of the gain (or rather the spontaneous emission) of the active medium, it is, therefore, expected that the pulse will be broadened by no more than 80% due to the insertion of the etalon. Because of practical constraints no quantitative measurements have been obtained to show the effect of the Fabry-Perot etalon on the pulse width. In a linear cavity configuration, pulses of 13ps duration have been obtained, with the Fabry-Perot etalon inside the cavity, at a modulation frequency of ∿320 MHz.

If a minimized pulse duration is the primary objective, then clearly the Fabry-Perot etalon is not recommended according to equation (2-34). Sometimes, however, frequency-tunable short pulses are desired and some sacrifice of pulse duration may be justified in order to gain the tunability unless some method can be found to tune the output frequency without increasing the pulse width. If the etalon is chosen to select the lasing wavelength rather than refining the band structure, then the thickness of the etalon can be chosen much less than 1mm (the standard set by Kuizenga et al for their Nd:YAG laser [16]) as was the case in this work. So long as the etalon is able to select the lasing wavelength properly and effectively, the etalon thickness can be kept as small as possible in order to keep the mode-locked pulse duration as close as possible to the value without etalon. In this work, an etalon thickness of 10μm has been used which permitted a tuning range of mode-locked pulse generation ∿14nm. As for the band structure of the mode-locked Brewster-angled diode laser, the insertion of the Fabry-Perot etalon did not have any observable effect on the spectral structure of the laser, as expected for an etalon having a pass bandwidth substantially in excess of the lasing bandwidth. The typical bandwidth from the mode-locked Brewster-angled diode laser, with or without the etalon, was $\sim$0.5nm which was about 5 times that corresponding to the transform-limited pulse (at $\lambda\sim$850nm) of duration $\sim$10ps. This might be attributed to the system instabilities and the transient frequency shift during the process of pulse generation [22], which will be discussed in Chapter 6.

(b) Now consider the case without the Fabry-Perot etalon in the cavity where the theoretically predicted pulse width, according to equation (2-34) with $\Delta\nu_F\to\infty$, is

$$\tau_p\sim[(2\ln 2)^{\frac{1}{2}}/\pi](Mg_o)^{-\frac{1}{4}}\ (\nu_m.\Delta\nu_d)^{-\frac{1}{2}} \qquad (2\text{-}35)$$

Assuming that the peak wavelength of the lasing modes is coincident with the peak wavelength of the medium gain and using the following figures, $\Delta\nu_d\sim1.2\text{x}10^{13}$Hz, $Mg_o\sim0.4$, then for $\nu_m\sim3.2\text{x}10^8$Hz, the pulse width, according to equation (2-35), is $\tau_p(\sim320\text{MHz})\sim8$ps, and for $\nu_m\sim4.8\text{x}10^8$Hz, $\tau_p(\sim480\text{MHz})\sim6$ps. These figures are in reasonable agreement with the experimental results of 10ps for $\nu_m\sim3.2\text{x}10^8$Hz and 7ps for $\nu_m\sim4.8\text{x}10^8$Hz. In practice, the modulation frequency might not be equal to the external cavity mode spacing [23], the system was not very stable, the pulses were not Gaussian (which will be discussed in Chapter 6), and so on, therefore, the theory presented in this chapter can only be regarded as an approximation to the experiment.

Experimental observation did not indicate any systematic change of the pulse duration with the dc bias level in these actively mode-locked Brewster-angled diode lasers. This has been implied in equation (2-35) where the pulse duration is not sensitive to the parameters M and g_o. Because of other reasons (for example, system stabilities which might be changed with the injection current via the induced temperature changes in the active region), the variation in pulse duration as a function of dc bias is likely to be unobservable.

2.4. Streak Camera Measurements of the Optical Pulses

2.4.1. The image tube

Since the measurement technique involved in this work was a synchroscan streak camera system which provided a direct record of the light intensity, this section will be limited to giving a description of this system. The Synchroscan streak camera comprised an image tube (modified Photochron I with an S20 photocathode) with RF deflection circuitry. It was the synchrononism of the actively mode-locked pulses with external events which brought about the realization of the Synchroscan streak camera system [25].

A diagrammatic representation of an image tube is shown in Fig. (2-3). A light pulse incident on the photocathode

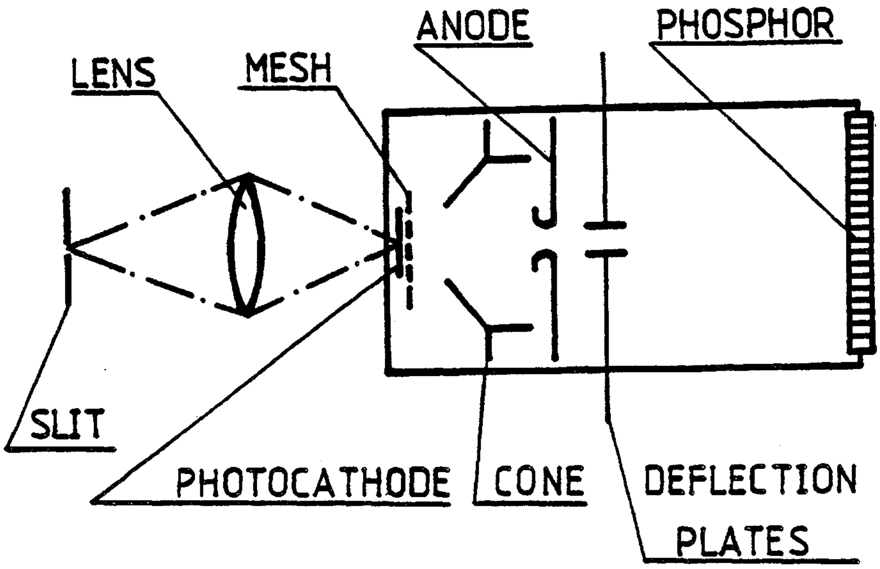

Fig. (2-3) A schematic of the etectron-optical image tube.

produces a temporal distribution within the emitted photoelectrons. These electrons are then accelerated along the tube by the mesh, cone and anode electrodes, after which the electrons pass into a drift space where a ramp voltage is applied across the deflection plates thereby yielding a spatial distribution on the phosphor. The resulting streak images can then be recorded on photographic film or by an optical spectral analyser (OSA).

2.4.2. Synchroscan streak camera system

The streak camera used in the work was a repetitively scanned streak camera. The principle of the synchroscan had been suggested in 1973 by Sibbett [26]. The repetitive deflection ramps enabled each light pulse to be streaked and overlaid on the previous record. As a result, there was no need for image intensification. Taking advantage of the actively mode-locked semiconductor injection laser in which the pulse repetition rate was the same as that of the sinusoidal modulation signal, the Synchroscan deflection could be obtained from the modulation voltage supply. About half of the output signal from the synthesizer (RACAL 9081), which was operated at a full output power of 1mW, was supplied to a preamplifier whose output was then sent into a power amplifier. The output of the power amplifier was coupled into the deflection plates, as shown in Fig.(2-4). Because of the limitation imposed by the commercially available

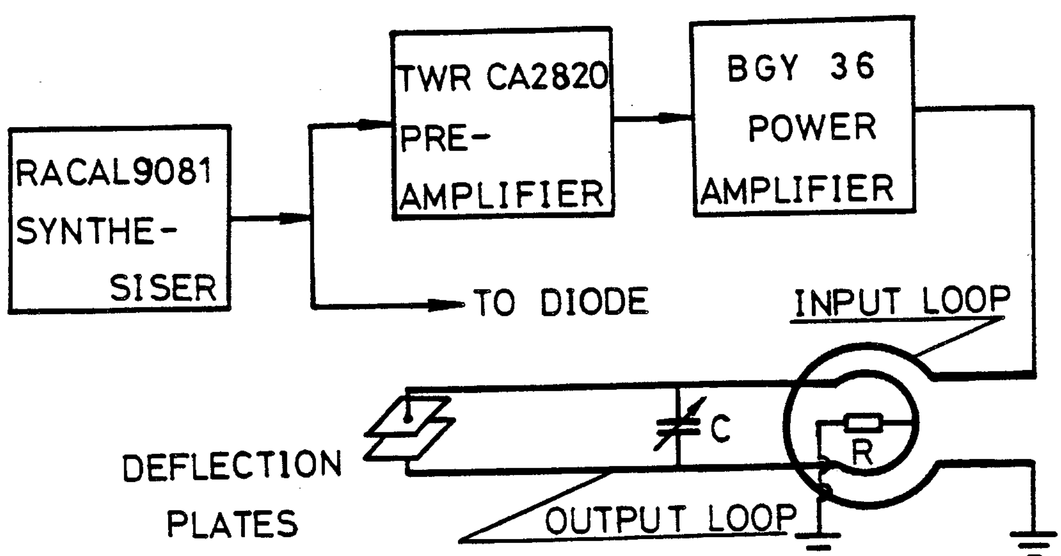

Fig. (2-4) Block diagram of the deflection circuit for the Synchroscan.

power amplifier (Mullard BGY36) with a working frequency range of 148-174 MHz, a synthesizer output at $\sim$160 MHz was chosen. Because the power amplifier needed 150mW drive power, a preamplifier (CA2820) was inserted between the synthesizer and the power amplifier which gave an output power $\geqslant$10W. The output from the power amplifier was coupled into the deflection plates of the image tube through an L-C resonant circuit. A trim capacitor, parallel to the deflection plates, was used to ensure that the resonant frequency of the circuit was equal to the signal frequency from the power amplifier. The optimization of the tuned deflection plate circuitry was checked with a Standing Wave Ratio and Power meter (Coax NDK-200). In practice, once the circuitry was set up, the tuned deflection plate circuitry was optimized by observing the maximum scan amplitude on the phosphor. Proper choice of the cable length into the driving circuitry made it possible that the two subpulses produced from one laser pulse by a beam splitter (50/50) and delayed by the preset time Δt by an optical delay line could appear at the linear part of the driving sine wave. This meant that the pulses should appear about the middle of the phosphor, otherwise the pulse would be distorted and thus lead to incorrect interpretation of the results.

2.4.3. Time resolution

According to [27], for a single shot camera the time resolution Δt_s can be expressed

$$\Delta t_s = [(\Delta t_D)^2 + (\Delta t_{tech})^2]^{\frac{1}{2}} \qquad (2\text{-}36)$$

where Δt_D is the time dispersion due to the initial energy distribution of the photoelectrons emitted from the photocathode, Δt_{tech} is the system technical time resolution. It was derived that Δt_D satisfies the following formula [26]

$$\Delta t_D = 2.34 \times 10^{-6} (\Delta E)^{\frac{1}{2}}/E \qquad (2\text{-}37)$$

where Δt_D is in seconds; ΔE, in electron-volts, is the FWHM of the energy distribution function of the photoelectrons, which is dependent on the energy of the incident photon and the type of the photocathode; E, in mks units is the extraction field between the mesh and the photocathode. For the S20 photocathode and an incident photon wavelength of 850nm, ΔE is about 0.1 eV [28]. The extraction field used in these experiments was $\sim 3 \times 10^5$ Vm^{-1}. From equation (2-37), the time dispersion can be calculated to be $\Delta t_D \sim 2.5$ps.

The system technical time resolution can be obtained as follows. According to [26],

$$\Delta t_{tech} = (\nu \delta)^{-1} \qquad (2\text{-}38)$$

where ν is the writing speed of the streak camra, and δ is the spatial resolution which was ~ 60 line pairs per centimetre in this case [28]. The writing speed was measured from the experiment as $\sim 2.7\times10^9$ cm/s. This gives a time resolution $\Delta t_{tech} \sim 6.2$ ps from equation (2-38). From equation (2-36), it can be found that the time resolution of the single shot streak camera is $\Delta t_s \sim 7$PS.

When the streak camera is operating in the synchroscan mode, the images displayed on the phosphor are due to many pulses overlapped with each other. Any jitter from the laser or the driving signal could affect the recorded pulse width on the phosphor, so that the time resolution of the Synchroscan streak camera Δt should be no less than Δt_s. At present, some sources of jitter have been identified, but the quantitiative descriptions of the effects of the known jitter on the measured pulse width are far from being specified, and even less can be related to unknown sources of jitter. In this work, the increase of the recorded pulses due to various jitter sources of the laser and measurement system was unlikely to exceed 30%. The pulse duration $\sim$9ps and the spectral width $\sim$ 0.5nm have been measured for these pulses. The spectral width indicated that the real pulse width should be larger than 2ps (for a Gaussian pulse at $\lambda \sim 850$nm). In the single shot regime, a 2ps pulse would be recorded as $\sim$7ps on the screen due to the inherent temporal resolution of the streak camera. Under the worst jitter conditions, ie, if the pulse widths were 2ps and various jitter contributions caused these pulses to be recorded as $\sim$ 9ps on the screen, then the increase of the recorded pulse width due to jitter would be ∿30%. If the system jitter was minimized, it might be possible that the increase of the pulse width due to jitter would be much smaller than 30%.

2.5. Conclusion

In this chapter, the basic concepts of mode-locking Brewster-angled diodes in external cavity configurations have been discussed. Pulse durations from an actively mode-locked diode laser have been related to laser parameters such as the spectral width of the medium gain lineshape, modulation frequency (which is equal to the mode spacing of the external cavity or its submultiple/multiple), modulation index and the peak gain coefficient. Theoretical results show that increasing the modulation frequency is an effective way of shortening the pulse duration and further theory, which incorporates the effect of a Fabry-Perot etalon on the pulse duration has also been outlined.

A description has also been given of the repetitively operating streak camera used in this research work. The image tube with an S20 photocathode has been found to have a resolution limit ∿7ps. Experiments have now proceeded to the stage that the pulse duration of the mode-locked injection diode laser is comparable to the resolution limit of the detection system.

Appendix

In this appendix equation (2-24) will be solved with the effective gain expressed in equation (2-31). Using the following substitutions,

$$\left.\begin{aligned} &\omega/(\Delta\omega_d/2) = \Omega,\ (\omega_g-\omega_F)/(\Delta\omega_d/2) = a \\ &\Delta\omega_d/\Delta\omega_F = b \text{ and } \omega_m/(\Delta\omega_d/2) = c \end{aligned}\right\} \qquad \text{(A-1)}$$

equation (2-31) may be re-written as

$$g(\Omega) = g_o[1+(\Omega-a)^2]^{-1} - (b\Omega)^2 \quad (\Omega\to 0) \qquad \text{(A-2)}$$

$$\sim \frac{g_o}{1+a^2} \cdot \frac{1}{1-\dfrac{2a}{1+a^2}\Omega + \left[\dfrac{1}{1+a^2} + \dfrac{(1+a^2)b^2}{g_o}\right]\Omega^2} \qquad \text{(A-3)}$$

For simplicity, the following symbols are introduced

$$\left.\begin{aligned} &g_o/(1+a^2) = G\ ,\ a/(1+a^2) = x \\ &1/(1+a^2) + (1+a^2)b^2/g_o = y \end{aligned}\right\} \qquad \text{(A-4)}$$

The final form of equation (A-3) is then:

$$g(\Omega) = G(1-2\,x\,\Omega + y\Omega^2)^{-1} \qquad \text{(A-5)}$$

Adopting equation (A-1), equation (2-24) takes the form:

$$\{1-1/g(\Omega)\}U+MC^2\frac{d^2U}{d\Omega^2} = 0 \qquad \text{(A-6)}$$

Substituting equation (A-5) for $g(\Omega)$ in equation (A-6), results in

$$\{1 - (1-2x\Omega+y\Omega^2)/G\}\ U+MC^2\ \frac{d^2U}{d\Omega^2} = 0 \qquad \text{(A-7)}$$

or $$\{(G-1) - (y\Omega^2-2x\Omega)\}\ U + MGC^2\ \frac{d^2U}{d\Omega^2} = 0 \qquad \text{(A-8)}$$

An algebraic calculation leads to

$$\left[(G-1)/y+x^2/y^2\right]U-(\Omega-x/y)^2U+ \frac{MGC^2}{y} \cdot \frac{d^2U}{d(\Omega-x/y)^2} = 0 \qquad \text{(A-9)}$$

Equation (A-9) is similar to the linear harmonic oscillator equation in quantum mechanics,

$$-\hbar^2/(2m)\ \frac{d^2\psi}{dx^2} - E\psi + \tfrac{1}{2}\ ms^2x^2\psi = 0 \qquad \text{(A-10)}$$

Solutions to equation (A-10) are

$$\psi_\ell\ (x) = N_\ell \cdot H_\ell\ (\alpha x)\ \exp(-\alpha^2x^2/2) \qquad \text{(A-11)}$$

here $H_\ell\ (x)$ is the ℓth order Hermitian polynomial and N_ℓ is the normalization constant, and

$$\left.\begin{aligned} N_\ell &= \{\alpha/(\sqrt{\pi}\ 2^\ell\ \ell!)\}^{\frac{1}{2}} \\ \alpha &= (ms/\hbar)^{\frac{1}{2}} \\ E_\ell &= (\ell+\tfrac{1}{2})\hbar s \end{aligned}\right\} \qquad \text{(A-12)}$$

By making the following substitutions,

$$\left.\begin{aligned} &MGC^2/y = p \rightarrow \hbar^2/(2m) \\ &(G-1)/y+x^2/y^2 = Q\rightarrow E \\ &1\rightarrow\tfrac{1}{2}\ ms^2 \end{aligned}\right\} \qquad \text{(A-13)}$$

then equation (A-9) will be identical to equation (A-10), and the solutions to equation (A-9) are

$$U_\ell(\Omega) = N_\ell \cdot H_\ell\,[\alpha(\Omega - x/y)]\exp\{-\tfrac{1}{2}\alpha^2(\Omega - x/y)^2\} \qquad \text{(A-14)}$$

and α, s, m can be derived from equation (A-13),

$$\left.\begin{aligned} \alpha &= (p)^{-\frac{1}{4}} \\ s &= 2\sqrt{P}/\hbar \\ m &= \hbar^2/(2P) \end{aligned}\right\} \qquad \text{(A-15)}$$

Finally,

$$\begin{aligned} V(\Omega) &= U(\Omega)/g(\Omega) \\ &= N_\ell \cdot \{(1-2x\Omega+y\Omega^2)/G\}.H_\ell\,[\alpha(\Omega-x/y)]. \\ &\quad \exp\{-\tfrac{1}{2}\alpha^2(\Omega-x/y)^2\} \end{aligned} \qquad \text{(A-16)}$$

It can be seen from equation (A-4), that if the value of g_o is found, then $V(\Omega)$ can be determined. Using equations (A-12), (A-13) and (A-15), one has

$$(2\ell+1)\sqrt{P} = (G-1)/y + x^2/y^2 \qquad \text{(A-18)}$$

Because P is a function of variables G and y, while G is proportional to g_o, and y varies with g_o according to equation (A-4), so g_o can be found from equation (A-18). Once g_o has been evaluated, the oscillating field amplitudes can be obtained. Through Fourier transformation, the pulse can be derived as

$$|\nu(t)|^2 \propto |\int_{-\infty}^{\infty} V(\omega)\exp(i\omega t)d\omega|^2 \qquad \text{(A-19)}$$

Haus has pointed out [21] that all higher order supermodes, a term used to refer to the solutions (A-16) with $\ell \neq 0$, could not be excited in the steady state, because they would be unstable. This limits the solution to the fundamental "supermode" only, namely

$$V(\Omega)=\{(1-2x\Omega+y\Omega^2)/G\}N_o\exp\{-\tfrac{1}{2}\alpha^2(\Omega-x/y)^2\} \quad \text{(A-20)}$$

From equations (A-13) and (A-15), it can be found that

$$\alpha = p^{-\frac{1}{4}} = [y/MGC^2)]^{\frac{1}{4}} \quad \text{(A-21)}$$

Considering the actual figures in experiment, the round numbers for y and G are several, M is a fraction of a unit, while C is a very small figure, $\sim 10^{-4}$, it can be estimated that α^2 has an order of 10^4. While in equation (A-20), the expression at the right hand side can be re-written as

$$(No/G)\{(1+\tfrac{1}{2}y/\alpha^2-x^2/y)H_o[\alpha(\Omega-x/y)]+[y/(4\alpha^2)]H_2[\alpha(\Omega-x/y)]\}$$
$$\exp\{-\tfrac{1}{2}\alpha^2(\Omega-x/y)^2\} \quad \text{(A-22)}$$

Comparing the coefficients of the Hermitain polynomials H_o and H_2, it can be realized that $V(\Omega)$ is approximately decided by H_o, ie,

$$V(\Omega)\sim (1+\tfrac{1}{2}y/\alpha^2-x^2/y)(N_o/G)\exp\{-\tfrac{1}{2}\alpha^2(\Omega-x/y)^2\} \quad \text{(A-23)}$$

Therefore, the pulse can be found, with the aid of Fourier transformation

$$\nu(t)\propto\exp\{-t^2\Delta\omega_d^2/(8\alpha^2)\} \quad \text{(A-24)}$$

The pulse width is thus given by

$$\tau_p \sim \alpha (4 \ln 2)^{\frac{1}{2}} / (\pi \Delta\nu_d) \tag{A-25}$$

From equations (A-21), (A-1) and (A-2), it can be found that

$$\alpha^4 = \frac{g_o \Delta\nu_d{}^2 \Delta\nu_F{}^2 + [\Delta\nu_d{}^2 + 4(\nu_g - \nu_F)^2]^2}{4Mg_o{}^2 \nu_m{}^2 \Delta\nu_F{}^2} \tag{A-26}$$

Therefore,

$$\tau_p \sim \left(\frac{2\ln 2}{\pi^2} \right)^{\frac{1}{2}} \left\{ \frac{g_o(\Delta\nu_F/\Delta\nu_d)^2 + [1 + 4(\nu_g - \nu_F)^2/(\Delta\nu_d)^2]^2}{Mg_o{}^2 \nu_m{}^2 \Delta\nu_F{}^2} \right\}^{\frac{1}{4}} \tag{A-27}$$

References

[1] D. Faubert, S. L. Chin, Opt. and Laser Technology, Vol. 14, 197 (1982), 245 (1982).

[2] G. H. C. New, Rep.Prog.Phys., Vol. 46, 877 (1983).

[3] G. H. C. New, Phil.Trans.R.Soc.London, Vol.A289, 247(1980).

[4] J. M. Halbout, C. L. Tang, IEEE J. Quantum Electron., Vol.QE-19, 487 (1983).

[5] I. V. Tomov, R. Fedosejevs and M. C. Richardson, Sov.J.Quantum Electron., Vol. 10, 797 (1981).

[6] P. G. May, W. Sibbett and J. R. Taylor, Appl.Phys., Vol. B26, 179 (1981).

[7] G. Mourou and T. Sizer, Opt.Commun., Vol. 41, 47(1982).

[8] J. P. van der Ziel, R. A. Logan and R. M. Mikulyak, Appl.Phys.Lett., Vol. 39, 867 (1981).

[9] A. Yariv, "Quantum Electronics", John Wiley and Sons, U.S.A.(1975).

[10] G. H. C. New, IEEE J. Quantum Electron., Vol. 10, 115 (1974).

[11] E. M. Garmire and A. Yariv, Ibid, Vol. QE-3, 222 (1967).

[12] H. Bachert et al, Ibid, Vol. QE-9, 1101 (1973).

[13] W. Ruhle et al, J.Appl.Phys., Vol. 51, 5949 (1980).

[14] H. Kawaguchi et al, IEEE J. Quantum Electron., Vol. QE-16, 706 (1980).

[15] P. Brosson et al, Ibid, Vol. QE-17, 714(1981).

[16] D. J. Kuizenga and A. E. Siegman, Ibid, Vol. QE-6, 694 (1970).

[17] H. A. Haus, J.Appl.Phys., Vol. 51, 4042 (1980).

[18] Y. Sumatsu, Proc. IEEE, Vol. 71, 692 (1983).

[19] H. Kressel, J. K. Butler. "Semiconductor Lasers and Heterojunction LEDs", Academic Press,(1977).

[20] Y. Yamamoto, H. Tsuchiya, Electron.Lett., Vol. 16, 235 (1980).

[21] H. A. Haus, IEEE J. Quantum Electron., Vol. QE-11, 323 (1975).

[22] C. Lin, T. P. Lee and C. A. Burrs, Appl.Phys.Lett., Vol. 42, 141 (1983).

[23] A. Scavannec, Opt.Commun., Vol. 17, 14 (1976).

[25] M. A. Adams, Ph.D. Thesis, University of London, (1979).

[26] W. Sibbett, Ph.D. Thesis, Queen's University, Belfast, (1973).

[27] D. J. Bradley, "Methods of Generation", Ultra Short Light Pulses, Topics in Applied Physics, Vol. 18, (1977).

[28] W. Sibbett, Private communication.

Chapter 3

BASIC PRINCIPLES OF SEMICONDUCTOR LASERS

3.1. Introduction

In this chapter the basic principles of semiconductor laser operations are introduced and the evolution of the technology is traced from the original homojunction structure to the present heterojunction which relates specifically to the research described in this thesis. The reason and practicality of constructing external cavity lasers will also be discussed in this chapter. In the following chapters results will be presented for such a laser system incorporating a Brewster-angled diode, which has been operated in (1) the frequency-tuning regime, (2) the mode-locking regime and (3) the combination of both.

3.2. Basic Principles

In some lasers (such as ruby) discrete atomic states are involved. Within a semiconductor material, however, the electron transitions take place between conduction and valence bands rather than two well defined energy levels [1]. Usually, the electrons in a solid can be divided into three categories [2]. Firstly, there are the "core electrons" whose movements are screened from the effect of neighbouring atoms; we are not interested in these electrons because they contribute a negligible effect to the lasing event. Then, there are the "valence electrons" which are to some extent affected by the neighbouring atoms, but remain in bound states in the vicinity of their parent atoms. These electrons are responsible for the cohesion of the solid. Finally, there are the "free" or "conduction electrons" which become detached from their parent atoms and move about the crystal subject both to thermal excitations imparted to them by the lattice and external forces such as applied electric or magnetic fields. The free electrons are responsible for the conductivity of the solid.

Owing to the high electron concentration in the solid state, the ele-ctronic wave functions overlap. Consequently the electronic energy distribution in a semiconductor is broadened into bands of states, ie, conduction band and valence band. In equilibrium, the probability of occupation of these states is governed by Fermi-Dirac statistics, ie,

$$f(E) = \{1+\exp[(E-E_F)/(kT)]\}^{-1} \qquad (3\text{-}1)$$

where f(E) is the probability of occupation of one state with energy E by an electron in equilibrium states and E_F is the Fermi-level.

Another problem to be solved before the free carrier density can be evaluated is the total number of available electron states within a unit volume of the semiconductor. This is accomplished in terms of the "density of states".

It has been given in reference 3 that the density of states per unit energy interval in the conduction band $Q_C(E)$ and valance band $Q_V(E)$ are

$$Q_C(E) = 8\pi[2M_c{}^3(E-E_C)]^{\frac{1}{2}}/h^3 \qquad (3\text{-}2)$$

$$Q_V(E) = 8\pi[2M_V{}^3(E_V-E)]^{\frac{1}{2}}/h^3 \qquad (3\text{-}3)$$

where E_C and E_V are the conduction band minimum and valance band maximum, respectively, and M_C represents the effective mass of an electron and M_V that of a hole. The subscripts c and v, according to convention, refer respectively to the conduction band and valence band.

The total number of free electrons per unit volume in the conduction band of the semiconductor is obtained by integrating the product of $Q_C(E)$ and $f(E)$ over the energy range of the conduction band.

$$N_C = \int_{E_c}^{E_o} Q_C(E)f(E)dE \qquad (3\text{-}4)$$

where E_o is the energy of an electron just outside the semiconductor. Substituting equations (3-1) and (3-2) into (3-4) gives

$$N_C = \int_o^\infty [8\pi(2M_C^3)^{\frac{1}{2}}/h^3] \frac{E^{\frac{1}{2}}dE}{1+\exp\{[E+(E_C-E_F)]/(kT)\}} \qquad (3\text{-}5)$$

Here, the upper limit of the integration has been extended to infinity and this is acceptable in view of the extremely low population above E_o[2]. Integrating equation (3-5), one gets

$$N_C=2\sum_{n=1}^{\infty}(-1)^{n+1}[2\pi kTM_C/(nh^2)]^{3/2}\exp[n(E_F-E_C)/(kT)] \qquad (3\text{-}6)$$

The same argument applies to the valence band, the only difference is that where the hole population is of importance and the probability of occupation of a state by a hole is given by the expression

$$1-f(E) = \{1+\exp[(E_F-E)/(kT)]\}^{-1} \qquad (3\text{-}7)$$

and so the hole density in the valence band is given by

$$N_V=2\sum_{n=1}^{\infty}(-1)^{n+1}[2\pi kTM_V/(nh^2)]^{3/2}\exp[n(E_V-E_F)/(kT)] \qquad (3\text{-}8)$$

Note that in equations (3-6) and (3-8) the values of N_c and N_V are convergent only when the Fermi level E_F is outside the conduction and valence bands. For $(E_C-E_F)>>kT$ and $(E_F-E_V)>>kT$, which are valid for intrinsic semiconductors at room temperature, the first terms of equations (3-6) and (3-8) are usually used to approximate N_c and N_V, respectively, and these approximations lead to

$$N_c \cdot N_V \propto T^3\exp(-E_g/(kT)] \qquad (3\text{-}9)$$

where $E_g=(E_c-E_v)$ is the extent of the energy gap.

In an intrinsic (undoped) semiconductor, in the state of thermal equilibrium, the Fermi-level is practically in the middle of the energy gap. When the semiconductor is doped, there is the presence of bands of impurity states just below the conduction band for n-type dopants and just above the valance band for p-type dopants, and the Fermi-level begins to shift. As the doping level increases to significant values, the semiconductor becomes degenerate [4], in that the Fermi-level moves into the conduction band for n-type dopants and into the valence band for p-type dopants, as shown in Fig. (3-1).

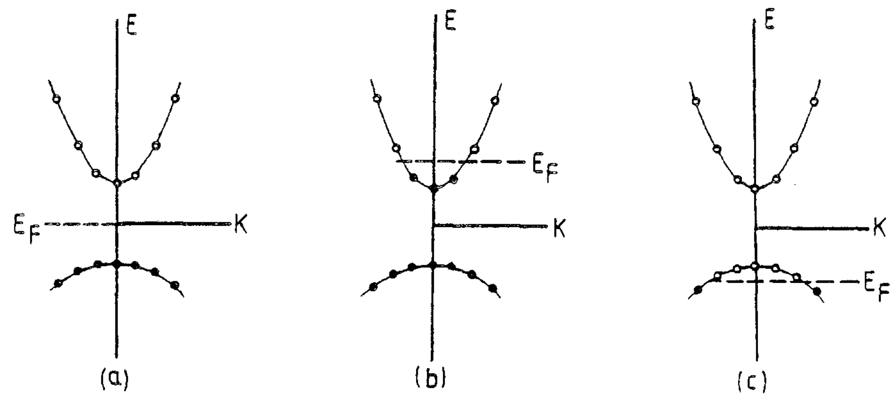

Fig.(3-1) (a) an intrinsic semiconductor, (b) an n-type degenerate semiconductor and (c) a p-type degenerate semiconductor. A dot "." indicates the state is taken by an electron and circle "o" represents the state is empty, k is the propagation constant, and the temperature is OK.

For the distinct case shown in Fig.(3-2), which can exist only under non-thermal equilibrium conditions, the valence band occupation is like that of the p-type degenerate semiconductor shown in Fig.(3-1c), whereas the conduction band resembles the n-type degenerate semiconductor. This is a double degenerate semiconductor, which is characterized by two Fermi levels E_{Fv} and E_{Fc},

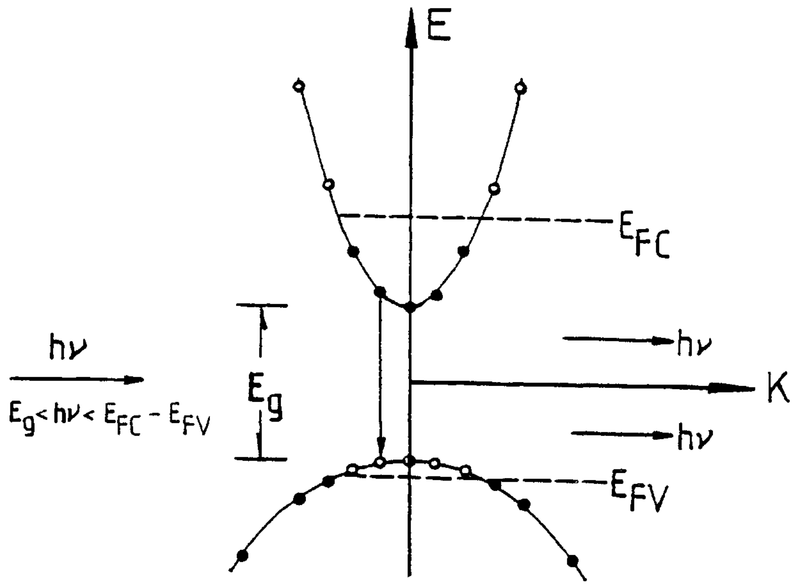

Fig.(3-2) A double degenerate semiconductor. An incident photon with energy hν, which satisfies $E_g < h\nu < E_{Fc} - E_{Fv}$, may induce stimulated emission.

referred to as "quasi-Fermi levels". A photon with frequency ν such that $E_g < h\nu < E_{Fc} - E_{Fv}$ propagating through this semiconductor may induce a stimulated transition. This criterion was first derived by Bernard and Duraffourg [5].

The double degenerate situation shown in Fig.(3-2) may be brought about by various techniques such as electron beam excitation and optical pumping. The most convenient method is by forward biasing a p-n junction and this will be discussed later in this chapter.

Another important condition which is usually accepted as the "conservation of crystal momentum" was investigated by Dumke [6] in 1962, although this condition has now been questioned in the context of high injection carrier densities [3]. This condition predicts that transitions occur mostly between initial and final states with near-identical $\underline{k}$ values. In a direct bandgap semiconductor, whose conduction band minimum and valence band maximum have the same propagation constant $\underline{k}$, electronic transitions with no change of $\underline{k}$ are possible between the minimum energy states at the bottom of the conduction band and the maximum energy states at the top of the valence band. In an indirect material, however, no such transitions are available. Certain radiative transitions do take place across the minimum energy gap, but they involve the participation of another quantum, eg, a phonon, to balance the $\underline{k}$ relation. Since a four-particle interaction is much less probable than a three-particle interaction, transitions across the narrow part of the bandgap have a much lower probability in indirect than in direct gap materials. Using available data at that time, Dumke predicted that in germanium using the indirect transitions, maser action would be prevented by absorption due to free carriers. In

GaAs, or other materials with a direct bandgap, however, it is entirely possible that maser action could be achieved [6]. $Al_xGa_{1-x}As$ has been measured to be a direct transition type material for $x<0.37$ [3], and has played a vital role in the development of CW semiconductor lasers.

In a semiconductor, if an electron is excited into the conduction band, then it thermalizes rapidly through the empty states with a characteristic time of 0.1ps [7], while the spontaneous emission lifetime between bands is much larger, $\sim$1ns [3]. Thus, the system is actually a quasi-four-level system and could reasonably be treated as any other four-level laser. Similar to other laser systems, the exponential gain of the semiconductor material is derived as [1]

$$g(\nu) = \frac{c^2(N_2-N_1)/(Wld)}{8\pi n^2\nu^2\tau_{rec}} f(\nu) \qquad (3\text{-}10)$$

where τ_{rec} is the spontaneous emission lifetime; n, the material refractive index; ν, the light frequency; $f(\nu)$, lineshape function; N_2, N_1, the electron populations of the upper and lower bands; l, the length of the diode; W, the width of the active region; and d, the thickness of the active region. The population of the conduction band N_2 can be related to the total injection current by requiring that in the steady state the rate of recombination be equal to the rate of injection, ie,

$$N_2/\tau_{rec} = I\eta/e \quad (3\text{-}11)$$

where I is the injection current, η is the fraction of the injection electrons which recombine radiatively, and e is the electron charge.

From equations (3-10) and (3-11), we get

$$g(\nu) = [c^2 f(\nu)\zeta\eta/(8\pi n^2\nu^2 ed)]J \quad (3\text{-}12)$$

where J is the injection current density, and $\zeta = (1-N_1/N_2)$ is the inversion factor. By matching the gain coefficient to the system losses, the laser threshold current density can be derived.

Fortunately, due to the waveguide effect, the diffractive loss is less important than other losses [4], especially in the double heterostructure diode laser [8]. By equating the system gain coefficient expressed in equation (3-12) to the distributed and reflection losses, the oscillation condition at frequency ν can be written as

$$\alpha-[1/(2l)]\ln(R_1 R_2)=c^2\zeta\eta f(\nu)J_{th}(\nu)/(8\pi^2\nu^2 n^2 ed) \quad (3\text{-}13)$$

or

$$J_{th}(\nu)=\{8\pi n^2\nu^2 ed/[c^2\zeta\eta f(\nu)]\}\{\alpha-[1/(2l)]\ln(R_1 R_2)\} \quad (3\text{-}14)$$

where α, the distributed loss coefficient, includes the absorption of the flux outside the active region α_{out}, semiconductor imperfect absorption, scattering and free carrier absorption [3]; R_1 and R_2 are the cavity mirror reflectivites.

3.3. <u>p-n Junction</u>

At present, all injection semiconductor lasers are based on the p-n junction structure. When a p-type semiconductor and an n-type semiconductor are put together, a well defined p-n junction is obtained. If these two semiconductors possess the same bandgap energy, the junction is called homojunction, otherwise heterojunction. Using Poisson's equation with proper boundary conditions, the characteristics of the junction region can be derived [1]. This region is called the "depletion" or "space charge" region.

If a p-n junction is forward biased properly, there will be a region within which electrons appear in the states higher in energy than the hole occupied states. This region is often referred to as the "active" or "recombination region". In one-dimensional geometric space, this situation can be described with Fig.(3-3).

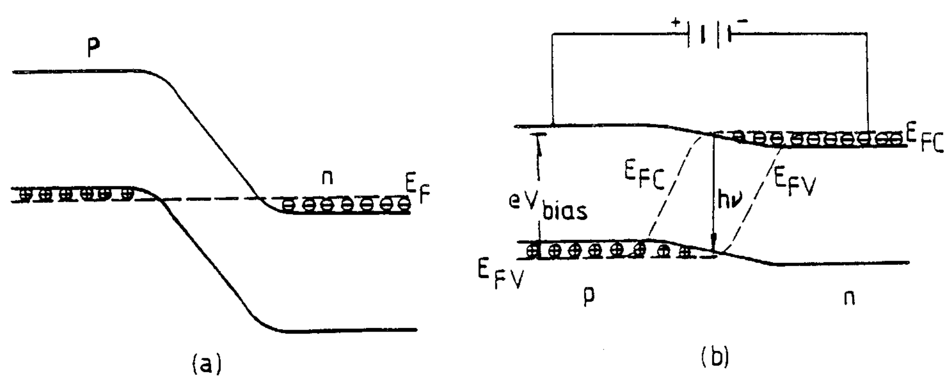

Fig. (3-3) By biasing a p-n junction with proper voltage, a double degenerate region at the junction can be produced ("⊕" represents the hole, and "⊖" electron).

When the amplifying medium shown in Fig.(3-3) or (3-2) is enclosed in an optical resonator, laser action may be achieved provided there is enough gain. Usually, the mirrors of the optical resonator are provided by the cleaved facets of the semiconductor crystal. For GaAs, which has a refractive index of 3.6, the cleaved facet has a reflectivity of 0.32 for normal incident light.

In the initial stages in their development, diode lasers were homojunction devices and had to be operated at very high injection current densities, low temperatures and low duty cycles [3]. This was mainly attributed to the lack of confinement of injection carriers and the weakness of the optical waveguide effect in homojunction lasers [3]. These problems were finally solved by the construction of the heterojunction laser, which made room temperature CW semiconductor lasers a practical reality.

3.4. Heterojunction

A heterojunction can be a p-n, p-p, or n-n junction. Because of its importance to the room temperature CW operation of semiconductor lasers, the inclusion of a dedicated section is justified.

It was found that $Al_xGa_{1-x}As$ material had a larger bandgap energy and lower refractive index than GaAs, and the bandgap energy and the refractive index could be changed by adjusting the aluminium content x. Also, the crystallographic lattice parameters of GaAs and $Al_xGa_{1-x}As$ matched very well. It was relatively easy to epitaxially grow $Al_xGa_{1-x}As$ layers on the top of a GaAs substrate. These factors made possible the realization of high quality heterojunction semiconductor lasers. Up-to-date, manufacturing technology for AlGaAs/GaAs diodes is such that the diodes can be produced very reliably. Substantial ongoing research has also concentrated on InGaAsP/InP semiconductor lasers in order to meet the demands arising from optical fibre communication. Nevertheless, the study on GaAs diode lasers is still being intensively continued. Many of the results obtained with GaAs are applicable to other materials and can provide guidelines for their preparation [3].

With the introduction of aluminium into the cladding layers, between which the active layer is sandwiched, a potential barrier is introduced into the interfaces between the active layer and the passive layers to prevent the injection carriers from diffusing away from the recombination region. Because the injected carriers are effectively confined to the active region, their utilization is greatly increased and as a result, the threshold current density is decreased drastically [9]. Moreover, with the active layer thickness being much less than the carrier diffusion length (the accepted figure is $d<0.5\mu m$ in GaAs), the concentration of the injected carriers may be regarded as constant over the whole thickness of the active layer [8].

Exploitable refractive index differences between the active and passive layers are also introduced by this means. It is estimated [3] that the refractive index step Δn at the interface of the $Al_xGa_{1-x}As/GaAs$ heterojunction, at λ=900nm, satisfies the relationship that

$$\Delta n = 0.62\ \Delta x \qquad (3\text{-}15)$$

where Δx is the aluminium content difference between the materials of the two layers concerned. Consequently, a waveguide structure is built up. It can be shown that, for a symmetric three-layer waveguide which is composed of a higher refractive index (n) layer of d in thickness sandwiched between two semi-infinite layers of lower index n_c, the FWHM of the guided fundamental TE mode is

$$FWHM = d + \lambda \ln 2/[2\pi(n^2-n_c{}^2)^{\frac{1}{2}}] \qquad (3\text{-}16)$$

Putting the following values into equation (3-16), λ=850nm, n=3.6, n_c=3.42, and d=0.2μm, the FWHM is approximately 0.28μm, which agrees with the value cited in reference 9. Taking into account that the active layer is 0.2μm, it can be concluded that the major part of the light is confined within the active region and an effective waveguide effect is, thus, achieved. Fundamental transverse mode operation can be expected according to reference 3, using the parameters suggested by the manufacturer for the zero degree diode, when d satisfies 0.07μm<d<0.46μm.

3.5. Stripe Geometry Lasers

The idea of confining light and carriers to the active region can also be applied to the lateral direction of a semiconductor laser. This brought about the so-called stripe geometry diode laser. The lateral confinement serves several purposes [10] which include (i) reduction of the cross-sectional area which in turn reduces the operating current, (ii) single filament operation and fundamental mode emission along the junction plane for stripe width W<15μm, (desirable dimension of the coherent light source for special optical fibres by controlling the stripe width), and (iii) reduced degradation effects by removing most of the junction perimeter from the surface. It is worth pointing out that the temperature rise of the active region of a stripe-geometry double heterojunction laser does not significantly differ from that of a broad-area double heterojunction laser [10].

The SiO_2 stripe-geometry diode used in the experiments described in this thesis was defined by a photolithographic process. The light was confined to the area of the stripe without the use of a deliberate dielectric waveguide simply by supplying optical gain to the stripe region only and leaving the outer regions in optically lossy conditions. Photons naturally accumulated in the regions where there was gain and were removed from the regions where there was loss

[8]. A diagrammatic illustration of the oxide stripe double heterojunction is shown in Fig. (3-4).

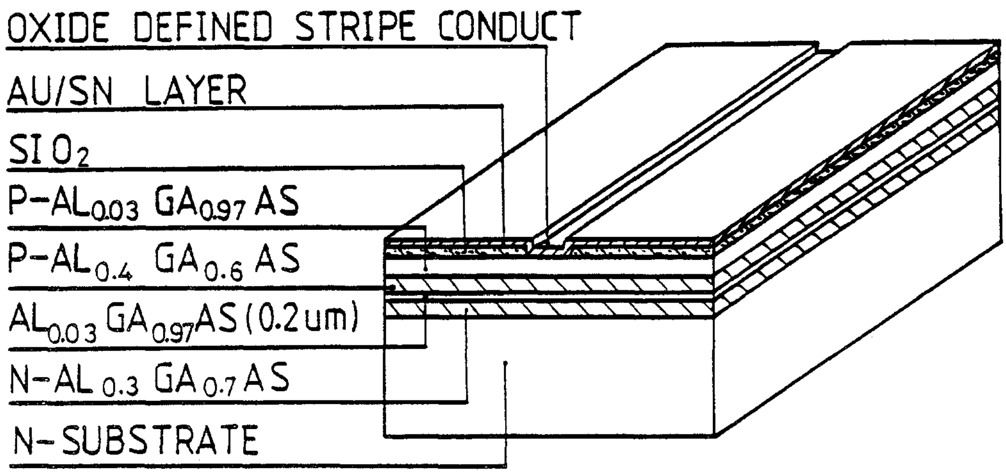

Fig. (3-4) Diagrammatic illustration of an SiO_2 stripe double heterojunction diode used for the results presented in this thesis.

The diodes used were Brewster-angled diodes where the stripes were tilted at the Brewster angle to the facet normals so that the guided waves would strike the facets near the Brewster angle and so the TE mode would pass through the facets without being subject to much loss. The laser feedback was provided by reflectors external to the diode rather than the diode facets, and the diode acted solely as an amplifying medium around which the external cavity was configured. It must be remembered that the basic physical properties are not altered for these "angled-stripe" laser diodes.

3.6. Brewster-Angled Diode Lasers Operating in External Cavity Configurations

It was found that the FWHM of the spontaneous emission of the GaAlAs/GaAs diode, used in this work, was ∿14nm. This provided the potential, in principle at least, of tuning the output wavelength about the same range and generating ultrashort pulses. Due to the fact that the material (GaAs)has a refractive index of 3.6, a diode with two parallel facets whose normals are coincident with the stripe direction, operates as an oscillator so the ways of tapping this potential are largely confined.

The solitary diode laser is not suitable for mode-locking. There is an alternative approach to obtaining short optical pulses from the diode by the gain switching method. Although impressively short pulses have been produced in this way [11,12,13], unfortunately, the resulting pulse widths were of the order of several cavity round-trip times, and it was unlikely that transform-limited pulses would be generated in this manner [14]. Also, because these pulses were composed of broad backgrounds superimposed by several spikes defined by the cavity round-trip time, this would largely reduce the usefulness of these pulses in time multiplexing. Spectral measurements also showed several cavity modes, which would affect frequency multiplexing as well. Haus concluded [15] that if simplicity of the structure is the dominant consideration, the modulation method will prevail. However, one may surmise that for a given modulation power the mode-locking principle will be capable of producing "cleaner" (with less structure) pulses at higher repetition rates than the direct modulation process. This follows from the fact that in a mode-locking configuration the pulse does not build up from noise but from a pulse "stored" in the external resonator from the preceding passage. Also, various relaxation oscillations that follow a rapid turn-on of the diode do not affect the mode-locked pulse shape but have to be combatted in direct pulse generation from a laser diode.

According to mode-locking theory and practice, in order to actively mode-lock a laser system, a modulation frequency equal to (or harmonically related to) the cavity mode spacing must be used. For an isolated diode of length $\sim$500μm, the mode spacing would be $\sim$83GHz (taking the refractive index of GaAs $\sim$3.6). Apart from the high frequency generator, two obstacles need to be overcome before such a diode laser can be mode-locked actively. Firstly, the modulation frequency achieved at present is relatively low, even taking into account the latest result reported by Lau et al [16] where the modulation frequency does not even reach one-tenth of the diode mode spacing. Secondly, the injection efficiency of a high frequency signal into the injection diode is not practical . It is very difficult to couple an RF signal ~100GHz into a diode laser [3]. As pointed out by Suematsu [17], the diode impedance will limit the modulation frequency, typically, to several gigahertz.

On the other hand, the solitary diode laser is not amenable to frequency-tuning. The output frequency can be controlled only by externally induced variation of the gap energy and refractive index (through changes in temperature, pressure or magnetic field) [18,19]. For example, in Fig. (3-5), temperature tuning ranges for four different semiconductor materials are shown [20].

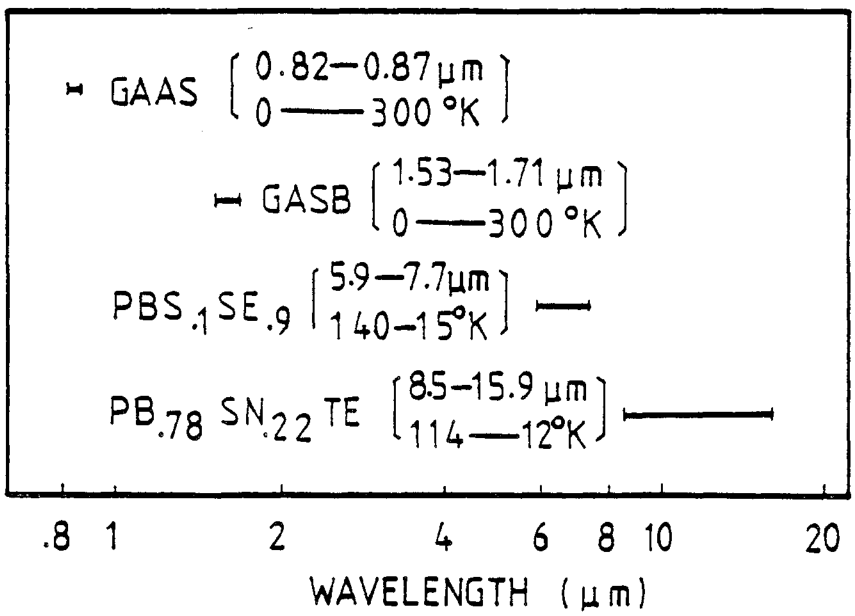

Fig. (3-5) Representative temperature tuning ranges for several semiconductor materials.

A simple way of achieving the temperature tuning is by altering the injection current which induces a temperature change in the active region. Unfortunately, in order to ensure reliable operation and durability, current changes are limited to small range, and this will be discussed further in Chapter 4. In the case when the single mode operation is desired, the injection current needs to be controlled more carefully.

Operating the semiconductor diode in an external cavity configuration seems to be a proper choice, and experiments have proved that this is a successful method for achieving continuous frequency-tuning and mode-locking of a semiconductor injection laser. Because the extended cavities are usually two or three orders of magnitude longer than the diode optical length, mode-locking frequencies compatible to these external cavities are reduced substantially. Moreover, the longer cavities provide the opportunity of inserting conventional frequency-tuning elements, which are usually much larger in dimensions than the diode chips, into the cavities. These include diffraction gratings [19,21-23], birefringent filters [24], Fabry-Perot etalons [25], etc. This makes the frequency-tuning more reliable and practical. Many workers have also observed that the external cavity operation injection laser gives very narrow spectral width with appreciably high stability [19,22,26,27]. For instance, Wyatt et al [23] have claimed a spectral width of 10KHz from their semiconductor laser.

The key point of coupling a semiconductor diode into an external cavity is to spoil the diode laser resonator defined by the two parallel cleaved facets. One method is to deposit an anti-reflection coating (AR) on the cleaved facet(s), for example, a layer of silicon monoxide of $\lambda/4$ thickness in the case of GaAs. Another method is to tilt the direction of the diode stripe at the Brewster angle with respect to the normal(s) to the end facet(s), as has been adopted here. This angle is $\sim 15.5^{o}$ for GaAs, as shown in Fig. (3-6).

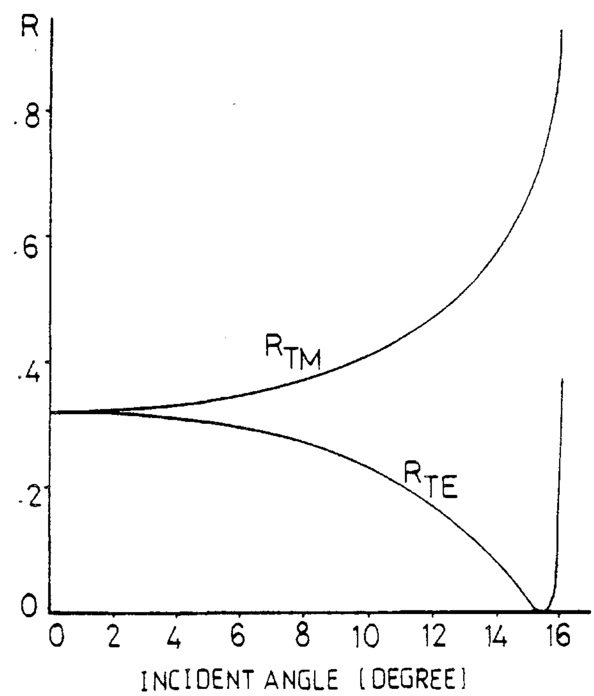

Fig. (3-6) Reflectivities for two orthogonally polarized plane waves incident upon a GaAs - air interface at different angles.

At present, AR coating techniques have achieved a modal reflectivity of less than $2x10^{-4}$ [28]. Ironically, it was the residual reflectivity which created diode modes that made Kaminow's measurements possible. This residual reflectivity manifested itself as a train of pulses separated by the diode chip round trip time, appearing in any result from the mode-locked diode laser system which used an AR coated zero degree diode as the active medium [29,30-33]. The effect of the spurious reflectivity on the quality of the mode-locking pulses has long been realized [34]. AuYueng et al summarised [14] that the external periodic current modulation locked the pulses of a group of external cavity modes centred at each individual laser diode mode. However, there was no phase coherence among the mode groups, giving rise to fluctuations within the optical pulses. The temporal width of the pulse envelope corresponded to the inverse spectral width of a single mode group. This indicated that so long as the diode modes were recognisable from an AR coated diode laser system, the spectral width of the external cavity modes which were phase locked together would be no more than the (internal) mode spacing of the diode. Therefore the possible pulse width would be restricted to the order of a picosecond (for transform limited Gaussian pulse at λ=850nm), unless perfect AR coating was achieved. The problem, which affects the result of AR coating, arises from the fact that the guided wave inside the diode does not strike the facet at the desired angle and the emergent light from the diode facet, which is equivalent to a narrow slit, will diffract into a large angle. It is, therefore, very difficult to choose the direction with which the normal to the $\lambda/4$ coating layer coincides.

Careful consideration revealed that the actual difficulty did not come from the waves incident upon the facets at angles slightly different from the designated angle, but from those parts of the reflected beams which were still travelling inside the waveguide giving rise to the diode modes. This suggested that the mode formation of the diode could be broken by letting the reflected light from the facets travel outside the gain area (stripe region). This is finally extinguished, partly due to the absorption when propagating through the loss area outside the excited stripe and partly due to the scattering when striking the sawn walls of the diode. The Brewster-angled diode embodied this idea, and experimental results have confirmed that it acted solely as an amplifying medium in the external cavity laser system. Of course, the Brewster-angled diode has its own shortcomings, for example, a more complex diode mount is needed due to its geometric shape (discussed in Chapter 4), extra effort is required to align the system compared to the conventional zero degree diode laser, and the beam profiles are more complicated, etc.

A photograph of the Brewster-angled diode used in

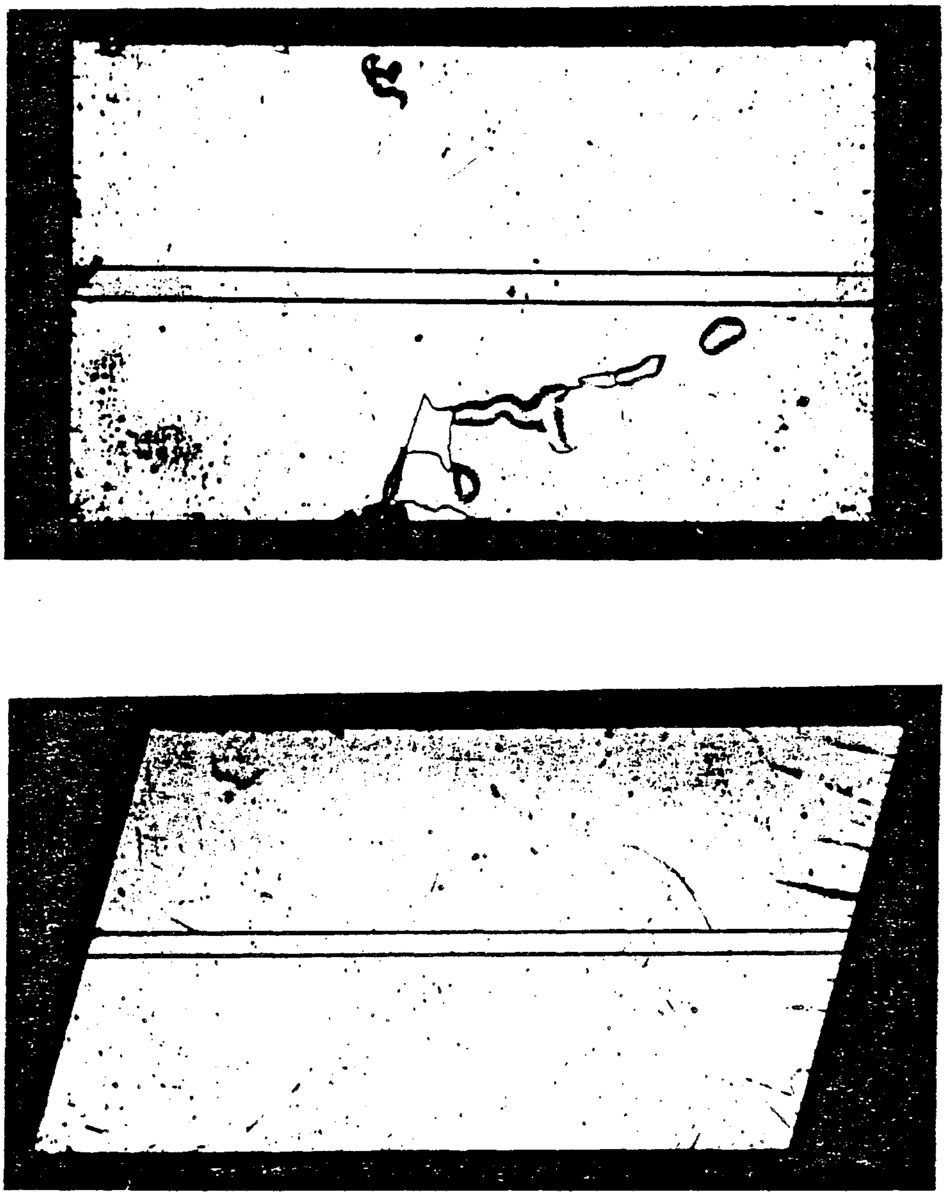

Fig. (3-7) Photographs of a zero degree diode and a Brewster-angled diode.

this work, taken through an optical microscope (x200), is shown in Fig. (3-7), together with a zero degree diode for comparison.

The angle between the stripe direction and the facet normal has been measured to be 15.5 ± 0.2^{o}. The optical paths of the two orthogonally polarized plane waves, one with its electric field oscillating inside the junction plane referred to as the TE wave, and the other perpendicular to the junction plane called the TM wave, are shown in Fig. (3-8). From Fig. (3-6), it is clearly

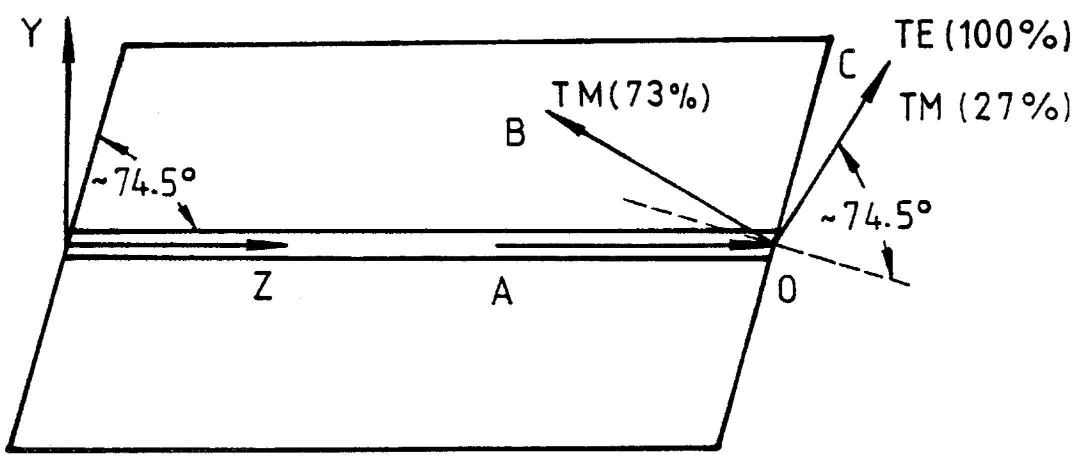

Fig. (3-8) Diagram showing the optical paths of the TE and TM plane waves incident at the Brewster angle upon the diode facet-air interface.

seen that the TE wave, whose reflectivity is denoted by R_{TE} can pass through the end facet without loss if the incident angle is exactly equal to the Brewster angle.

Most of the TM wave will be reflected at the diode facet, and the reflected light no longer travels inside the diode stripe area. This is eventually frustrated by absorption in the area outside the active region and scattering at the sawn side walls of the diode.

It is highly unlikely that the TM mode can compete with the TE wave in the Brewster-angled diode laser system, because of the large difference in the losses between the two orthogonally polarized waves. In fact, in the conventional zero degree diode laser, with a thin submicron active layer, the laser output is always dominated by the TE mode due to small difference of the mode reflectivities at the facet [35].

Experimental observation has confirmed that the output of the Brewster-angled diode laser was indeed dominated by the TE mode as shown in Fig. (3-9), which was recorded by inserting a polarizer in front of the photodiode detector. Furthermore, when the polarizer was included in the external cavity, the lasing action was quenched when only the TM wave was admitted. In fact, no lasing action was observed when the bias level was increased to 300mA, (about twice the threshold needed for the TE mode to lase), if the polarizer favouring the TM mode was placed inside the external cavity.

Observations of the output from the Brewster-angled diode without an external cavity have also been made, as

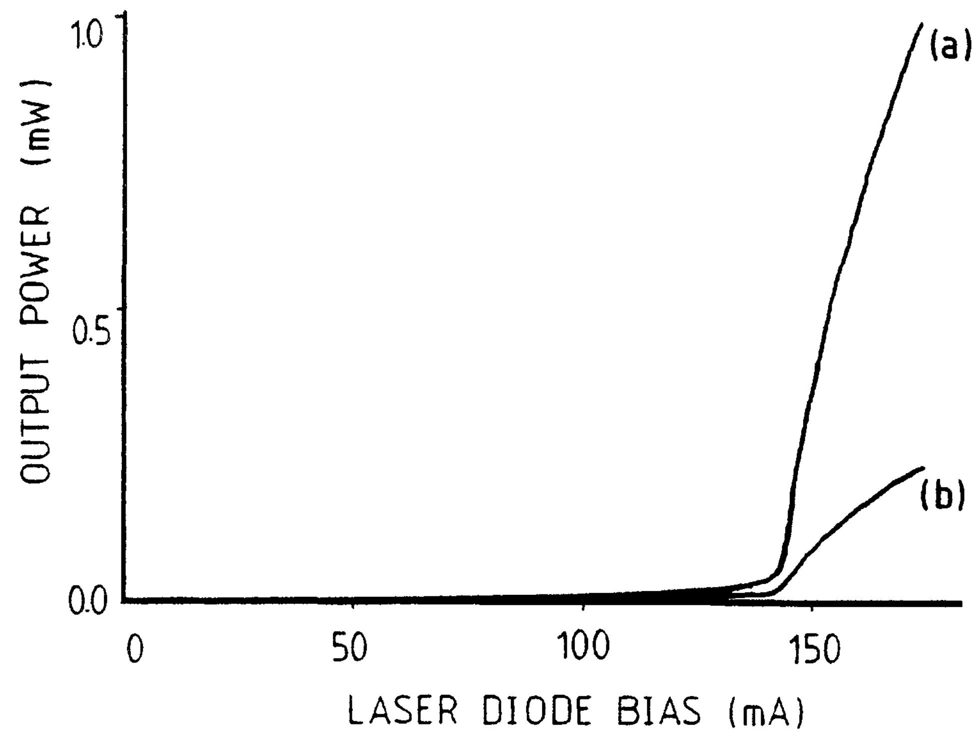

Fig.(3-9) Curves showing that the output of the Brewster-angled diode laser is dominated by the TE mode. (a) TE mode, (b) TM mode.

illustrated in Fig. (3-10). There was no evidence to suggest that the Brewster angled diode could oscillate on its own, even with an injection curent level as high as 3 times the threshold value when the external cavity was aligned. The output spectrum of the Brewster-angled diode without external cavity has also been monitored at an injection current of 300mA, using a monochromator of resolution better than 0.05nm. The result is shown in Fig. (3-11). For comparison, the spectrum of a conventional 500μm long zero degree diode biased at its threshold level (143mA for the diode tested) is also given in Fig. (3-11). The spectrum of the zero degree diode clearly shows the diode mode structures which are defined by the two parallel facets and separated by 0.17 to 0.19nm. In fact, as early as 1967, Mohn et al had reported that the spectra from their Brewster-angled diode operating in an external cavity showed no internal diode resonances [36]. In 1980, Holbrook et al obtained a complete elimination of feedback reflections from the cleaved facets of a GaAlAs/GaAs double-heterostructure injection laser by combining the AR coating technique with tilting of the diode stripe at 5° to the facet normal [37] and reported that bandwidth limited pulses of 16ps duration had been observed [38]. In this work, 9ps pulses (shorter than the round-trip time of the diode chip $\sim$12ps) have been recorded from the Brewster-angled diode laser (see Chapter 6).

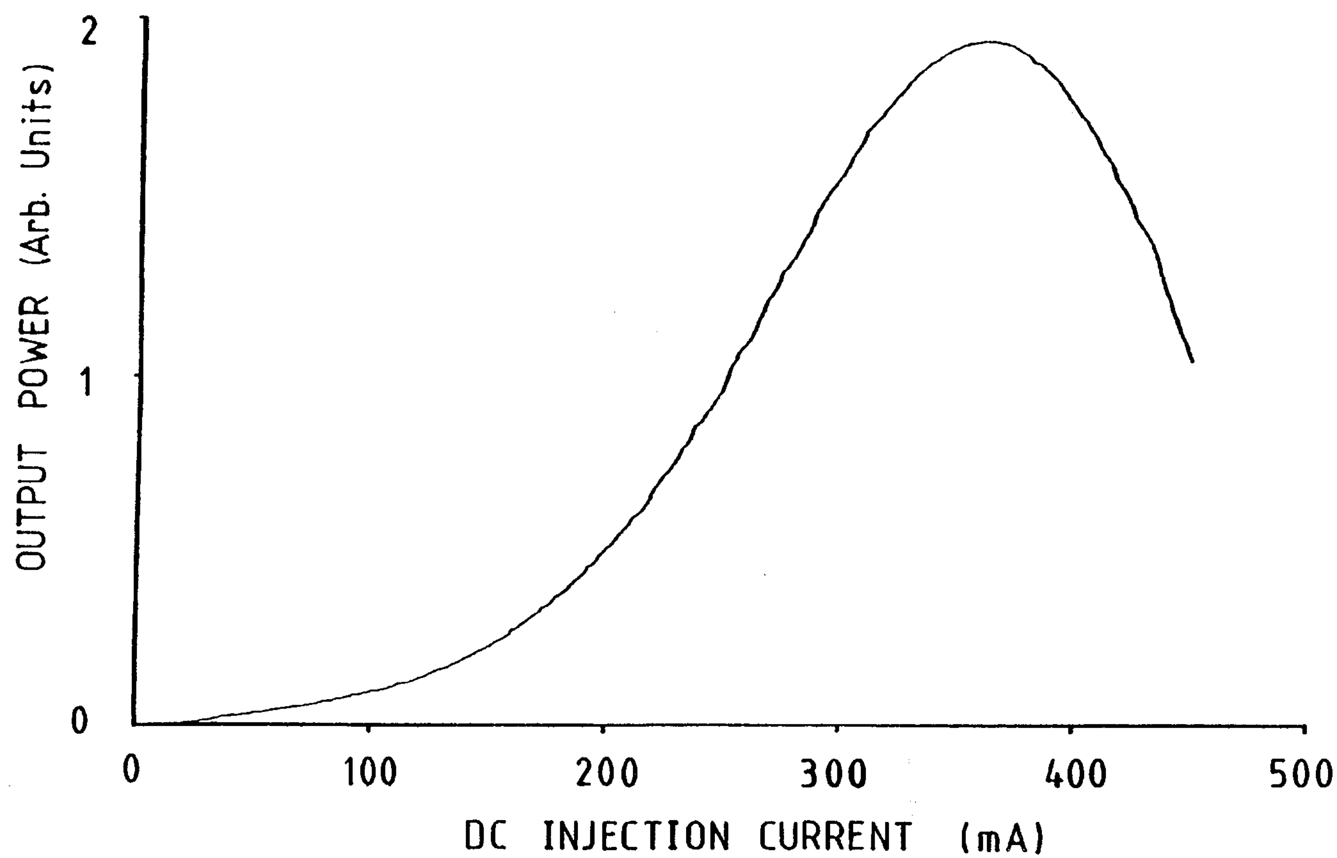

Fig.(3-10) Spontaneous emission of a Brewster-angled diode varies with dc injection current.

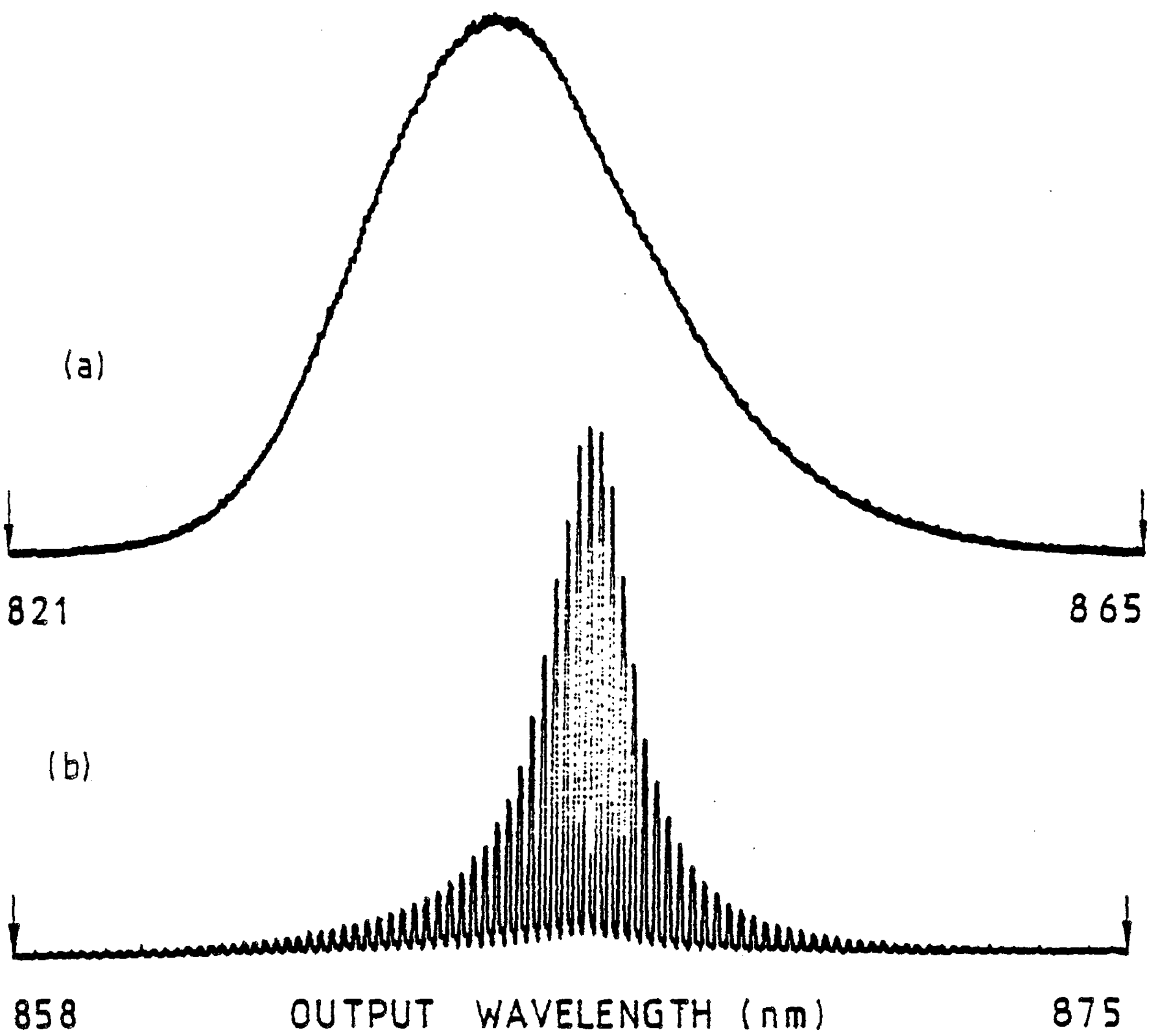

Fig.(3-11) (a) Spontaneous emission spectrum from a Brewster-angled diode biased at 300 mA.

(b) Output spectrum of a zero degree diode biased at its threshold (~143 mA).

3.7. Conclusions

In this chapter, the basic principles underlying the construction of the semiconductor injection laser have been outlined. Two key issues, effective exploitation of the injection carriers and tight confinement of the optical field to the proximity of the active region, have been jointly solved by the employment of the heterostructures. This has led to the successful CW operation of the semiconductor injection laser at room temperature. The necessity and practicality of a laser having an external cavity have been made clear in this chapter with emphasis directed towards a "Brewster-angled" diode laser system.

References

[1] A. Yariv, "Introduction to Optical Electronics", Holt, Reinhart and Winston, (1976).

[2] P. Hlawiczka, "Introduction to Quantum Electronics", Academic Press, (1971).

[3] H. Kressel, J. K. Butler, "Semiconductor Lasers and Heterojunction LEDs", Academic Press, (1977).

[4] A. Yariv, "Quantum Electronics", John Wiley and Sons, (1975).

[5] M. G. A. Bernard and G. Duraffourg, Phys.Stat.Solidi, Vol.1, 699 (1961).

[6] W. P. Dumke, Phys.Rev., Vol. 27, 1559 (1962).

[7] Y. Nishimura, Jpn.J.Appl.Phys., Vol.13, 109 (1974).

[8] G. H. B. Thompson, "Physics of Semiconductor Laser Devices", John Wiley and Sons, (1980).

[9] Zh.I.Alferov et al, Sov.Phys.Semicond., Vol. 3, 1107 (1970).

[10] H. C. Casey, M. B. Panish, "Heterostructure Lasers", Academic Press, (1978).

[11] G. J. Aspin, J. E. Carroll, R. G. Plumb, Appl.Phys.Lett., Vol. 39, 860 (1981).

[12] J. P. van der Ziel, R. A. Logan, IEEE J. Quantum Electron., Vol. QE-18, 1340 (1982).

[13] N. Onodera, H. Ito, H. Inaba, Electron.Lett., Vol.18, 811 (1982).

[14] J. C. AuYueng, A. R. Johnston, SPIE, Vol. 322, 25 (1982).

[15] H. A. Haus, Jpn.J.Appl.Phys., Vol. 20, 1007 (1981).

[16] K. Y. Lau et al, Appl.Phys.Lett., Vol. 43, 1 (1983).

[17] Y. Suematsu, Proc. IEEE, Vol. 71, 692 (1983).

[18] P. G. Eliseev, N. N. Shiukin, Sov.J. Quantum Electron., Vol. 3, 181 (1973).

[19] M. W. Fleming, A. Mooradian, IEEE J.Quantum Electron., Vol. QE-17, 44 (1981).

[20] B. D. Guenther, R. G. Buser, Ibid, Vol. QE-18, 1179 (1982).

[21] R. Ludek, E. P. Harris, Appl.Phys.Lett., Vol. 20, 499 (1972).

[22] S. Saito, Y. Yamamoto, Electron.Lett., Vol. 17, 325 (1981).

[23] R. Wyatt, W. J. Delvin, Ibid, Vol. 19, 110 (1983).

[24] C. L. Tang, V. G. Kreismanis, J. M. Ballantyne, Appl.Phys.Lett., Vol. 30, 113 (1977).

[25] C. Voumard, Opt.Lett., Vol. 1, 61 (1977).

[26] F. Favre, D. Le. Guen, J. C. Simon, IEEE J. Quantum Electron., Vol. QE-18, 1712 (1982).

[27] V. Yu. Bazhenov et al, Sov.J.Quantum Electron., Vol. 10, 1546 (1980).

[28] I. P. Kaminow, G. Eisenstein, L. W. Stutz, IEEE J.Quantum Electron., Vol. QE-19, 493 (1983).

[29] J. P. Van der Ziel, J.Appl.Phys., Vol. 52, 4435 (1981).

[30] J. P. Van der Ziel et al, Appl.Phys.Lett., Vol. 39, 525 (1981).

[31] J. P. Van der Ziel et al, Ibid, Vol. 39, 867 (1981).

[32] Ch. Harder et al, Ibid, Vol. 42, 772 (1983).

[33] Y. Suzuki, T. Sato, Electron.Lett., Vol. 18, 821 (1982).

[34] D. J. Bradley in "Topics in Applied Physics", edited by S. L. Shapiro, Springer-Verlag, Vol. 18, 17 (1977).

[35] T. Ikegami, IEEE J. Quantum Electron., Vol. QE-8, 470 (1972).

[36] E. Mohn et al, Phys.Lett., Vol. 24A, 561 (1967).

[37] M. B. Holbrook, D. J. Bradley, P. A. Kirkby, Appl.Phys.Lett., Vol. 36, 349 (1980).

[38] M. B. Holbrook, Ph.D. Thesis, University of London, (1980).

Chapter 4

DESIGN AND ASSESSMENT OF SEMICONDUCTOR LASER MOUNTS

4.1. Introduction

In this chapter, problems arising from the mounting process of the Brewster-angled diode are discussed in view of the temperature rise of the active region of the diode and its consequences. The obvious deliterious effects of the thermal excursions on the system threshold and operational lifetime imply that the laser diode should be operated at as low an active region temperature as possible. This has led to the design and construction of a special type of diode mount which is compatible to the Brewster-angled diode and also offers a low heat resistance. The mounting of the diode is described and the laser performance assessed from the "thermal" viewpoint.

4.2. Influences of Operational Temperature on Diode Laser Threshold and Lifetime

Good conduction between laser diodes and their heat sinks, both electrical and thermal, are of vital importance for efficient laser operation. Generally, the electrical contact does not impose a serious restriction on the CW operation of the injection laser, and this chapter is mainly devoted to addressing the issue of adequate heat sinking.

Ever since the advent of the semiconductor laser, the operational temperature of the laser diode has been studied extensively. When semiconductor lasers had a homojunction structure they failed to exploit the injection carriers and confine the optical fields in the proximity of the active regions effectively and as a result, threshold current densities in excess of 50,000A/cm^2 at room temperature were required [1]. Consequently, these diode lasers only operated at low duty cycles, usually a small fraction of 1 per cent [1], to ensure a low operational temperature in the active regions. In fact these semiconductor lasers were operated at low ambient temperature (77k) [2-4].

When the heterojunction laser was developed [5-8], it was possible to operate the semiconductor laser CW at room temperature. This achievement does not mean, however, that reducing the operational temperature in the active region is no longer of basic importance. Good thermal contact between the diode and its heat sink is still necessary, because without adequate thermal contact the temperature of the active region may be raised unnecessarily, which is very detrimental to the laser operation. This can be understood in terms of the threshold dependence and lifetime dependence of the injection laser on the operational temperature.

4.2.1. Threshold dependence of the diode laser on the operational temperature

The threshold dependence of the diode laser on the operational temperature of the active region is very complex, and it is very difficult to give a comprehensive description, because there are still some aspects that are not yet fully understood. Nevertheless, there exists the following commonly acknowledged semi-empirical formula, put forward by Pankove [9], relating threshold current to active region temperature,

$$I_{th}(T) = I_o \exp(T/T_o) \qquad (4\text{-}1)$$

where I_o is the laser threshold current extrapolated to zero degree Kelvin, T is the temperature of the active region and T_o is a characteristic temperature for the particular diode. According to reference [1], T_o varied from 50 to 100 K for GaAlAs/GaAs double heterojunction diode lasers.

Experimental measurements have been carried out to find the parameter T_o for the batch of diodes used in this work which was received in May 1982. The experimental results are shown in Fig. (4-1 a and b). In Fig. (4-1a), the threshold of a Brewster-angled diode operating in an external cavity configuration is measured against the heat sink temperature. A similar result has also been obtained from a zero degree diode made by the same manufacturer, as shown in Fig. (4-1b). These curves are in agreement with

(a)

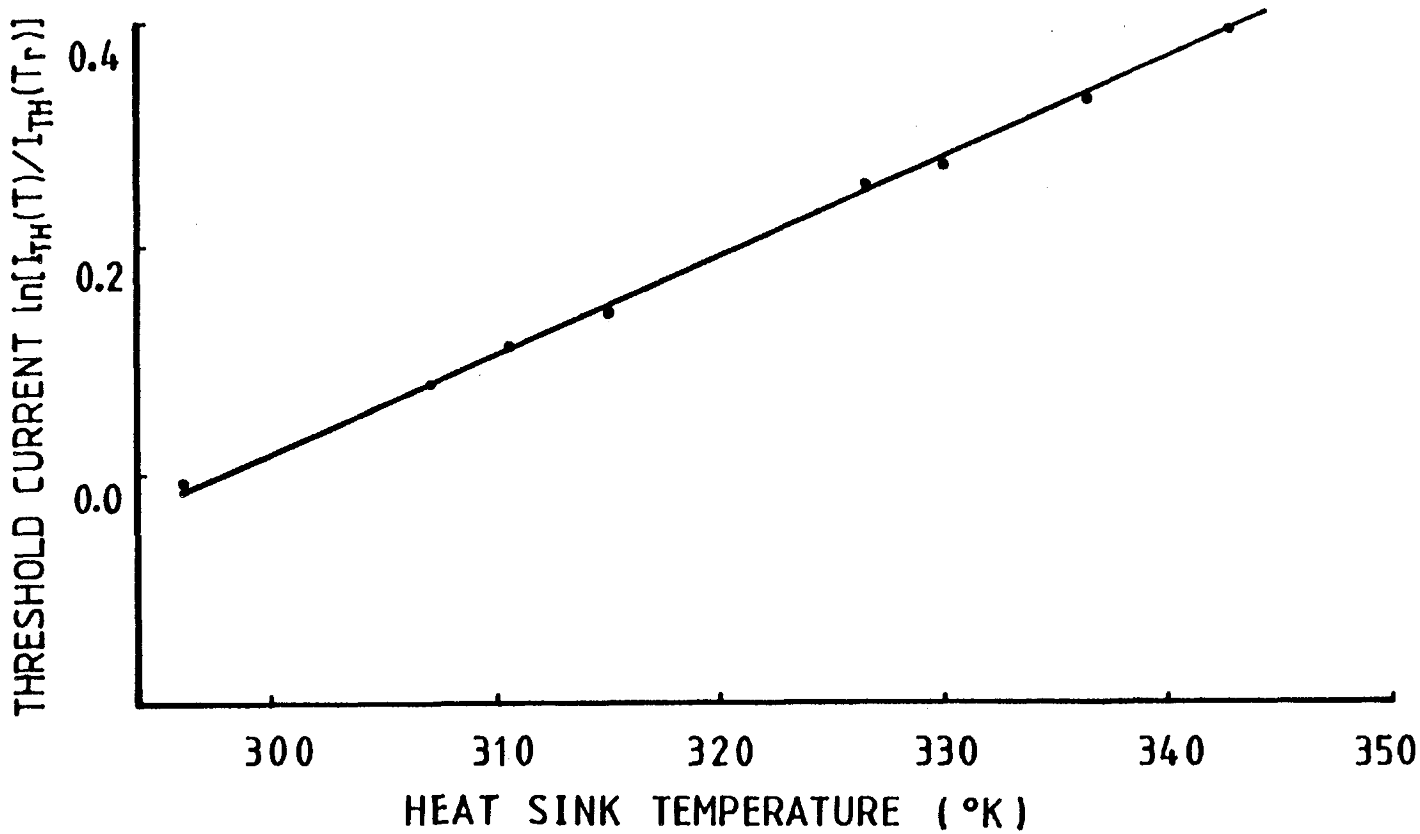

Fig. (4–1) Variation of laser threshold $I_{th}(T)$ as a function of the heat sink temperature, where $I_{th}(Tr)$ is the threshold at room temperature,

(a) taken for a Brewster-angled diode laser,

(b)

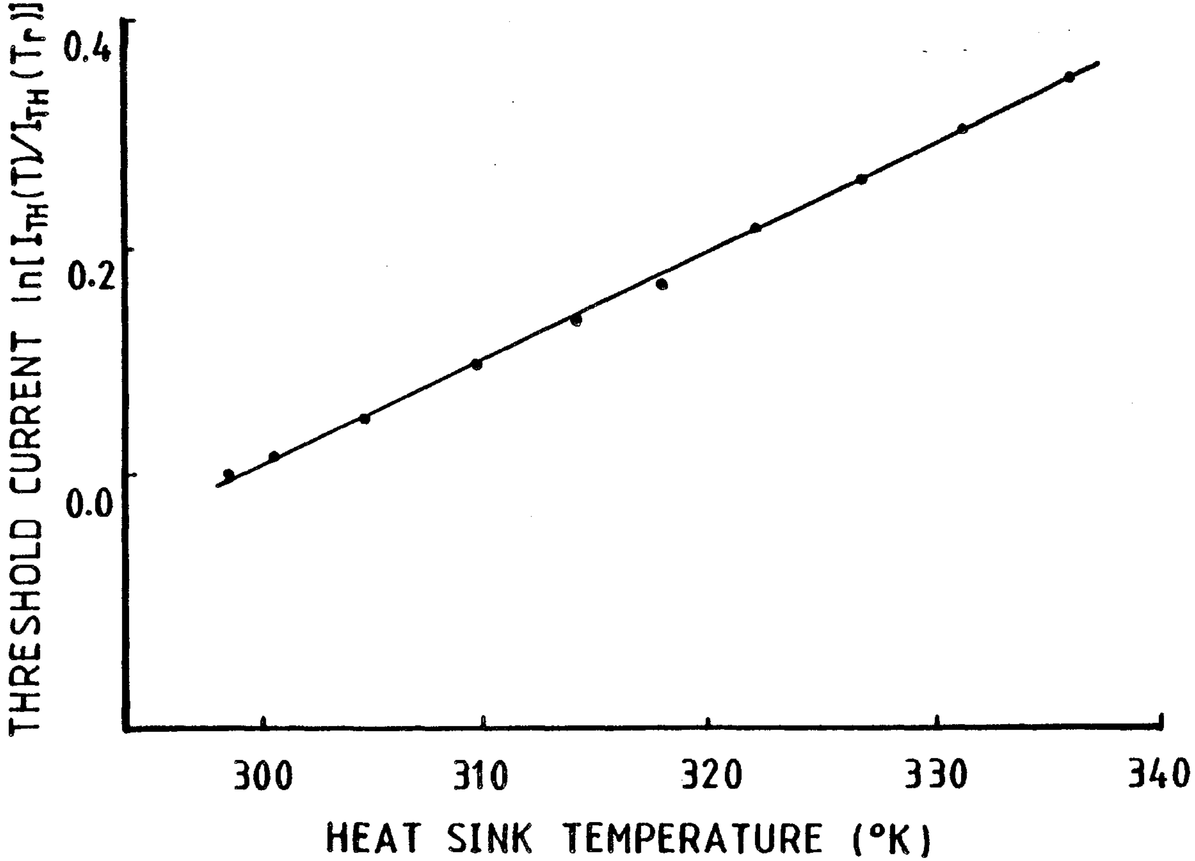

(b) taken for a zero degree diode laser with identical dimensions to the Brewster-angled diode laser.

equation (4-1) within the temperature range involved. From Fig. (4-1), T_o is deduced to be 112K for the Brewster-angled diode laser and 107K for the zero degree diode with identical dimensions.

For a more detailed consideration of equation (4-1), it is necessary to introduce another parameter R_h, the heat resistance of the system, which is defined as the temperature increment of the system when unit power is dissipated in it. Taking the case where the contact heating can be ignored, then the temperature T of the active layer is given by

$$T = T_s + R_h VI \tag{4-2}$$

where T_s is the heat sink temperature, V is numerically equal to the bandgap energy in electron volts, and I is the injection current [11]. Combining equations (4-1) and (4-2), one gets

$$I_{th} = I_o \exp\{(T_s + R_h V I_{th})/T_o\} \tag{4-3}$$

From equation (4-3) it can be seen clearly that a large R_h implies a high threshold current and this in turn increases the temperature of the active region. This will lead to a correspondingly higher threshold current. Under certain circumstances, namely when R_h is large enough and T_o is small enough, the diode can never reach its CW threshold when the ambient temperature is higher than a certain value $T_s(c)$, as shown in Fig. (4-2). The curve (as described by

Gooch [12]) in Fig. (4-2) shows the relationship between

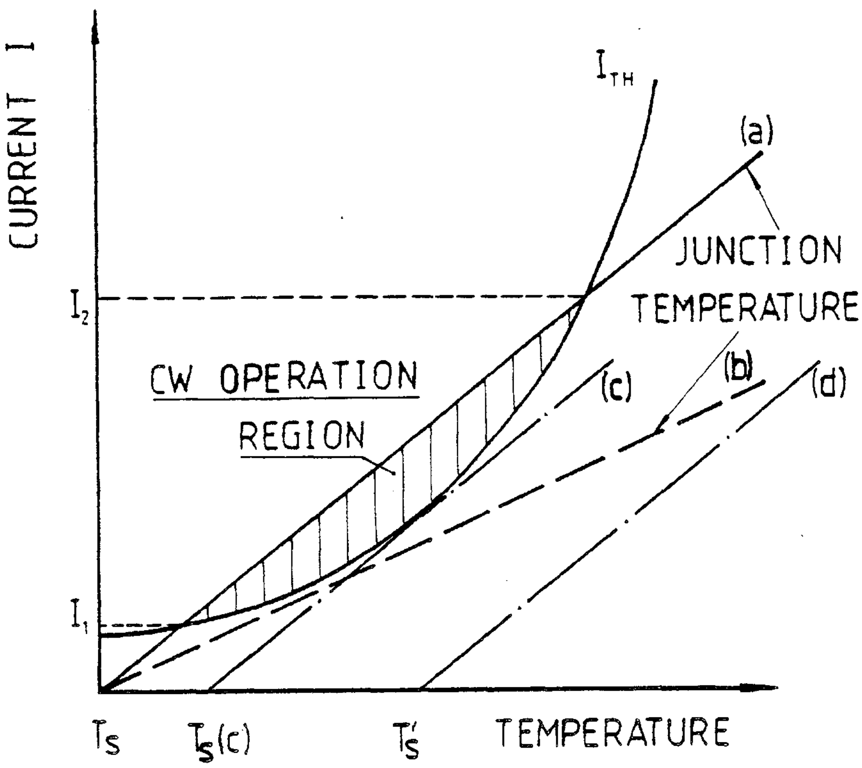

Fig. (4-2) The curve shows the threshold current dependence on the operational temperature of the active region. Straight lines (a) and (b) represent two different systems with different heat resistances; lines (a), (c) and (d) represent one system operating at different ambient temperatures T_s, $T_s(c)$ and T_s', respectively.

the diode laser threshold and its active region temperature. Lines (a) and (b) represent two different systems with different heat resistances operating at the same heat sink temperature T_s. The system with smaller heat resistance (line (a)) can oscillate CW when the injection current is between I_1 and I_2, while the system with larger heat resistance (line (b)) can not reach the CW threshold. Lines (a), (c) and (d) show one system operating at different heat sink temperatures T_s, $T_s(c)$ and T_s', respectively. When the heat sink temperature is larger than a certain temperature $T_s(c)$, the system can not oscillate continuously. From Fig. (4-2), it can also be seen that the diode laser, represented by line (a), starts to lase at current I_1. When the injection dc current is increased, the laser will give more output power. After passing through a maximum level, the output power begins to decrease with increasing injection current due to the thermal influence. Another point I_2 is reached when the system stops oscillating. This situation is more clearly shown in Fig. (4-3) where the threshold is plotted as a function of the injection dc current which changes the temperature of the active region which in turn alters the threshold current [13]. The laser does not turn on at current I_s, the threshold current if the temperature of the active region is equal to the ambient temperture T_s, because the injection current heats the active region. The laser turns on at current I_a when the current itself begins to exceed the threshold current I_{th}. The upper part of Fig. (4-3), which is proportional to $(I-I_{th})$ and therefore related to the output, passes through a maximum at current I_m. Above I_m the threshold current increases with injection current more rapidly than the current itself and the system ceases to oscillate at current I_b, where the threshold current again exceeds the applied current.

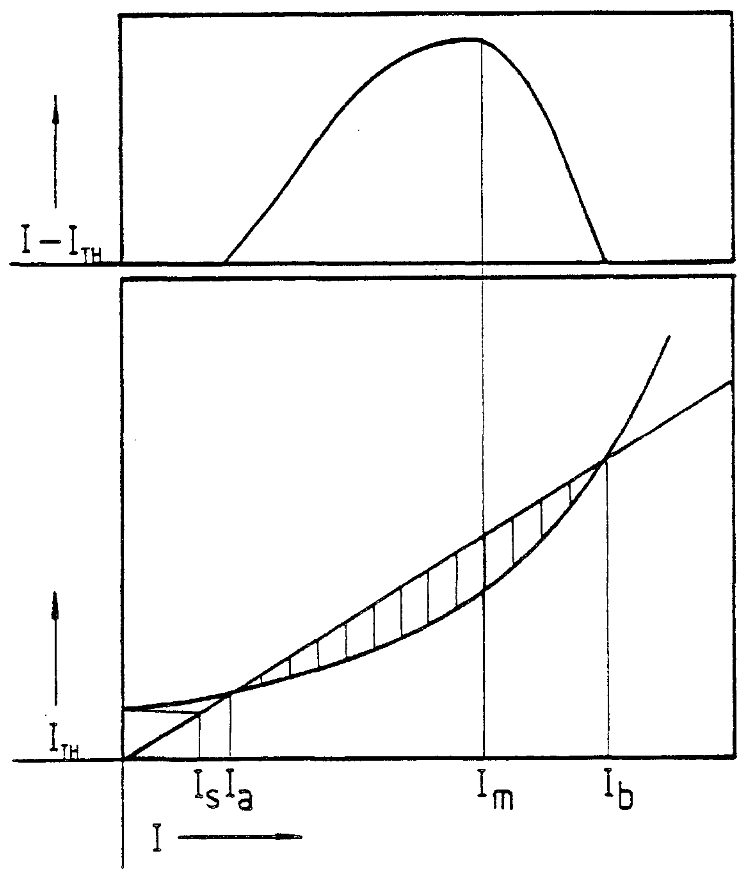

Fig. (4-3) Laser threshold and output vary with the injection dc current.

The output from one Brewster-angled diode laser has been measured at different injection current levels. Due to the large heat resistance of the diode mount chosen to obtain this curve, the diode did not oscillate under dc injection but lased under ac/dc injection conditions. The output power versus dc injection current, at fixed ac injection, is shown in Fig. (4-4). The light output/current input characteristic (L/I) of this Brewster-angled diode laser is featured by several points from A to E. From point A to point B, the system is below its threshold. Around point B, laser action begins, and between points B and C, the output increases almost linearly with the increase of the dc injection current. After point C, the output becomes a sublinear function of the dc injection current. Finally, point D is reached when the output is a maximum following which the output decreases as the injection current is increased. In fact, when the Brewster-angled diode was mounted on the heat sink with much smaller heat resistance, there existed a maximum on the spontaneous output versus dc injection current characteristic, as shown in Fig. (3-10) (see Chapter 3).

4.2.2. Dependence of the usable lifetime of the diode on its operational temperature

So far, only the effect of the operational temperature on the diode threshold and output has been discussed. The relationship between the operational lifetime of the diode and its temperature must also be considered. In 1975, Hartman et al [14] summarised their experimental results and deduced the following formula, which relates the diode lifetime to its operational temperature T,

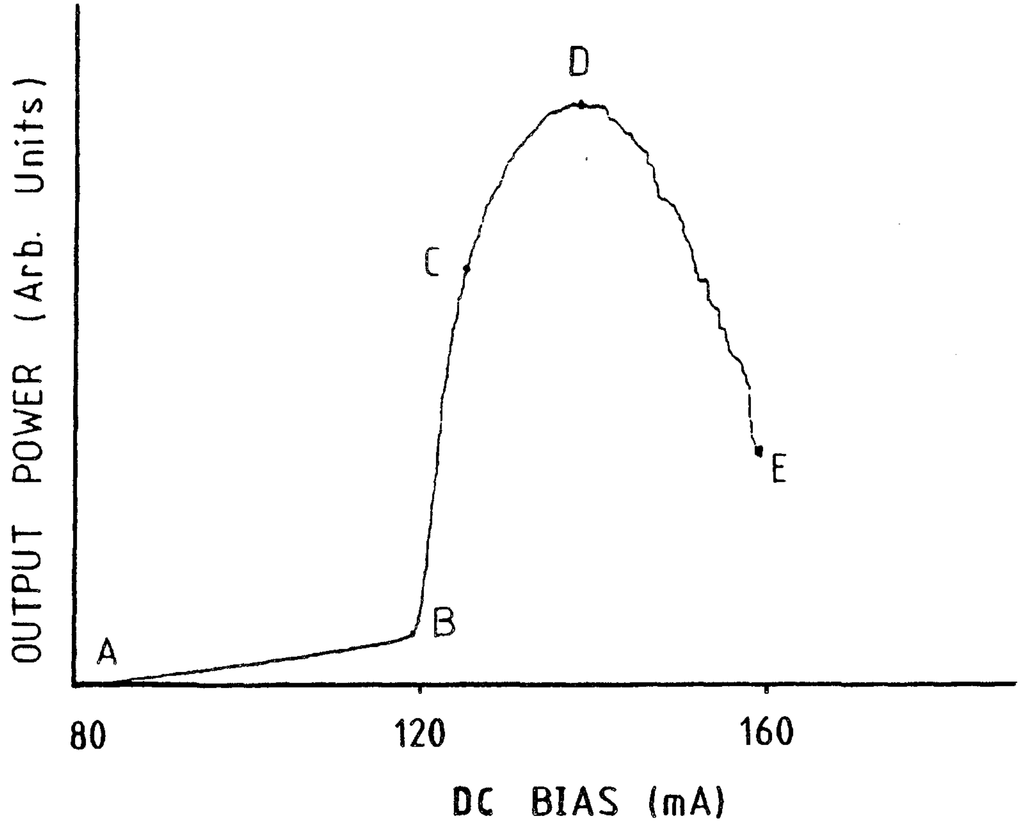

Fig. (4-4) Variation of output power of a Brewster-angled diode laser with injection d.c. current.

$$\tau(T) = C\exp[E_A/(kT)] \qquad (4\text{-}4)$$

where $\tau(T)$ is the diode lifetime when operating at an active region temperature of T Kelvin, C is a constant, k is the Boltzmann constant, and E_A is called "activation energy" of the diode. For those diodes tested by Hartman and his co-worker, the activation energy was measured to be 0.9±0.2eV. Kressel et al [15] measured their oxide-defined stripe-contact double heterostructure $Al_{0.3}Ga_{0.7}As$/ $Al_{0.08}Ga_{0.92}As$ diodes and found E_A to be 0.95±0.2eV. For an operational temperature T, the temperature increase ΔT_h which reduces the diode lifetime to half of that at T is derived from equation (4-4) as

$$\Delta T_h = kT^2\ln 2/(E_A - kT\ln 2) \qquad (4\text{-}5)$$

For E_A = 0.95eV, it can be calculated that the diode lifetime operating at 299.5k is half of that for operation at 294k. It thus becomes clear that keeping the operational temperature of the diode laser as low as possible is very important to achieve long lifetime. Attention will be paid in this chapter to minimizing the system heat resistance, especially by designing an appropriate diode mount.

Before discussing the diode mount, it is worthwhile to give a brief account of other factors by which the system heat resistance can be minimized. In this work various precautions were taken to keep the temperature rise of the active region as small as possible and the most important are described below.

(i) The diodes and their mounts were carefully cleaned before mounting. After laser operation, several diodes have been taken off their mounts and both diodes and mounts were checked under an optical microscope. It was observed that the indium solder, used to bond the diodes to their mounts, covered the tops of the mounts and the p-sides of the diodes acceptably, although some voids were evident, these were within the allowable size suggested by Kobayashi et al [16].

(ii) Each diode was mounted with its p-side in contact with the mount. If the diode had been mounted with its n-side down, this would have introduced an extra heat resistance of 13K/W to the system. This estimation was made from a simple one-dimensional approximation [17] which predicted that the heat resistance of a layer of thickness d and cross-sectional area A is

$$R_h = d/(\sigma A) \qquad (4-7)$$

where σ is the thermal conductivity of the material with its weak dependence on the temperature being omitted. If a two-dimensional approximation [18] was used, the heat resistance would be larger with reference to the results of Joyce et al [18] who claimed that the heat resistance of their diode system was 82.9K/W when the diode was mounted p-side up compared to 20.6K/W when the p-side was down.

(iii) The thickness of the indium was carefully controlled. The indium sphere which was used to bond the diode to its mount had a diameter of 0.15mm, that is a volume of $1.8 \times 10^{-3} mm^3$. If the indium contained in one sphere spread homogeneously when molten and formed a layer which had the same area as that of the p-side of the diode ($0.15 mm^2$), the layer thickness would be 12μm. According to Manning's figure [19], for his oxide-defined stripe-geometry diode of stripe area $8 \times 200 \mu m^2$, an indium layer of 10μm thickness had a heat resistance of 10K/W and so it could be expected that for the diode used in this work, which had a stripe area of $18 \times 500 \mu m^2$, the 12μm thick indium layer would have a heat resistance below 10K/W.

4.3. Design of Diode Mounts

Besides the points mentioned in section 4.2, the diode mount also played an important role in diode operation. Owing to the special shape of the Brewster-angled diode used in this work, attention was inevitably drawn to the design of the diode mounts which satisfied the working conditions of the Brewster-angled diodes. During this investigation the five types of mount that were constructed and tested shared several common features. Firstly, the dimension of the surface of the mount in contact with the diode was made 10 to 20μm shorter than the diode length (500μm). Lynch [20] pointed out the poor light output/injection current characteristic of the diode with an unbonded region ranging from 5 to 20 per cent, but in this case, the unbonded region was 2% or less at each side. Moreover, the heat problem arising from the unbonded areas at both sides of the diode was partly alleviated by the surplus indium stuck to the p-side of the diode outside the mount during the mounting process. With this overhang of $< 10\mu m$ at each side of the diode it was ensured that the light from the diode facet could travel without obstruction to the neighbouring optical components. The thermal singularity reported by Lynch [20] has not been observed in this work at least for the injection level of $1.4I_{th}$. Secondly, the top surfaces of these mounts were polished but did not have a gold layer because it was decided [18] that a gold-plated heat spreader is thermally unnecessary. Indeed, initial experiments with a diode mounted on the diode mount type DM1, which will be discussed later in this section, showed no observable change whether the top surface was gold plated or not. Thirdly, no special expansion coefficient matching material such as BeO [21] was sandwiched between the diode and its mount top to avoid stress. This was because the soft solder material, indium, was used to bond the laser to its mount.

The five different diode mounts, referred to as DM1 to DM5, respectively are depicted in Figs. (4-5 a to d) and (4-6). In Fig.(4-5), four different diode mounts which were

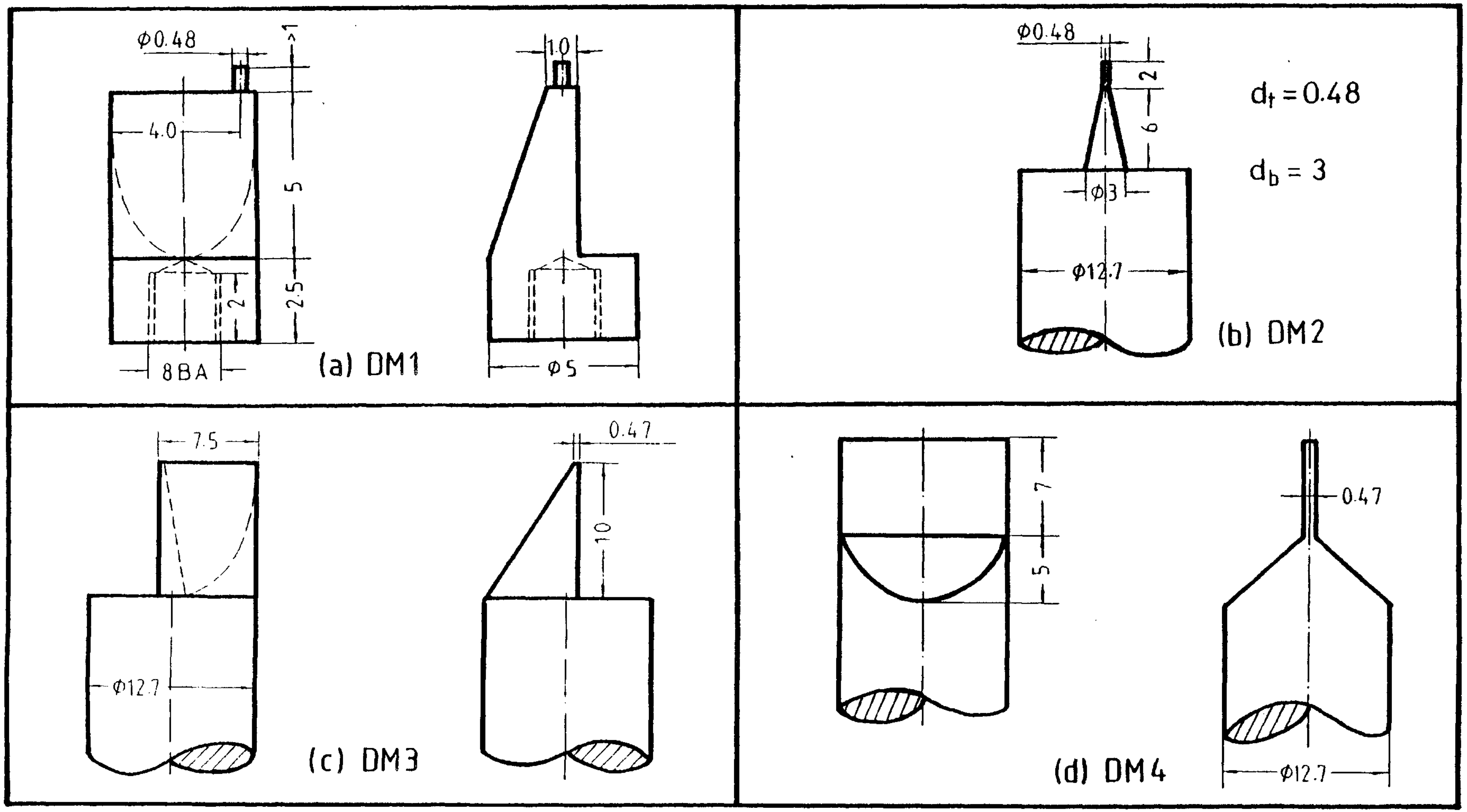

Fig.(4-5) Four diode mount designs DM1 to DM4 (dimensions in mm).

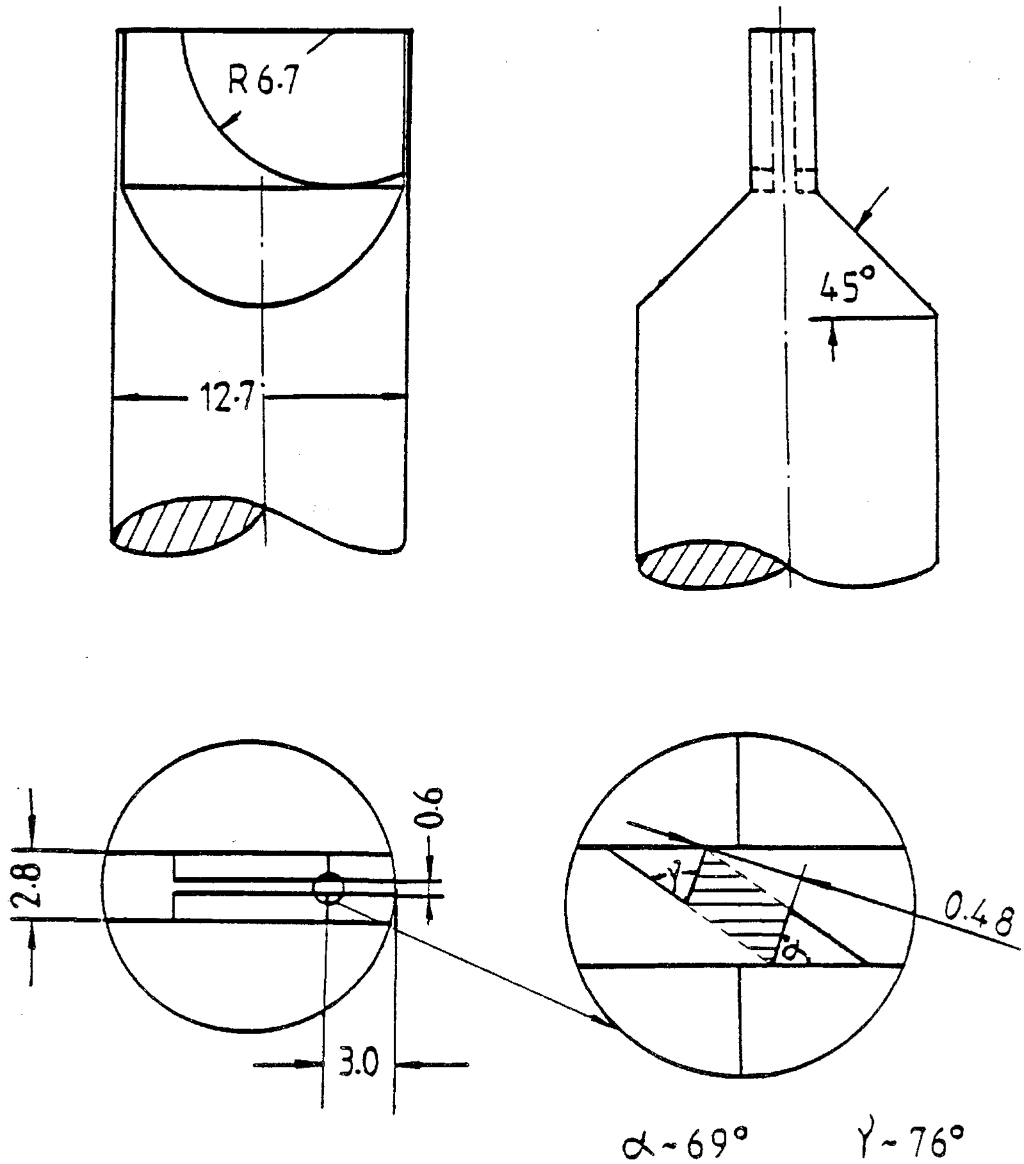

Fig. (4–6) Diode mount of type DM5, used to conduct most experiments reported in this thesis.

precursors to the final version are shown, and will be judged from the thermal viewpoint later. Fig. (4-6) shows the final version of the diode mount, DM5, which has been used in most of the experiments reported in this thesis. With the dimensions of these mounts as indicated, it is possible to assess their quality by evaluating their heat resistances using either one-dimensional approximation adopted by Dyment et al [17] or with reference to the results obtained by Joyce et al [18] from the two-dimensional approximation. Both approximations will be used in this section to find the heat resistances of the mounts, and the predictions will be compared with the experimental observations.

Preliminary calculation using the one-dimensional approximation with the figures given in Figs. (4-5) and (4-6), shows that the heat resistance of these mounts can be primarily attributed to the upper parts of the mounts. The heat resistance of the bottom parts of these mounts, a cylinder of $\sim$12.7mm in diameter and $\sim$50mm in height, is less than 1K/W for copper and 4K/W for brass. Attention is, therefore, concentrated on the upper parts of these mounts.

4.3.1. Diode mount type DM1

This type of mount was the early version used in initial experiments. Only a few diodes from this batch were mounted on this type. DM1 can be used in cavity type

C1 (see section 5.3) with the slope side of the mount facing the spherical mirror, while the other side (which is accessible to the microscope objective) facing the flat mirror. The small stud of DM1 was soldered on to the mount with tin solder at a temperature higher than the melting point of the indium before the diode was mounted. The bottom part of the mount (not shown in Fig. (4-5a)) is a cylinder of ∿12.7mm in diameter and ∿50mm in height. the upper part of the mount head is a cylinder of diameter ∿0.48mm and length >1.0mm. According to equation (4-7), this brass stud has a heat resistance in excess of 55K/W and the other part of the mount head, made of copper, contributes a heat resistance of ∿3K/W. When the bottom brass part of the mount is included, DM1 has a heat resistance $R_h(1)$ ∿62K/W. Replacing the circular stud with a 480x480μm^2 square stud, the two-dimensional approximation predicted a heat resistance of this "square stud" to be ∿48K/W compared to 55K/W given by equation (4-7). Because the cross-sectional area of the square stud is bigger than the circular counterpart its heat resistance will be lower and so it can be concluded that the circular stud would have a heat resistance larger than 48K/W. Therefore, 55K/W will be used as the heat resistance of the circular stud, and in later discussions $R_h(1)$ ∿62K/W will be used. When diodes were mounted on DM1 they could oscillate under dc injection conditions. The average threshold, from 4 diodes on DM1, was 177mA in an external cavity configuration type C1. Because this cavity is asymmetric, attempts were made to acquire accessibility to both sides of the Brewster-angled diode by the microscope objectives in order to configure different types of symmetric external cavities. This stimulated the construction of diode mount type DM2.

4.3.2. Diode mount type DM2

The shape and dimension of DM2 are shown in Fig.(4-5b), the main advantages of this diode mount are: accessibility of the microscope objectives to both sides of the Brewster-angled diode; convenience of rotating the diode axis to a desirable direction; fabrication from a solid block rather than multiple fitted metal components. Unfortunately, DM2 had a very high heat resistance because it was made of brass to overcome the poor rigidity of copper.

The upper part of the mount, composed of a cylinder and a sub-base, possesses a heat resistance of $\sim$163K/W according to the one-dimensional approximation [17] which suggests that the heat resistance of the brass rod is

$$R_h'(2) \sim 4l/(\pi \sigma d_t^2) \sim 110 \text{ K/W} \qquad (4\text{-}8)$$

and that of the brass sub-base is

$$R_h''(2) \sim 4\int_0 \{\pi\sigma[d_t-(d_b-d_t)y/h]^2\}^{-1}dy$$
$$\sim 53 \text{ K/W} \qquad (4\text{-}9)$$

This figure is larger than the characteristic temperature T_o of 110K of the diode. With the method due to Joyce et al [18], the estimated heat resistance of the rod, again using the "square stud" as adopted in the previous sub-section, is larger than 100K/W, slightly smaller than that given in equation (4-8). For the same reason as mentioned in the preceding sub-section, a value of $R_h(2)$ of 164K/W will be used later. Of the thirteen Brewster-angled diodes that had been mounted on this type of mount, only one of them was observed to oscillate under dc injection conditions (with a threshold of 220mA), while five could not lase with dc injection but could oscillate under dc/ac injection conditions at room temperature. It was observed that, as shown in Fig. (4-4), about 10 to 20 mA extra dc current increment above the "threshold" would severely affect the lasing action. Seven of them did not lase at room temperature whatsoever. Moreover, it was observed that when the dc injection current was increased to about 210 to 240mA (without ac injection) the spontaneous emissions of these Brewster-angled diodes on DM2 began to decrease with increasing current, probably due to thermal effects. This indicated that the temperature rise caused by increasing the current raised the threshold current by more than in the current supplied, and in this case, the CW threshold at room temperature could not be achieved.

4.3.3. Diode mount type DM3

The approach of making the diode mount from one solid block was applied to the design of diode mount DM3, as shown in Fig. (4-5c). This type of mount, made of copper, only served as the first step towards the construction of diode mount DM5. Its heat resistance was estimated [18] to be in the range from 13 to 15 K/W; the value of 14(K/W) will be used in later discussions. It suffered from the shortcoming of less manoeuverability and, therefore, could only be used in cavity type C1. Only one Brewster-angled diode was mounted on DM3, and it had a threshold of 150mA operating in external cavity type C1.

4.3.4. Diode mount type DM4

Diode mount type DM4, as shown in Fig. (4-5d), was specially made for the diode to be accessible by the microscope objectives from two opposite directions. The heat resistance along the vertical direction according to the formula used by Dyment et al [17]

$$R_h(4) \sim \ln(4l/s)/(\sigma\pi l) \qquad (4\text{-}10)$$

is 7.5(K/W) for l=480μm and S=18μm. Using Joyce's method [18], $R_h(4)$ ranges from 10.4 to 11.4 K/W. Taking the bigger of the heat resistances given by these two methods, $R_h(4)$ =11K/W will be used for later discussions.

If the power dissipated in the diode was 0.3W (for I=200mA and a junction voltage of 1.5V), and neglecting the optical power, it could be estimated that with diode mount DM4 the temperature of the active region might increase by 3.3K. Six diodes had been mounted on DM4, and the average dc threshold was 159mA at room temperature. Because the geometric shape of the top of the mount was different from that of the Brewster-angled diode, extra uncontacted area in the stripe region was introduced in addition to that due to the diode overhang (< 20μm), and some difficulty was encountered in positioning the diode on the top of the mount. In order to overcome the drawbacks of DM4, it was decided to further refine the mount design as described in section 4.3.5.

4.3.5. Diode mount type DM5

The diode mount type DM5 is illustrated in Fig. (4-6). This type of mount retained the good thermal characteristics of DM3 and DM4 and easy accessibility by the microscope objectives from two opposite directions of DM4. The optimized matching of the geometric shapes of the diode and the mount top ensured that the total unbonded area was less than 20μm as on diode mounts DM1, DM2 or DM3 and greatly simplified the process of positioning the diode on the mount. (Most results presented in this thesis were obtained on this type of mount).

The heat resistance can be estimated, as in the case of diode mount DM4, to be 11K/W and this figure is used in the following discussions. The dc performance of eleven Brewster-angled diodes mounted on headers of DM5 has indicated that the average current threshold was 155mA when operating in external cavity configuration of type C2 (see section 5.3). This was slightly higher than that of the ordinary zero degree diode lasers (141mA) inferred from Aspin's results [22]. This might result from the higher losses of the external cavity configurations used in this work and extra losses introduced by the Brewster-angled diode itself. The lowest dc threshold of these diode lasers was 130mA when operating in configuration C2.

4.3.6. The effect of different mounts on diode laser thresholds

In the preceeding sections, it has been shown that the average dc thresholds of the Brewster-angled diode lasers were 177mA for DM1 (designated $I_{th}(1)$), $I_{th}(5)$ = 155mA and $I_{th}(4)$ = 159mA, while the lowest thresholds were 160mA (denoted $I_{th}(1,1)$), I_{th} (5,1)=130mA and $I_{th}(4,1)$ =137mA.

The threshold of 220mA, obtained from the only one diode which lased CW when mounted on DM2, could perhaps be regarded as $I_{th}(2,1)$. Only one diode was mounted on DM3; therefore, its threshold of 150mA will not be used for comparison.

Taking the heat resistance of the system (apart from the diode mount) as 35K/W (which is reasonable compared to the results obtained by Manning [19]) and other parameters as follows, heat sink temperature T_s=294K, diode characteristic temperature T_o=110k, junction voltage V=1.46V for λ=850nm, then it can be calculated, from equation (4-2) that the temperature of the active region at average threshold was T(1) = 319K for DM1, T(4) = 304.7k for DM4 and T(5) = 304.4K for DM5. (The number after the decimal point, for T(4) and T(5) was retained to show that they were practically the same). From equation (4-3), the ratio of the laser threshold for DM1 and DM5 at T_s = 294K is $I_{th}(1)/I_{th}(5)$ = 177/155, which is identical to the experimental result. The ratio of $I_{th}(4)/I_{th}(5)$ should be 1 because diode mounts DM4 and DM5 had the same heat resistance, and the experimental result of 159/155 is in good agreement with this expectation.

From equation (4-3), it can also be derived that

$$I_{th}(1) = I_{th}(5)\exp\{ \frac{VI_{th}(1)[R_h(1)+35]-VI_{th}(5)[R_h(5)+35]}{T_o} \} \tag{4-11}$$

and

$$I_{th}(2) = I_{th}(5)\exp\{ \frac{VI_{th}(2)[R_h(2)+35]-VI_{th}(5)[R_h(5)+35]}{T_o} \} \tag{4-12}$$

for the same heat sink temperature T_s. These two equations offer the possibility of comparing the thresholds of the same diode when mounted on diode mounts DM1, DM2 and DM5. From equations (4-11) and (4-12), using the values of the heat resistances predicted by theory and the experimental parameter 110K for T_o, and assuming that the voltage applied to the diodes remains constant (1.46V), the following table, Tab.(4-1), can be drawn up. From this table it can be seen that a diode with a threshold of 130mA when mounted on DM5 could lase CW when mounted on DM2 with a threshold of 208mA. However, for a diode with a threshold of 135mA on DM5, it is uncertain as to whether this diode could lase when mounted on DM2. If the reduction in the spontaneous emission occurs at the injection above 225mA (the figure shown in Tab.(4-1) for this diode to oscillate CW on DM2) this diode could lase under dc injection conditions, otherwise it can not lase CW at room temperature. In practice, in order to obtain the extrapolated threshold value, the injection current was usually increased by no less than 10mA higher than the threshold. For the diode of threshold 225mA, it was very difficult in practie to obtain its extrapolated threshold unless its output started to decrease at a current level 235mA. Moreover, some diodes could not oscillate CW when mounted on DM2, but had lased under ac/dc injection conditions when the thermal effects are partially alleviated.

It should be pointed out that the figures appearing in Tab.(4-1) were calculated from a very simple model, and therefore only provide an approximate guide. If the change of the voltage across the diode with injection current had

DM5($R_h(5)$=11K/W)		DM1($R_h(1)$=62K/W)		DM2($R_h(2)$=164K/W)	
$I_{th}(5)$ (mA)	Temperature rise $\Delta T(5)$ (^{o}k)	$I_{th}(1)$ (mA)	Temperature rise $\Delta T(1)$ (^{o}k)	$I_{th}(2)$ (mA)	Temperature rise $\Delta T(2)$ (^{o}k)
125	8.4	138.4	19.6	192.2	55.7
130	8.7	144.7	20.5	207.5	60.2
135	9.1	151.0	21.4	224.9	65.2
140	9.4	157.4	22.3	245.5	71.2
145	9.7	163.9	23.2	271.4	78.7
150	10.1	170.5	24.1		
155	10.4	177.1	25.1		
160	10.7	183.9	26.0		
165	11.1	190.7	27.0		
170	11.4	197.6	28.0		
175	11.8	204.7	29.0		
180	12.1	211.8	30.0		
190	12.8	226.5	32.1		

Table (4-1) Theoretical calculation of the diode threshold and temperature rise in the active region for different diode mounts.

been taken into consideration, the predicted currents from equations (4-11) and (4-12) would have been larger than those given. For example, if the diode series resistance is taken as 1 ohm [1], and suppose that the voltage corresponding to 130mA is 1.46V, then the voltage across the diode at 208mA should be 1.538V. Substracting the bandgap narrowing of 0.024V between temperatures 354K and 303K (according to the formula given by Blakemore [23] for GaAs), the voltage across the diode would be 1.514V. Substituting 1.514V into equation (4-12) results in a predicted threshold of 218mA instead of 207.5mA given in Tab. (4-1).

The thermally-induced termination of laser action has been made for one Brewster-angled diode mounted on DM5 by externally increasing the heat sink temperature. It was found that when this temperature was increased to 343K, the CW threshold of 270mA was barely recognisible from the light output/input current curve. Above this temperature the CW threshold could not be extrapolated for the diode tested. From equation (4-2), it could be estimated, using the experimental parameters, that the temperature of the active region was 364K (ie, 70K higher than the room temperature). This figure indicated that a diode which had a threshold of 135mA when mounted on DM5 might have been just able to oscillate CW if it had been mounted on DM2. In the latter case, the active region temperature would be 362K. The "run-off" temperature around 364K might have implied that a diode with a threshold larger than 135mA when mounted on DM5 would not oscillate CW when mounted on DM2, and accounted for the fact that only one diode was observed to operate continuously when mounted on DM2. The spontaneous emission was observed to decrease at current levels in the range 210 - 240mA when the diode was mounted on DM2. At 230mA, the temperature of the active region could be calculated from equation (4-2) to be 363K which was, practically, equal to the inferred "run-off" temperature (364K) of the diode tested.

4.4. Diode Mounting Techniques

During the mounting process, several procedures were found to be of basic importance. For instance, each diode was initially examined using an optical microscope (magnification x 200). There were a few diodes which were not acceptable because they had part of their stripes missing.

After the examination of their visual appearance, the diodes were cleaned carefully at elevated temperatures using recommended solvents. This ensured that the stripe area could be wetted by the molten indium, so that a void-free indium layer could be created between the p-side of the diode and the top surface of the mount.

Two indium pellets have never been used because this avoided any unnecessary increase in the heat resistance of the system.

When the cleaned diode was transferred onto the diode mount, particular attention was paid to avoiding direct contact with either facet of the diode.

After the diode was positioned appropriately on the mount, a piece of printed circuit board was attached to the top of the mount near the diode. The short contact between the post and the driving circuit was composed of several fine wires in order to minimize electrical skin effects. A piece of gold foil was used to connect the n-side of the diode to the contact. The gold foil was configured so that it would not obstruct the light emitted from the diode. In Fig.(4-7), a diode mounted on DM5 is illustrated.

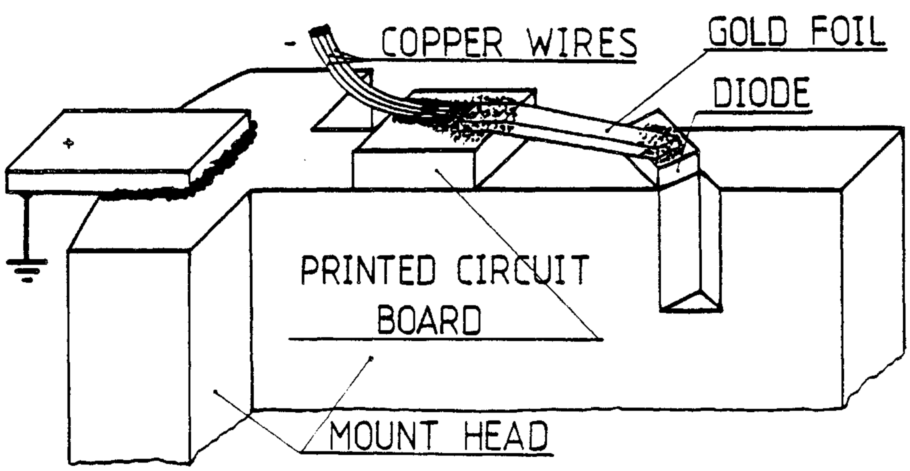

Fig. (4-7) The mounted Brewster-angled diode on its heat sink (DM5).

4.5. Electrical Connection to the Diode

In this section, a brief description of the electric driving circuit of the Brewster-angled diode will be given. The driving circuit used in this work is shown in Fig. (4-8).

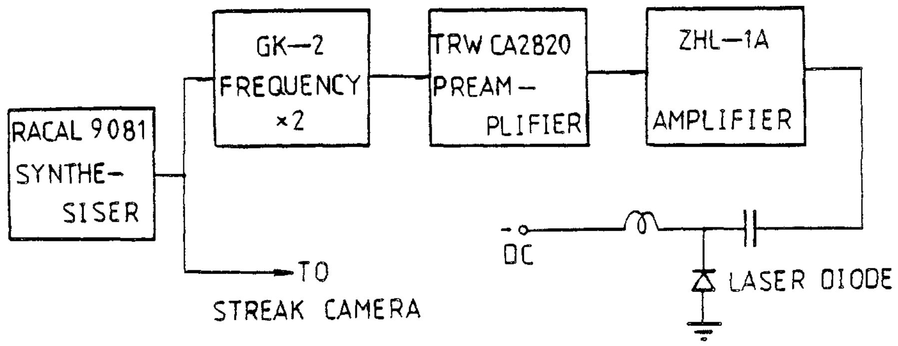

Fig. (4-8) Typical electrical driving circuit for the diode laser.

In an effort to boost the ac power injected into the diode, some workers have used a standard 47Ω resistor in the driving circuit so that the impedance of the diode system could approximately match the other electrical equipment. This is because the typical series resistance of the stripe diode was around 1 ohm [1]. However, the inclusion of a 47Ω resistor did not appear to be beneficial in this work, partly because the amplifier used was not seriously affected by the power reflected from the diode system and partly because the modulation frequencies used were not very high (< 500MHz). On the contrary, a series resistor introduced some additonal heat problem in the diode operation. About 1.9W (for I=200mA) would be converted into heat energy in the 47Ω resistor and some of this heat would reach the diode system. Consequently, in this work, no series resistor was used to match the diode system with the 50Ω impedance of the external electrical device.

4.6. Conclusions

In order to couple the Brewster-angled diode into different external cavity configurations, a specialised diode mount DM5, having good thermal, electrical and optical properties, has been designed and constructed through a series of refinement phases. Experimental observations have shown that the Brewster-angled diode mounted on this type of heat sink and positioned in an external cavity had an average dc threshold of 155mA at an ambient temperature of 294K; the lowest threshold obtained was 130mA for a diode having an oxide-defined stripe area $9\times10^{-5}cm^2$.

The variation of threshold current as a function of the heat sink temperature T_s, (measured for a Brewster-angled diode oscillating in an external cavity), has been plotted and the curve fitted to the relationship of $I_{th}(T)\propto\exp(T/T_o)$ for the temperature range of 294-343K. The characteristic temperature T_o of the Brewster-angled diode has been found to be 112K compared to 107K obtained from a zero degree laser. These figures, together with the theoretically predicted heat resistances of various diode mounts and the average heat resistance of the system (excluding the diode mount) taken as 35K/W, have been employed to give a reasonably good explanation of the experimental observations.

With the completion of the external cavity system incorporating the Brewster-angled diode, the frequency-tunable mode-locked semiconductor injection laser can be investigated and the experimental results will be presented in the following chapters.

References

[1] H. Kressel, J. K. Butler, "Semiconductor Lasers and Heterojunction LEDs", Academic Press, (1977).

[2] R. N. Hall et al, Phys.Rev.Lett., Vol. 9, 366 (1962).

[3] M. I. Nathan et al, Appl.Phys.Lett., Vol. 1, 62 (1962).

[4] T. M. Quist et al, Ibid, Vol. 1, 91 (1962).

[5] H. Kressel, H. Nelson, RCA Rev., Vol. 30, 106 (1969).

[6] M. B. Panish, I. Hayashi, S. Sumski, IEEE J.Quantum Electron., Vol. QE-5, 210 (1969).

[7] I. Hayashi, M. B. Panish, P. W. Fog, Ibid, Vol. QE-5, 211 (1969).

[8] Zh. I. Alferov et al, Sov.Phys.Semicond., Vol. 3, 1107 (1970).

[9] J. I. Pankove, IEEE J.Quantum Electron., Vol. QE-4, 119 (1968).

[10] N. K. Dutta, R. J. Nelson, Ibid, Vol. QE-18, 871 (1981).

[11] G. H. B. Thompson, "Physics of Semiconductor Laser Devices", John Wiley and Sons, (1980).

[12] C. H. Gooch, IEEE J.Quantum Electron., Vol. QE-4, 140 (1968).

[13] R. W. Keyes, IBM J.Res.Develop., Vol. 15, 401 (1971).

[14] R. L. Hartman and R. W. Dixon, Appl.Phys.Lett., Vol. 26, 239 (1975).

[15] H. Kressel, M. Ettenberg, I. Ladany, Ibid, Vol. 32, 305 (1978).

[16] T. Kobayashi and G. Iwane, Jpn.J.Appl.Phys., Vol. 16, 1403 (1977).

[17] J. C. Dyment, J. P. Ripper, T. H. Zachos, J.Appl.Phys., Vol. 40, 1082 (1969).

[18] W. B. Joyce, R. W. Dixon, Ibid, Vol 46, 855 (1975).

[19] J. S. Manning, Ibid, Vol. 52, 3179 (1981).

[20] R. T. Lynch, Jr., Appl.Phys.Lett., Vol. 36, 505 (1980).

[21] E. Duda, J. C. Carballes, J. Apruzzese, IEEE J.Quantum Electron., Vol. QE-15, 812 (1979).

[22] G. J. Aspin, J. E. Carroll, R. G. Plumb, Appl.Phys.Lett., Vol. 39, 860 (1981).

[23] J. S. Blakemore, J.Appl.Phys., Vol. 53, R123 (1982).

Chapter 5

FREQUENCY-TUNABLE BREWSTER-ANGLED DIODE LASERS

5.1. Introduction

In this chapter, the construction and performance of a frequency-tunable Brewster-angled diode laser with different external cavity configurations are described. The output wavelength was continuously selected with an intracavity etalon or grating reflector. The spectral characteristics of this laser under dc injection conditions will be presented and the origin of some relevant features of the tuning curves will also be explained.

5.2. General Remarks on Frequency-Tunable Semiconductor Lasers

There are several methods by which semiconductor lasers can be tuned, but basically, these methods can be divided into two categories. One is "coarse tuning", which is fulfilled by selecting appropriate constituent materials with different bandgap energies, and this provides a wide range of laser wavelengths [1]. Obviously, the compositional tuning gives a "wavelength range" choice, and so it only provides a coarse tuning.

The other category is "fine tuning" which makes it possible for the output wavelength from a laser to be changed by the amount which is comparable to the laser output linewidth, and the tuning technique is applied to each individual laser. Therefore, the term "frequency tuning" is mainly referred to this category throughout this chapter.

Frequency-tuning can be achieved without intracavity tuning elements. The simplest method used to alter the output wavelength is to change the diode laser bias current. Adjustments in bias current lead to changes of the injection carrier density, which in turn induce the refractive index change of the laser material [2,3,4,]. Also, current-induced temperature change in the material will alter the optical length of the diode. All these changes are related to the optical length of the cavity through which the passive cavity modes are determined. In a real laser system, not only should the passive cavity properties be considered, but the properties of the active medium must also be taken into account. As pointed out in reference 5, the two relevant factors affecting the lasing energy $h\nu_L$ are: the bandgap shrinkage and induced bandtail formation which depress $h\nu_L$; and secondly, the filling of the conduction band with electrons and the valance band with holes, an effect which tends to increase $h\nu_L$.

Sometimes, the frequency tuning is studied in terms of the operational temperature. Kressel et al [5] have indicated that the energy shift of the peak laser emission is

$$d(h\nu_L)/dT = -0.45 meV/K \qquad (5-1)$$

Kishino et al [4] suggested that above laser threshold, the carrier density was clamped at the threshold level and therefore it could be expected that thermal effects induced by the injection current would be mostly responsible for the observed shift in the laser wavelength. A conventional zero degree diode laser made by STL (Standard Telecommunication Laboratory) under the same conditions as the Brewster-angled diodes used in this work has been studied. It was found, (see Fig.(5-1)), that for a fixed bias current (190mA), the lasing peak wavelength of the AlGaAs diode varied with the heat sink temperature by an amount

$$d\lambda_L/dT = 0.25 nm/K \qquad (5-2)$$

It follows therefore, that the lasing photon energy changed with the heat sink temperature at a rate of

$$d(h\nu_L)/dT = -0.43 meV/K \qquad (5-3)$$

Unfortunately, neither the bias current nor the heat sink temperature is an ideal parameter for affecting the change in wavelength. The injection current can only be changed

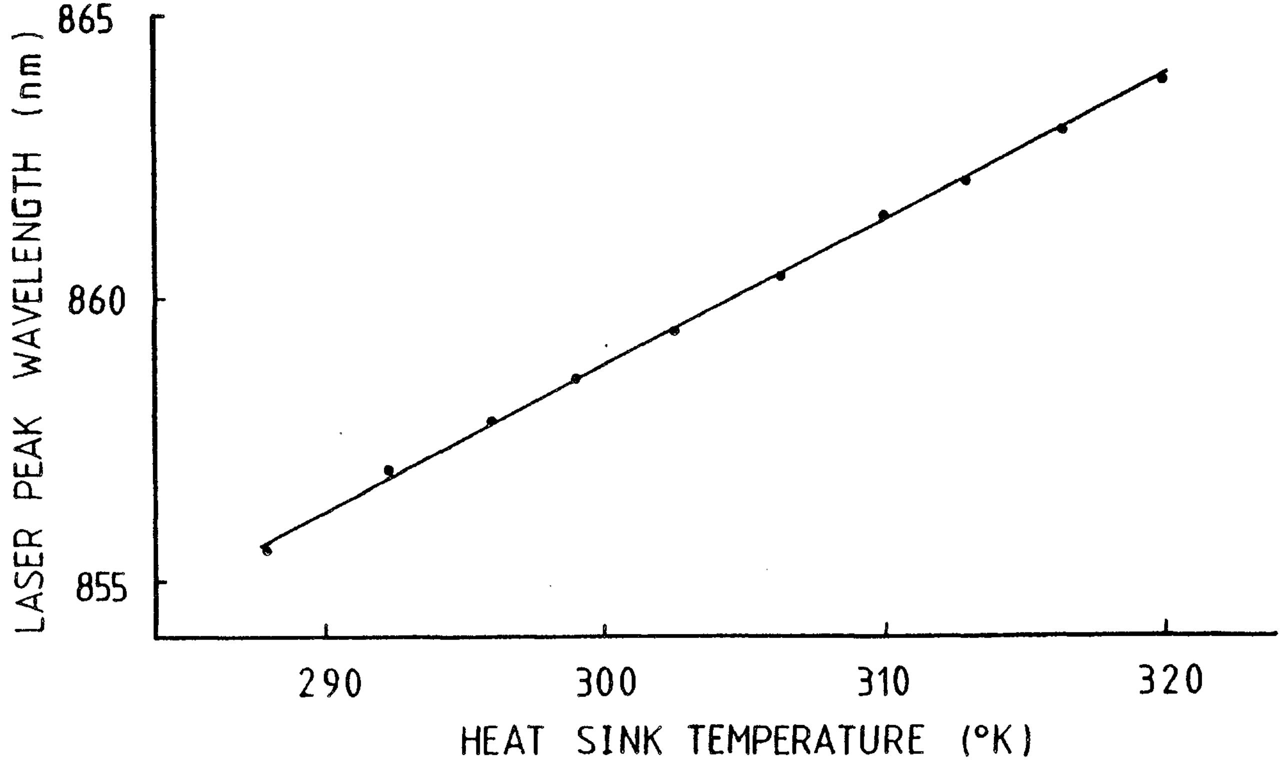

Fig. (5-1) The variation of the peak wavelength of a zero degree diode laser (with the same composition as the Brewster-angled diode) with the heat sink temperature.

within a limited range, from just above threshold to an upper limit which is dependent on the reliable operation and the acceptable span of lifetime. It is not easy to control the operating temperature and there is not much manoeuvrability in the upper side of the temperature scale without sacrificing the operational lifetime of the diode (see Chapter 4).

In contrast to this, the inclusion of intracavity tuning elements is a much simpler and more practical means of providing a frequency change. In external cavity semiconductor diode lasers, tuning elements can be inserted into the cavities and thereby the output wavelengths can be selected. Frequently adopted frequency-tuning elements include a grating reflector, which usually serves as an end mirror of the external resonator [6-10], a Fabry-Perot etalon [10,11], or a birefringent filter [12]. In this work, the two former elements have been employed.

5.3. Experimental Configurations of Frequency-Tunable Brewster-Angled Diode Lasers

Laser frequency-tuning experiments have been conducted in three external cavity configurations (shown in Fig.(5-2 a,b, and c)), which are referred to as cavity types C1, C2 and C3 respectively.

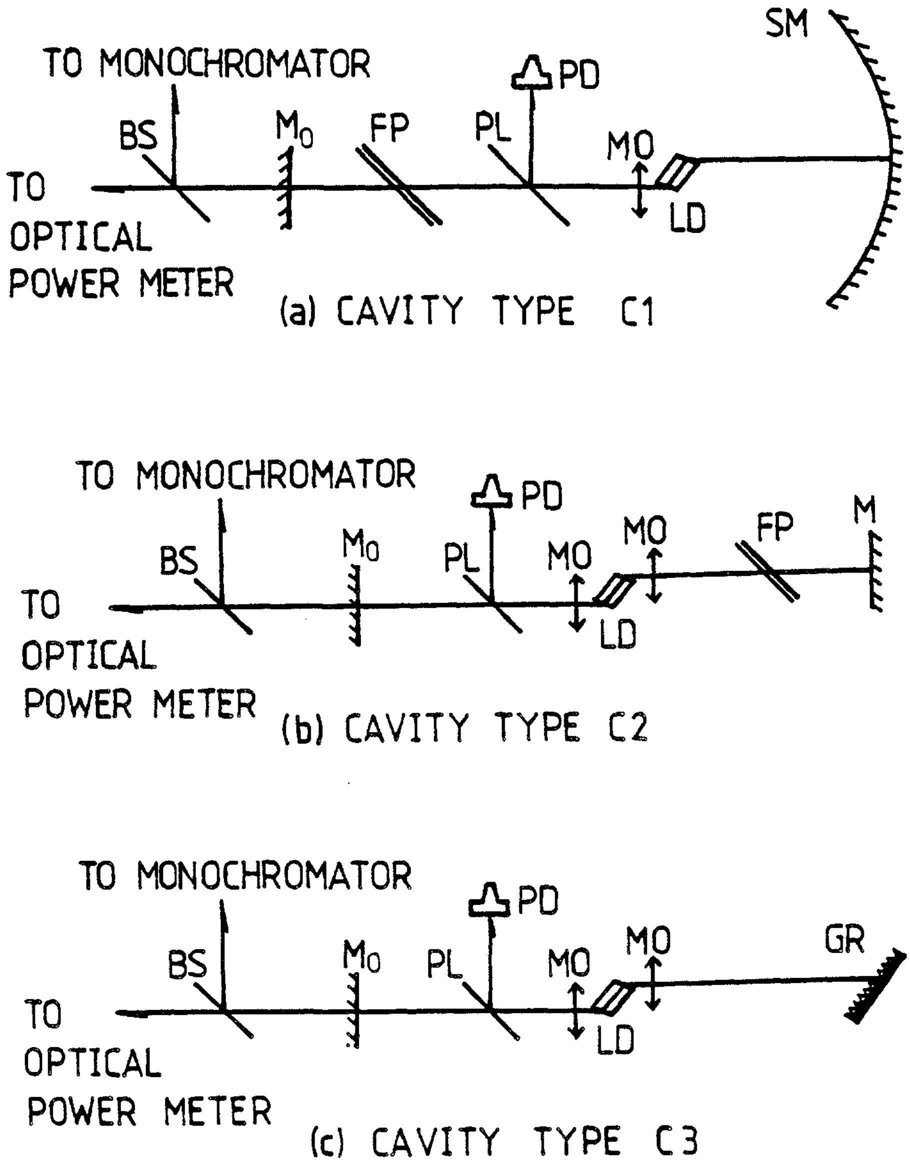

Fig.(5-2) Three different external cavity configurations used in frequency-tuning studies.

5.3.1. Cavity type "Cl"

Cl has a 100% reflectivity spherical mirror (SM) (radius of curvature of 50mm, diameter of 75mm), such that the angle subtended from the diode to the periphery of the mirror is 97°, which is much larger than the laser beam divergence angles that were measured to be 37° in the direction perpendicular to the junction plane of the diode and 9° in the junction plane. This resulted in negligible losses from this mirror. The output mirror (M_o) has a reflectivity of 75% in the spectral range from 830 to 870nm. A microscope objective (MO), with a magnification x20 and numerical aperture 0.5, was used to collimate the light from the diode and thereby the external cavity was constructed. This element (MO) was composed of three lens components, that is, six reflective surfaces, and introduced some extra loss into the cavity.

The alignment of the external cavity was considerably more difficult with a spherical mirror than with a microscope objective and a plane mirror combination [13]. Asymmetry was another primary feature of Cl in that losses at one side of the cavity (see Fig.(5-2a)) were much higher than at the other. These losses were introduced by the pellicle (PL) (inserted into the cavity to assist in the alignment), the Fabry-Perot etalon, the partially reflecting output mirror, and the microscope objective. This loss imbalance reduced the effectiveness of the amplifying medium. Some asymmetry was also due to different optical path lengths of the two sides of the cavity. The combination of these nonsymmetrical effects was expected to result in increased pulse duration when the laser was actively mode-locked. The round-trip time from the diode to the spherical mirror was 330ps so, as a result, the mode-locked pulse could be amplified once and attenuated once within each round-trip. The shortest pulse durations obtained from C1 were about 13ps.

5.3.2. Cavity types "C2" and "C3"

In C2, a microscope objective (MO) and a 100% reflection plane mirror (M) have been used to replace the spherical mirror in C1. C2 also included a Fabry-Perot etalon with an air gap of 10 μm and reflectivites of 65%. The free spectral range of this etalon was 36nm and its finesse was 7. In C3, a grating reflector of 1200 lines/mm has been used to replace the Fabry-Perot etalon and the total reflection mirror. Effort was made to distribute the cavity losses on both sides of the cavity in order to reduce the intensity difference between the two counter-propagating pulses which circulated inside the cavity (note that in C2 or C3, the modulation frequency has been set at twice the mode spacing of the external cavity) in the mode-locking regime. Meanwhile, the diode has been positioned in the middle of the cavity so that pulses reflected from both end reflectors of the cavity experienced gain when they collided within the active medium. It would therefore be expected that coherent "grating" effects would usefully contribute to the quality of the mode-locking as applied in the dye laser counterparts [14]. Another advantage of C2 and C3 over C1 was that the frequency-tuning element could be placed at the side of the active medium remote from the output mirror so that the tuning operation would not alter the output beam position.

All the microscope objectives in C1, C2 and C3, and the spherical mirror in C1 were mounted on x-y-z translation stages. Movement along any of these three directions was controlled by a micrometer (for coarse movement) and a piezoelectric device (for fine adjustment) which had a full range of 3μm for a drive voltage in the range 0-1000V. The plane mirrors were mounted on kinematically controlled mirror mounts which were fitted to the translation stages with a moveable range of 25mm along the axial direction. This made it possible to position the diode in the middle of the cavity.

In C2, the movement of the frequency-tuning element (Fabry-Perot etalon) could be rotated about the vertical direction, whereas in C3 the tuning element (diffraction grating) was mounted on an appropriate kinematic mirror mount. The rotational axis of the grating in the vertical direction was adjusted to intercept the laser beam in order to minimize the perturbance to the cavity length due to any rotational movement. This was useful for mode-locking operation which will be discussed in Chapter 6.

The pellicle directed <8% of the intracavity intensity onto a photodiode (SD-172) oscilloscope combination in order to monitor the alignment condition of the external cavity. The laser output was sub-divided in intensity by a beam splitter such that approximately 70% of the output was collected by the detector head of an optical power meter (Photometric Sensor Head Model 350 and Power Meter Model 44XL), while the remaining 30% was focused onto the input slit of a monochromator (Monospek 1000) which had an optimum resolution of 0.025nm. The light from the monochromator at the output slit was detected with a photomultiplier, which had an S20 photocathode, and this signal was supplied either to an oscilloscope or a chart recorder (Servogor XY 743) for measurement.

5.4. Characteristics of Brewster-Angled Diode Lasers

The light output vs injection dc current (referred to as the L/I characteristic) of a Brewster-angled diode laser is shown in Fig. (5-3). The threshold current of the laser was obtained by extrapolating the linear part of the L/I curve to the current axis. The system output with one reflector of the cavity blocked gave the spontaneous emission characteristic of the diode. Lasing action was

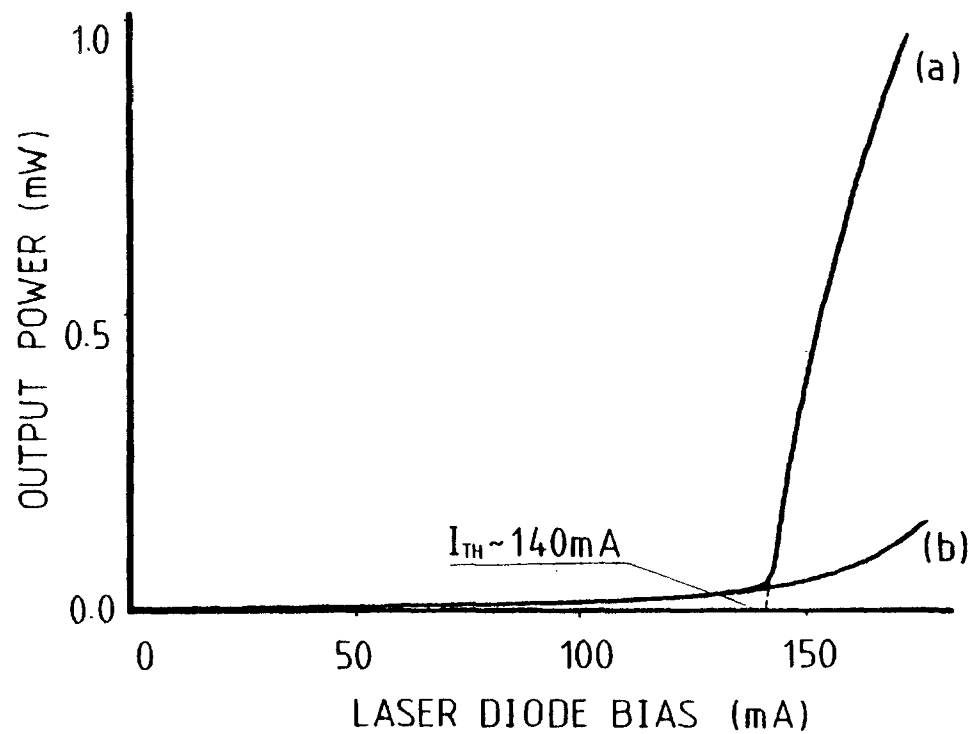

Fig.(5-3) Curves showing (a) the stimulated, and (b) the spontaneous outputs of the Brewster-angled diode as functions of the injection dc current.

also identified by the polarization measurement of the output and the accompanying spectral narrowing process. The polarization property of the output has been described in Chapter 3, Fig. (3-9).

The spectral development of the system output around the threshold is shown in Fig. (5-4). The current difference between two consecutive steps in the figure was $\sim$2mA ($\sim$1.3% I_{th}), and the extrapolated laser threshold was 157mA. At the threshold, the output spectral width was measured to be $\sim$5.6nm. The current difference between the threshold and the injection level ($\sim$163mA) at which the spectral width narrowed to $\sim$0.05nm was $\sim$6mA($\sim$4%I_{th}), which was well below the figure (10%) given by Kressel et al [5].

It is worthwhile to point out that the lasing spectrum evolved from a smooth, broadband characteristic. This is in contrast to the ordinary zero degree diode, in which the lasing mode(s) developed from the cavity modes, which were separated from each other by about 0.18nm for the cavity length of 500μm (see Fig.(3-11)), when the bias current was increased from below to above the extrapolated threshold. This confirmed that Brewster-angled diodes acted solely as the amplifying media and that the internal cavity effects had been suppressed.

In Fig. (5-5), a set of spontaneous emission spectra is presented for a Brewster-angled diode (recorded using a

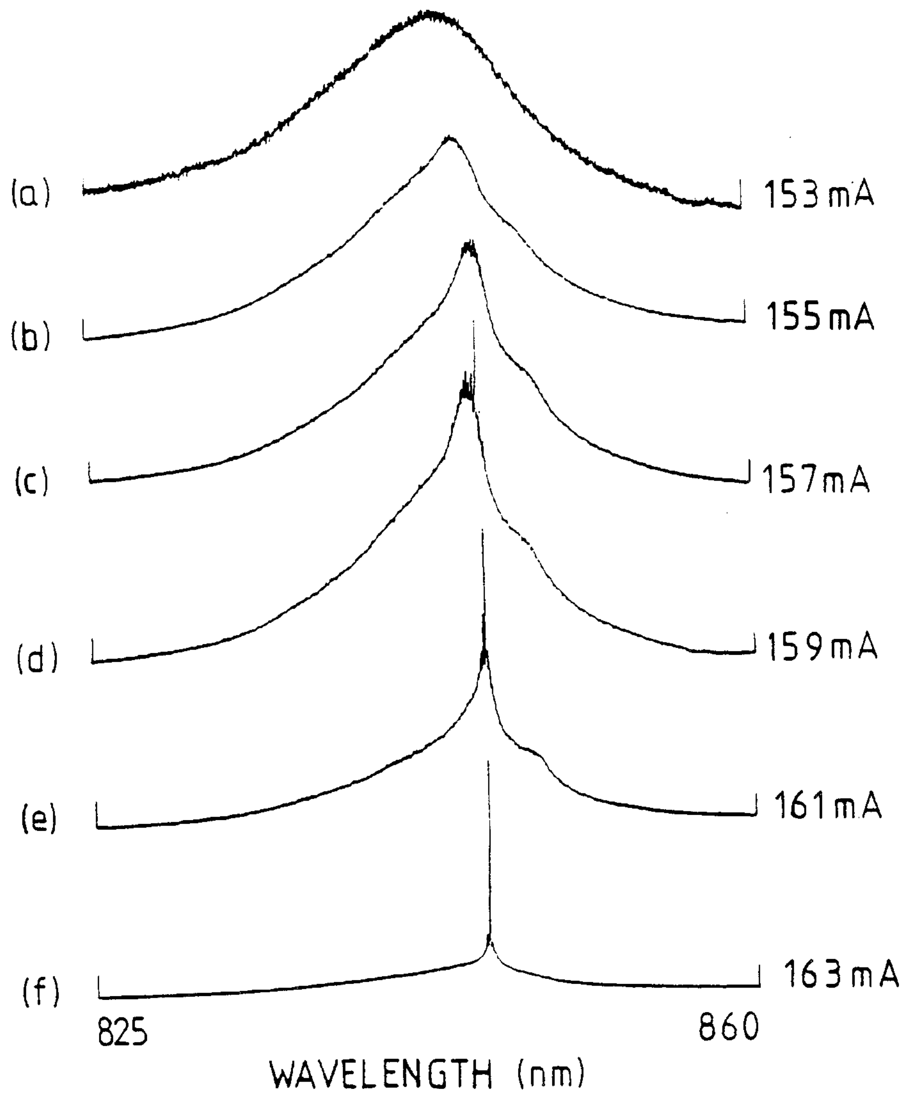

Fig.(5-4) Series of spectra showing the spectral development of the laser output from broad band spontaneous nature into narrow stimulated nature with increasing injection currents. I_{th}~157mA.

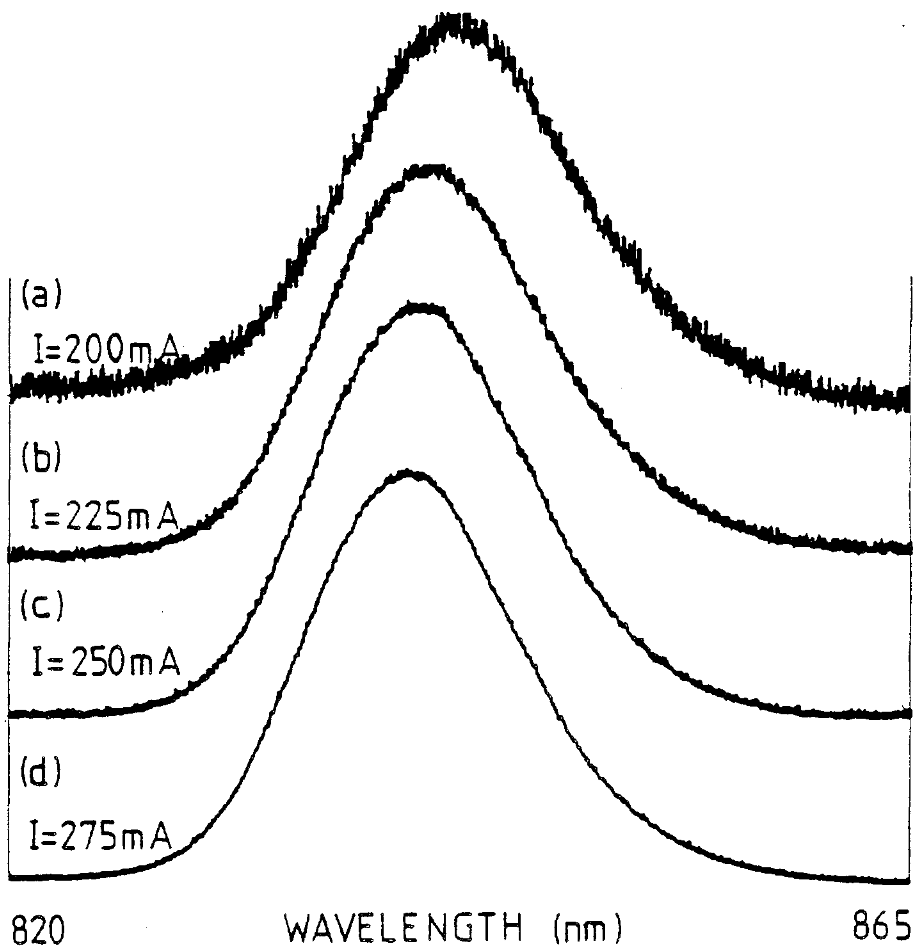

Fig.(5-5) Spontaneous spectra of a Brewster-angled diode at different levels of current injection.

chart recorder) at different injection levels. These curves show no evidence of lasing, even at injection currents as high as 275mA, which is approximately twice the threshold current when the external cavity was aligned. The peak wavelength of the spontaneous emission from the Brewster-angled diode shifted to the short wavelength side with increased bias currents while the spectral width remained almost unchanged. This indicated that the stronger pump produced increased separation of the two quasi-Fermi levels in the gain medium. Allowing for the red-shift of the peak wavelength due to the current induced temperature rise in the active region, the net effect of the wavelength shift with the injection current was towards the shorter wavelength side. In fact, the shifting of the peak wavelength towards the short wavelength side was one of the main features of the spontaneous emission [4,15]. In the lasing regime, however, because of the clamping-down of the separation of the quasi-Fermi levels, the temperature effect on the wavelength would dominate [4,15], and the output wavelength would be increased with stronger pumping. This situation is shown in Fig. (5-6) for different initial wavelengths from the same Brewster-angled diode laser. Increments of 0.15nm in wavelength are observed for the current increases of 30mA.

A typical spectrum of the stimulated emission from the Brewster-angled diode laser (in C2) is shown in Fig.(5-7).

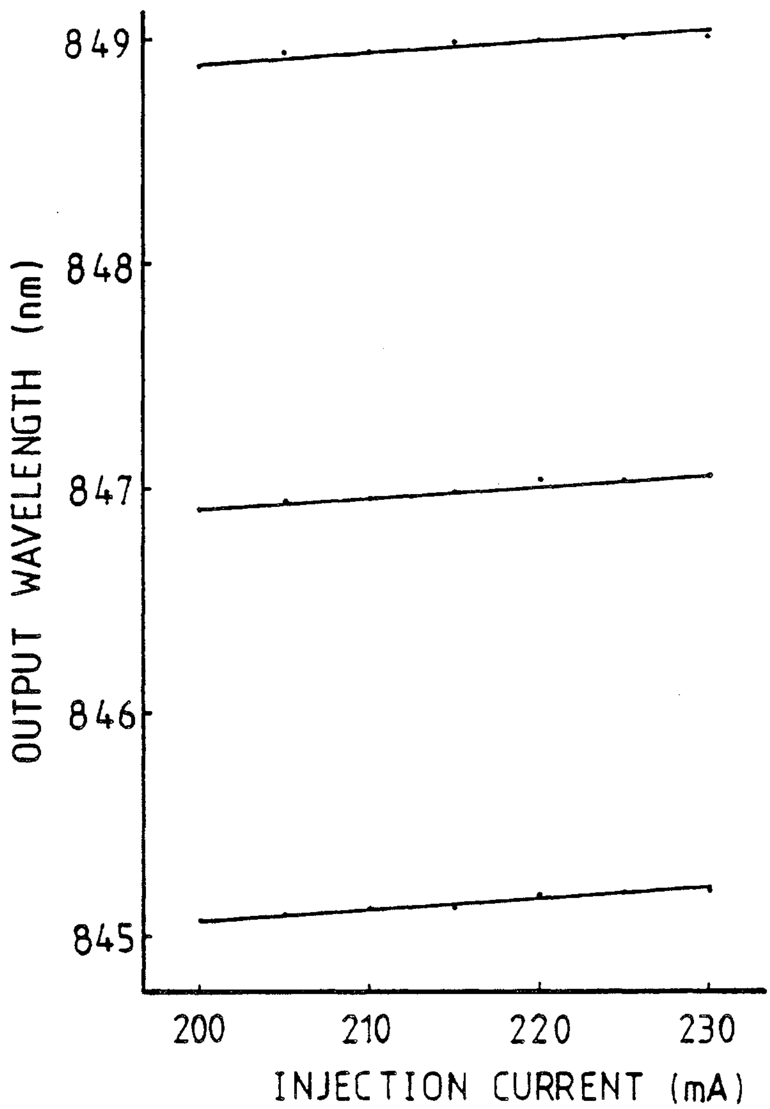

Fig.(5-6) Dependence of output wavelengths of a Brewster-angled diode laser on d c injection current.

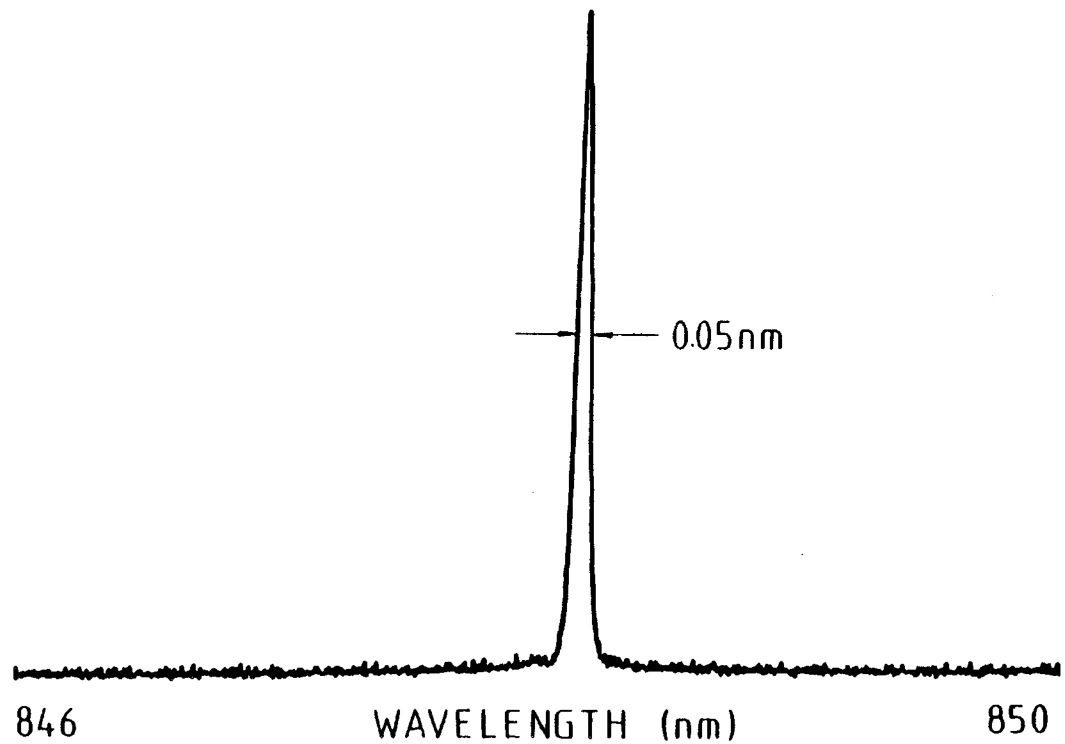

Fig.(5–7) Typical stimulated spectrum from a Brewster-angled diode laser (operating in cavity C2) with a spectral width ~ 0.05 nm.

There was no observed difference between the stimulated spectra from C2 and C3 laser arrangements. The spectral bandwidth was 0.05nm. For comparison, the spectra of both stimulated and spontaneous emission of a Brewster-angled diode (in C3), at the same bias current, are presented in Fig.(5-8). (The vertical scales are different for the two types of emission). It should be mentioned that due to the existence of the frequency-tuning element in the external cavity, the laser wavelength could be easily selected. In Fig. (5-4), the laser wavelength was tuned to the peak of the spontaneous emission while in Fig.(5-8) the system was aligned to oscillate at the longer wavelength side of the spontaneous emission spectrum.

The recorded stimulated spectral widths were larger than the resolution limit of the measuring system. This may have originated from the instability of the external cavity, because no special effort was made to stabilize the external cavity diode laser. The spectrum was, in fact, a time-averaged spectrum which could be quite different from the spectra obtained using high temporal resolution [16]. During the time averaging process, the lasing mode(s) may have strayed through many available cavity modes around the peak laser wavelength as a result of system instabilities. Mechanical movement of laser components could conceivably exist and also minute air turbulence in the external cavity could introduce some mechanical/optical instabilities and

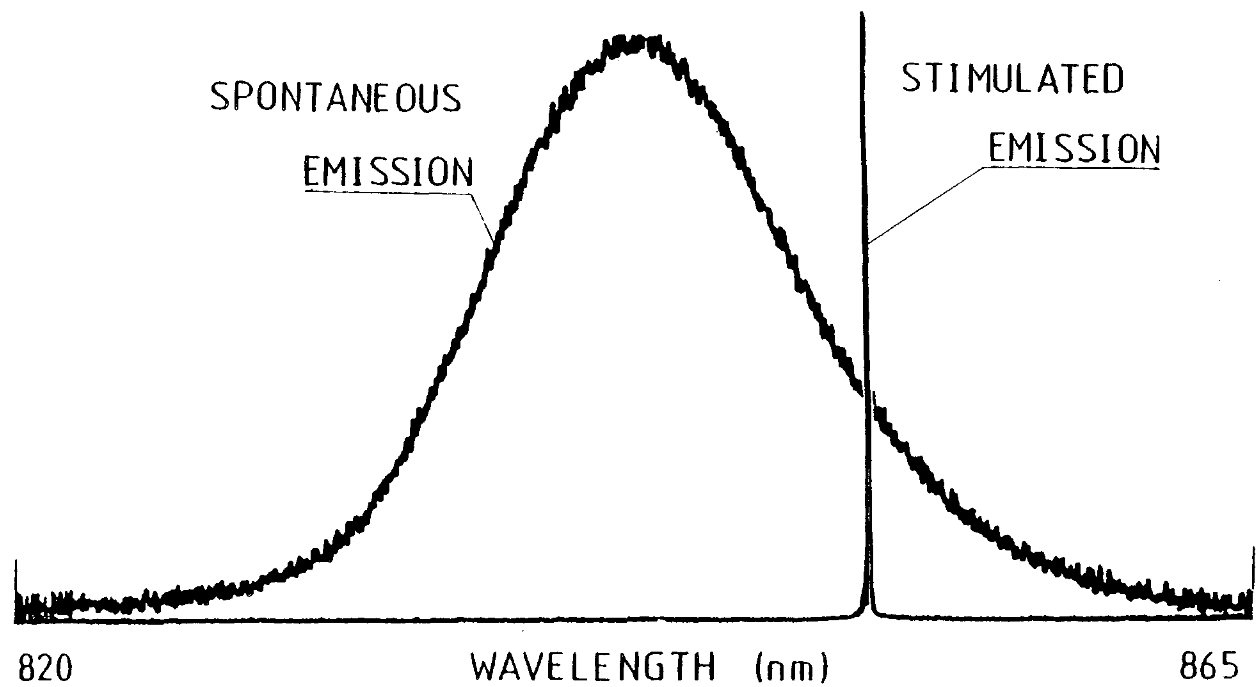

Fig. (5-8) The stimulated emission spectrum taken from a Brewster-angled diode laser (operating in cavity C3) shown together with its spontaneous emission spectrum for the same bias level (~200 mA).

thereby influence the output mode structure.

5.5. Frequency-Tuning with Intracavity Elements

By including an intracavity Fabry-Perot etalon or grating reflector, the wavelength of the Brewster-angled diode laser could be tuned easily and controllably within the medium gain spectrum. The output powers at different wavelengths of the Brewster-angled diode laser were measured with an optical power meter while the laser wavelengths were simultaneously monitored with a monochromator (see Fig.(5-2)). Typical spectra are shown in Fig.(5-9a) and in Fig.(5-9b) where the output of the frequency-tunable laser has been recorded on a photographic plate. Experimental observation did not show any difference between the etalon-tuned system and the grating-tuned laser as far as the spectral width and profile were concerned. There was, however, an observed difference in the threshold current for these two cavities. When the diode was operating in C2, the laser threshold was almost the same as that without the Fabry-Perot etalon. With C3, the threshold of the laser was about 5% higher than in C2 for the same diode, because of the losses introduced by the grating reflector.

In Fig.(5-10) the variation the output power of the frequency-tunable laser as a function of wavelength is shown for different bias currents. The recorded power

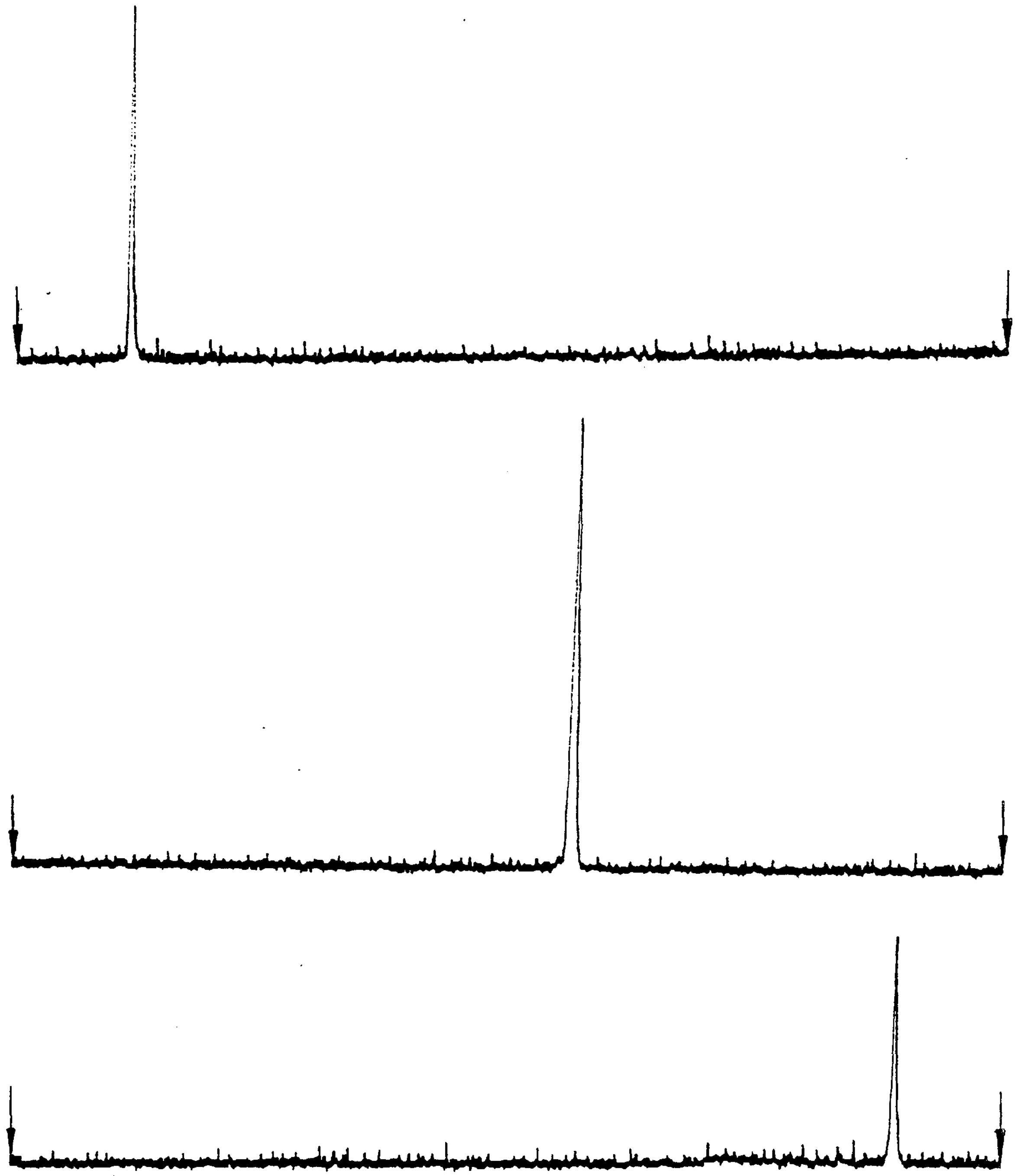

848 OUTPUT WAVELENGTH (nm) 865

Fig.(5-9) Output spectra of a Fabry-Perot etalon tuned Brewster-angled diode laser, (a) registered by chart recorder,

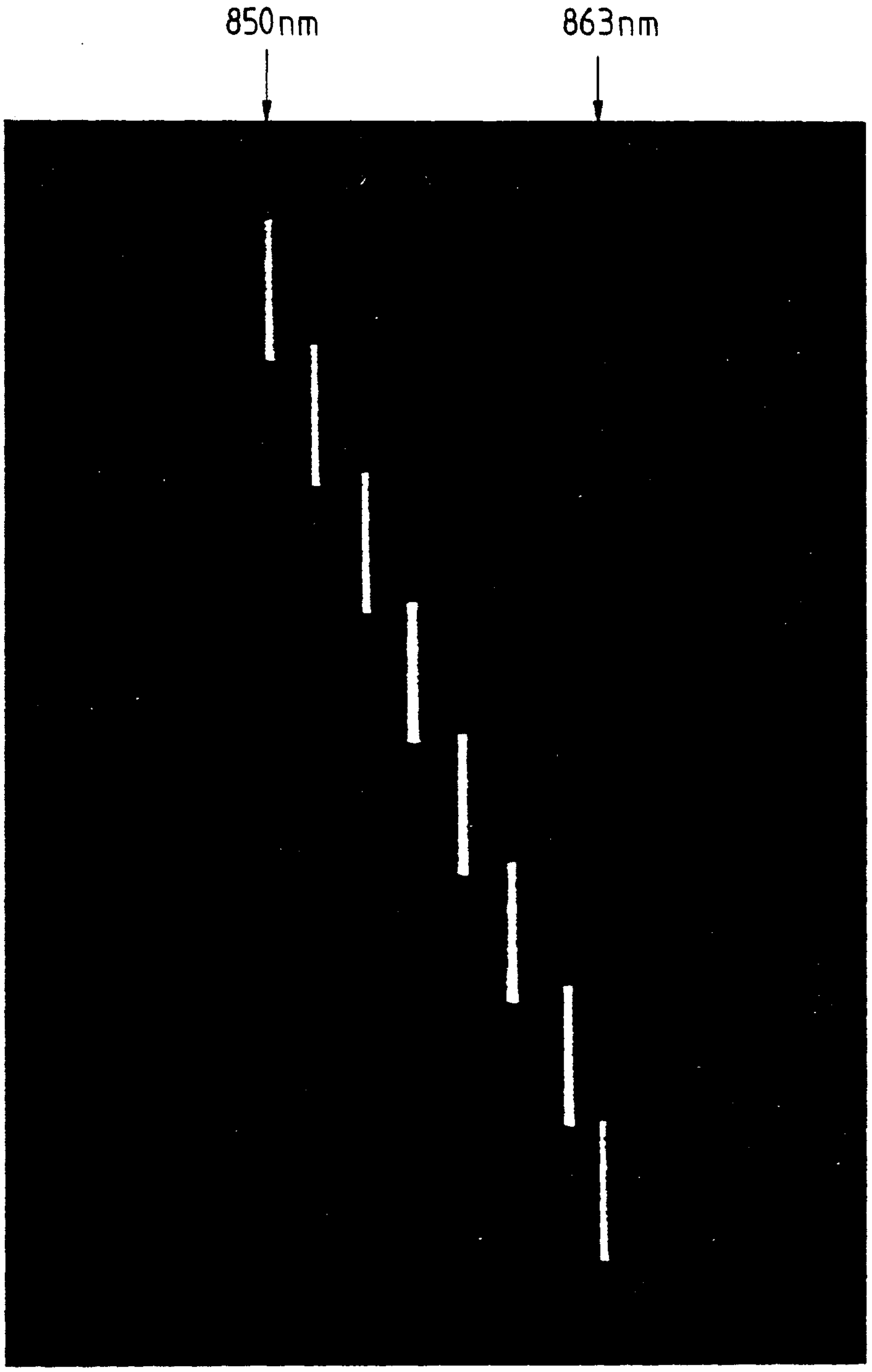

(b) recorded on a photographic plate.

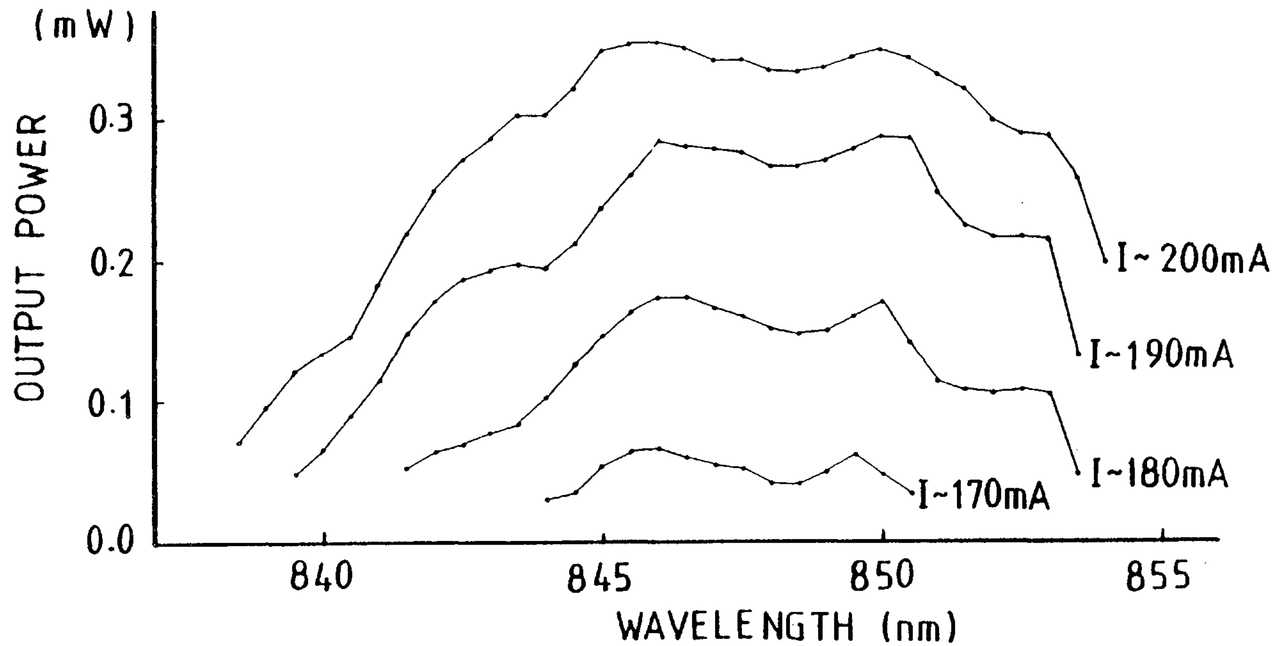

Fig. (5-10) Variation of the output power of a Brewster-angled diode laser with wavelength at different bias levels.

included the spontaneous emission power from the device. However, the spontaneous emission power was much smaller compared to the coherent output power, as can be seen from the L/I characteristic in Fig. (5-3) and from the stimulated emission spectrum in fig.(5-7). From Fig.(5-10), it can be concluded that the higher the injection current, the wider the laser tunability will be, where the tunability is defined as the wavelength separation between the two wavelengths at which the output powers are equal to half the maximum power. At $1.3I_{th}$ level, the system had a tunability of 14nm. Fig.(5-11) shows the tunability of the Brewster-angled diode laser operating in C3 at different injection currents. Similar results have also been obtained when the diode was operating in C2.

It can also be seen from Fig. (5-10) that the tuning curves fall away more markedly at the longer wavelength side than at the shorter wavelength side. The tunability was mainly acquired in the shorter wavelength side when the pumping current was increased in accordance with theoretical predictions. In reference 17, Stern had calculated the gain coefficient as a function of the photon energy for several different excitation levels, and a compresssion of the gain curves on the low energy side and an enhanced separation on the high energy side were inferred. From these curves it is to be expected that the tunability at high excitation currents should be extended mainly towards

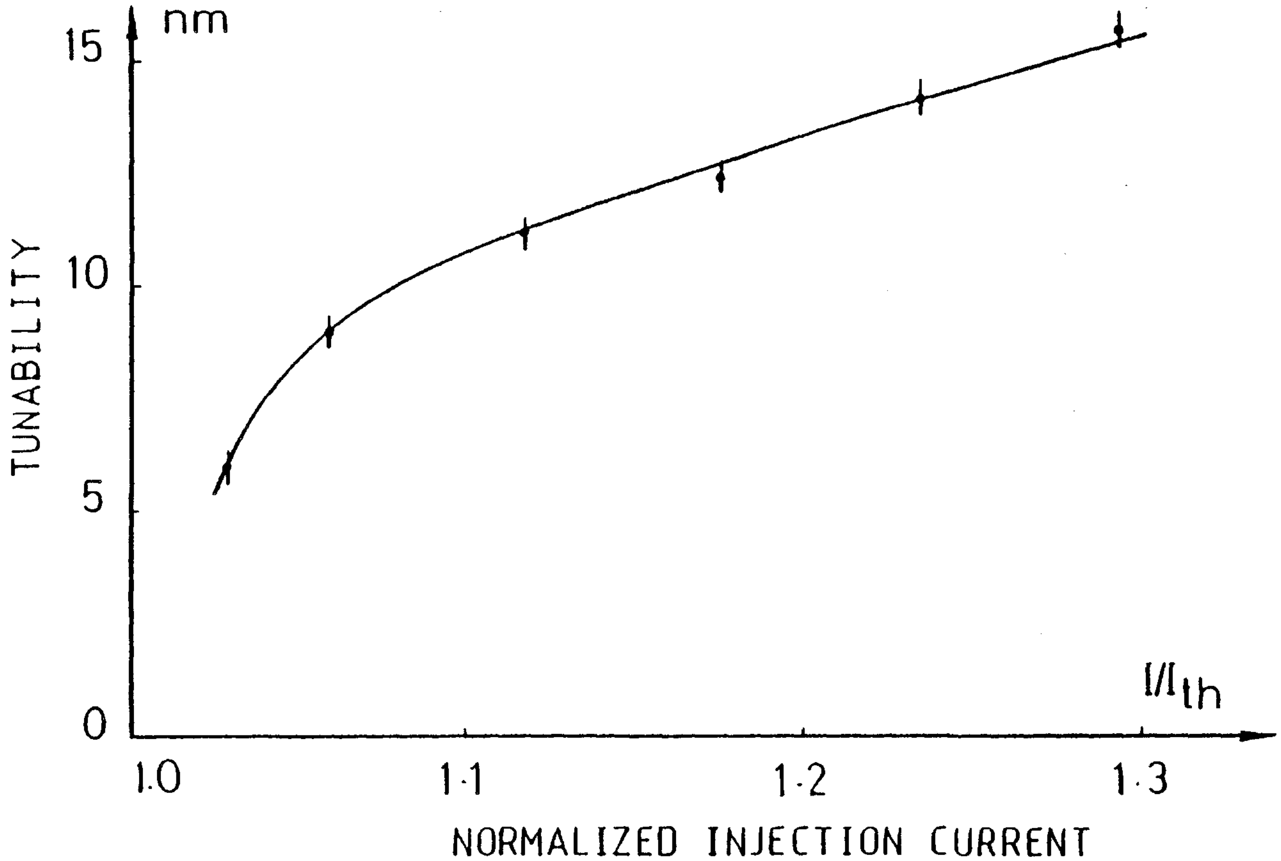

Fig.(5-11) Tunability versus the normalized injection current.

the shorter wavelengths.

5.6. Modulation Features of the Tuning Curve

An additional significant feature of Fig. (5-10) is that the tuning curves seem to have been "modulated" in that there are several "peaks" and "valleys" on these curves. From the experimental measurements, it was found that these "cycles" were separated by 3.0 to 3.5nm. The "depth" of the modulation was observed to alter from diode to diode. Even for the same diode, a small movement of the optical components of the external cavity by the piezoelectrically controlled cavity mounts would also change the modulation depth. It was observed that if the feedback into the diode was slightly defocused, the modulation depth was increased as reported in reference 10.

In an attempt to determine the nature of this phenomenon, spectra of the Brewster-angled diode with and without one-side-feedback have been taken. The spontaneous emission without any feedback did not display this modulation effect. For the system operated with one-side-feedback (this was investigated for the condition of the aligned laser followed by the removal of the output mirror) the recorded spectrum is shown in Fig. (5-12). The wavelength modulation seen in the laser regime is also apparent in Fig. (5-12). The wavelength separation between two consecutive peaks (or valleys) is measured as 3.2nm from

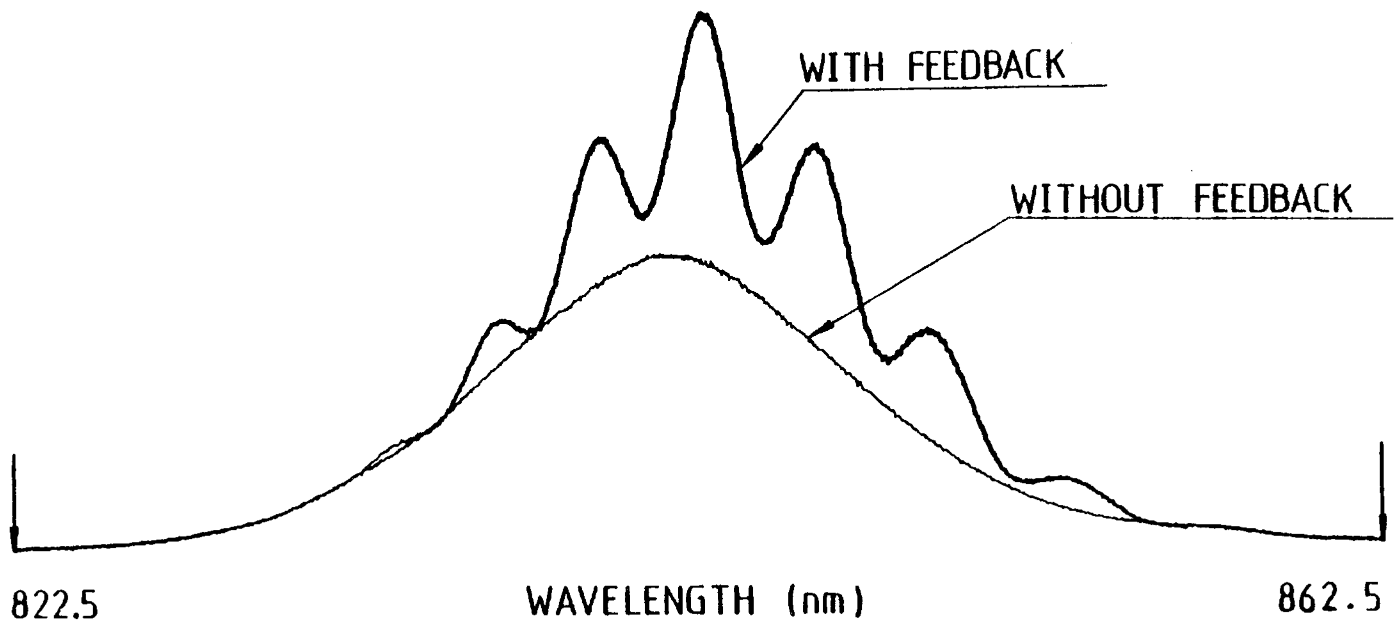

Fig. (5-12) Output spectra of a Brewster-angled diode with and without one-side-feedback.

this diagram which is the same as in the lasing case. Moreover, it can be seen from Fig. (5-12) that the spectrum with one-side-feedback is distorted on the high energy side due to selective internal absorption [18]. When feedback was provided by a spherical mirror and the output was focused onto the input slit of the monochromator with a one element lens of focal length of 10cm to eliminate any influence of the microscope objectives, the wavelength modulation still existed.

All these facts clearly show that the wavelength modulation phenomenon is related to the feedback and the diode chip. It is suggested here that this modulation may have resulted from light interference between the beam passing through the active layer and that propagating through the cladding layer(s). Part of the feedback light falling outside the active region would pass through the cladding layer without being subject to heavy loss because the passive layer has a wider energy gap. Passage of the two beams through the distinct semiconductor layers would incur a phase difference between them arising from the difference of the respective refractive indices. By assuming that the electric fields of the two beams have the same phase at the entrance facet, the refractive index difference needed to produce 3.0-3.5nm wavelength modulation at 850nm can be calculated as 0.41 to 0.48 using $\Delta n=\lambda^2/(l\delta\lambda)$ where l is the diode length and $\delta\lambda$ is the wavelength separation of two peaks. This was later substantiated by other workers [19].

When the diode was pumped, the effective index n_e in the active region could be as high as 4.2 [20,21]. An ordinary zero degree diode with identical dimensions has been examined and the laser mode separation was measured to be 0.17 to 0.19nm at 850nm (see Chapter 3, Fig. (3-11)). It can be calculated from the generally accepted formula [5]

$$n_e = \lambda^2/(2\Delta\lambda l) \tag{5-4}$$

that n_e ranged from 3.8 to 4.3, where $\Delta\lambda$ is the diode mode separation. With the passive layer having a refractive index ~3.4, then, within experimental error, this explanation is in good agreement with the measured data. A similar phenomenon had also been reported by Deutsch [22] for his homojunction lasers where the feedback was provided by the diode facet rather than the external resonator.

5.7. Laser Stability

When the Brewster-angled diode laser was operating in the external cavity, some mechanical/optical instabilities, such as the optical bench, the air turbulence within the external cavity would inevitably affect the system operation. In order to judge the external cavity, stability measurements have been carried out with these external cavity lasers.

Firstly, the time stability of the output powers of a Brewster-angled diode laser at different wavelengths was monitored. The output power of the laser was sampled by means of an intracavity pellicle, and directed on to a photodiode, the signal from which was recorded with a chart recorder. Typical results, at two wavelengths, are shown in Fig.(5-13 a and b). The ripple of the output within 40 minutes, which was limited by the chart recorder, was less than 1.5%. It is expected that particular design measures could be introduced to minimize most of the mechanical instabilities of the system and this observed ripple could therefore be reduced significantly below 1.5%. For example, the Brewster-angled diode may be coupled to an otpical fibre external cavity and the diode could be fixed to the fibre with refractive index matched epoxy. In such a compact system, improved mechanical formats should exist for external cavity configurations.

Secondly, the output wavelength stability with time was measured. Part of the laser output, divided by the beam splitter, was focused onto the input slit of the monochromator and the output of the monochromator was recorded every 15 minutes. In Fig. (5-13c), the output wavelength is shown to be only fluctuating within the resolution limit of the detection system over two hours. This indicated that the wavelength of the laser output was practically unchanged for the detection system employed.

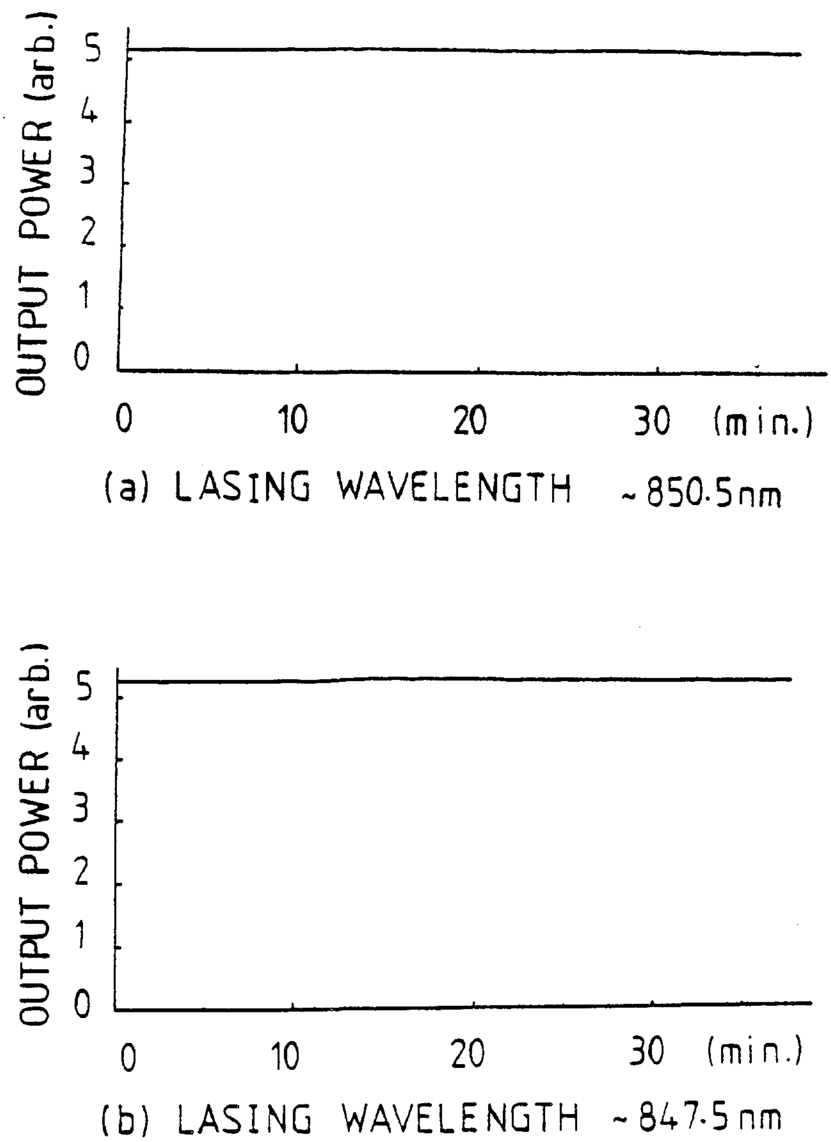

Fig.(5–13) Time stabilities of the Brewster-angled diode laser.

(a),(b) Output power time stability at ~850.5nm and ~847.5nm, respectively,

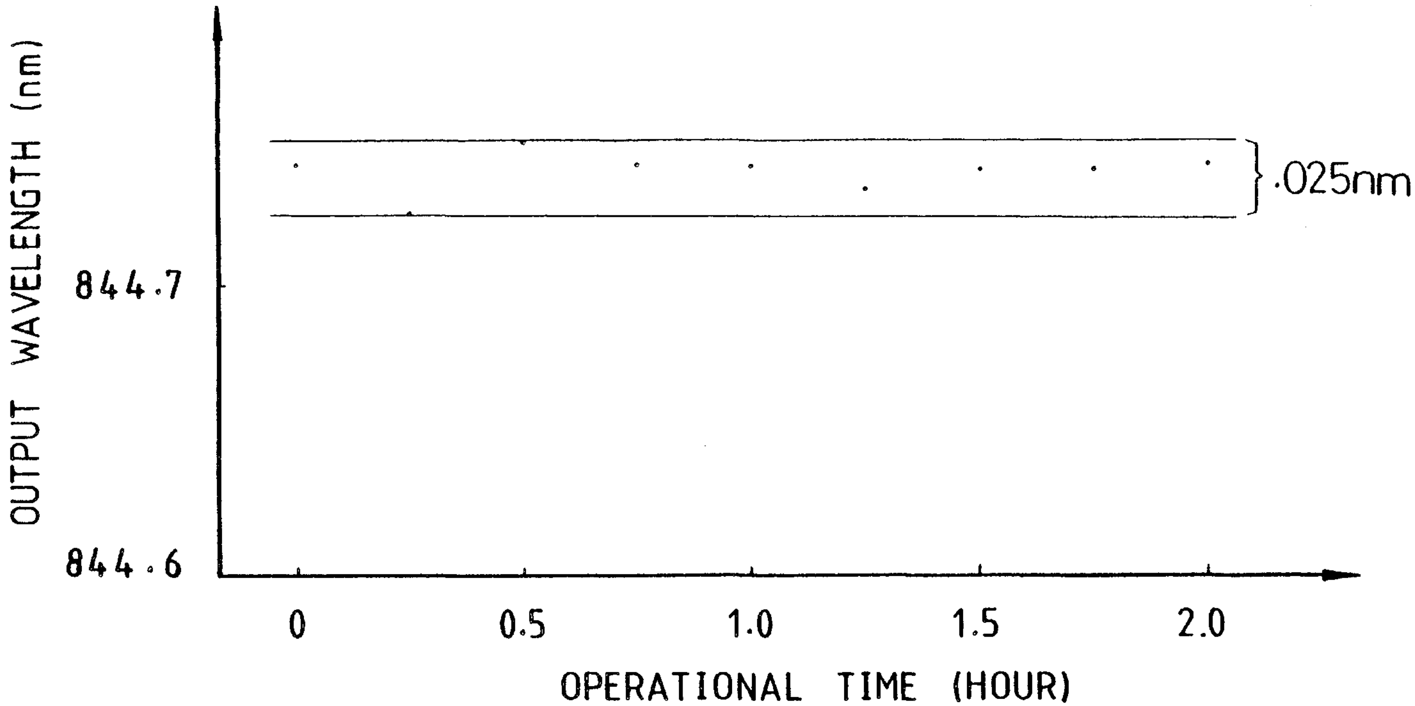

(c) time stability of the output wavelength.

5.8. Conclusions

In this chapter, data have been presented to show that the external cavity has a useful capacity for exploiting the broad-band emission of the AlGaAs diode, and thus provides the possibility of tuning the output wavelength of the Brewster-angled diode laser with the aid of an intracavity frequency tuning element. Spectral characteristics of such a Brewster-angled diode oscillator operating in several external configurations have been investigated including the features of spontaneous emission with and without one-side-feedback. The spectrum of the Brewster-angled diode laser has been observed to evolve from the smooth broad spontaneous emission below the threshold to a narrow stimulated emission of 0.05nm in width at a current injection level slightly higher ($\sim$4%) than threshold. Tunability of the Brewster-angled diode laser has been seen to increase with the injection current and observed to predominate at the shorter wavelength side for higher injection currents. At $1.3I_{th}$ level, the output wavelength of the Brewster-angled diode oscillator has been continuously tuned over 14nm with either an intracavity Fabry-Perot etalon or a grating reflector.

Two main features that distinguish the Brewster-angled diode from the ordinary zero degree diode at injection levels higher than the threshold of the external cavity laser have been identified. One is that at any current tested the direction of the peak wavelength shift with increasing bias current of the Brewster-angled diode was observed to be in accordance with that of the zero degree diode below its threshold. The other is that the spectral width of the emission from the Brewster-angled diode remained almost unchanged when the injection current was increased to 275mA. These two characteristics, together with the smooth appearance of the spontaneous emission spectrum, clearly show that for the Brewster-angled diode internal resonator effects are suppressed and suggest that this diode configuration offers the possibility of being used as an active medium both in oscillators and amplifiers.

It has also been observed that there was some evidence of a regular modulation on the tuning curve of the laser output. An explanation has been advanced where this effect is attributed to the interference between the light passing through the active layer with that passing through the cladding layer(s). The operational stabilities of the Brewster-angled diode laser have been measured both in terms of the output power and the output wavelength and good stability has been implied.

References

[1] B. D. Guenther, R. G. Buser, IEEE J.Quantum Electron., Vol. QE-18, 1179 (1982).

[2] H. S. Sommers, Appl.Phys.Lett., Vol. 42, 928 (1983).

[3] K. Stubkjaev et al, Jpn.J.Appl.Phys., Vol. 20, 1499 (1981).

[4] K. Kishino, S. Aoki, Y. Suematsu, IEEE J. Quantum Electron., Vol. QE-18, 343 (1982).

[5] H. Kressel, J. K. Butler, "Semiconductor Lasers and Heterojunction LEDs", Academic Press, (1977).

[6] R. Ludek, E. P. Harris, Appl.Phys.Lett., Vol. 20, 499 (1972).

[7] A. P. Bogatov et al, Sov.J.Quantum Electron., Vol. 12, 963 (1982).

[8] R. Wyatt, W. J. Delvin, Electron.Lett., Vol. 19, 110 (1983).

[9] M. W. Fleming, A. Mooradian, IEEE J. Quantum Electron., Vol. QE-17, 44 (1981).

[10] J. Chen, W. Sibbett, J. I. Vukusic, Opt.Commun., Vol. 48, 427 (1984).

[11] C. Voumard, Opt.Lett., Vol. 1, 61 (1977).

[12] C. L. Tang, V. G. Kreismanis, J. M. Ballantyne, Appl.Phys.Lett., Vol. 30, 113 (1977).

[13] J. C. AuYeung, A. R. Johnston, SPIE, Vol. 322, 25 (1982).

[14] R. L. Fork, B. I. Greene, C. V. Shank, Appl.Phys.Lett., Vol. 38, 671 (1981).

[15] M. Ito, T. Kimura, IEEE J. Quantum Electron., Vol. QE-16, 910 (1980).

[16] P. G. Eliseev, N. N. Shuikin, Sov.J.Quantum Electron., Vol. 3, 181 (1973).

[17] F. Stern, J.Appl.Phys., Vol. 47, 5328 (1976).

[18] H. F. Lockwood, H. Kressel, J. Crystal Growth, Vol. 27, 97 (1974).

[19] G. H. B. Thompson, Private Communication.

[20] R. A. Lang, K. Kobayashi, IEEE J. Quantum Electron., Vol. QE-16, 347 (1981).

[21] R. O. Miles et al, Appl.Phys.Lett., Vol. 37, 990 (1980).

[22] Ch.Deutsch, Phys.Lett., Vol. 24A, 467 (1967).

Chapter 6

MODE-LOCKED FREQUENCY-TUNABLE BREWSTER-ANGLED DIODE LASER

6.1. Introduction

The first attempt to mode-lock a semiconductor diode laser was made in 1968 [1]. By superimposing a radio frequency signal on a rectangular pump current pulse with a frequency equal to the mode spacing of the external cavity, Mohn achieved partial mode-locking of a Brewster-angled diode laser and obtained pulses of 600ps in duration. In 1978, Ho et al successfully mode-locked a semiconductor diode laser operating in an external optical resonator and measured output pulse durations of 20ps [2]. Thereafter, this area has been subjected to intensive research with an aim of achieving high information bit rates for optical fibre communication. [3-9].

In this chapter, the experimental results will be presented for an actively mode-locked Brewster-angled diode in an external resonator. The modulation mismatch effect will be discussed and it will be demonstrated that the frequency-tunable version of this laser is able to produce picosecond pulses within a spectral range of 14nm.

6.2. Experimental Set-Up of Mode-Locked Brewster-Angled Diode Lasers

6.2.1. Cavity types "C3" and "C4"

The experimental set-up for the active mode-locking of the Brewster-angled diode lasers was similar to that used for the frequency tuned lasers described earlier (see Section 5.3). Two frequently used cavity configurations were "C3" and "C4", depicted in Fig. (6-1a and b). In fact, mode-locking experiments have also been conducted in cavity type C2 (See Chapter 5, Fig. (5-1b)), and no observable difference has been found between C2 and C3 as far as the pulse profile and duration were concerned. The main consideration favouring C3 arises from the mismatch effect of the modulation frequency from the optimum frequency (which will be discussed in Section 6.4) that affects the frequency-tunable picosecond pulses. In C2, the rotation of the Fabry-Perot etalon could alter the cavity length by more than 300μm, and this in turn required that the modulation frequency be changed by about 100 KHz (for a cavity length of 93cm). If the comparison between different output wavelengths was to be made at the same modulation frequency, the reflector of the resonator near the etalon had to be moved accordingly, otherwise the pulse duration would be increased considerably if the rotation of the etalon lengthened the cavity or the pulse formation was completely frustrated if the tuning movement resulted in the reduction

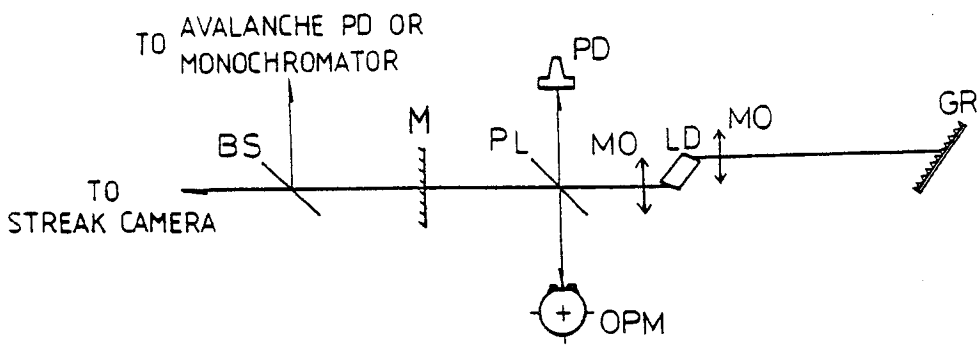

(a) CAVITY TYPE C3

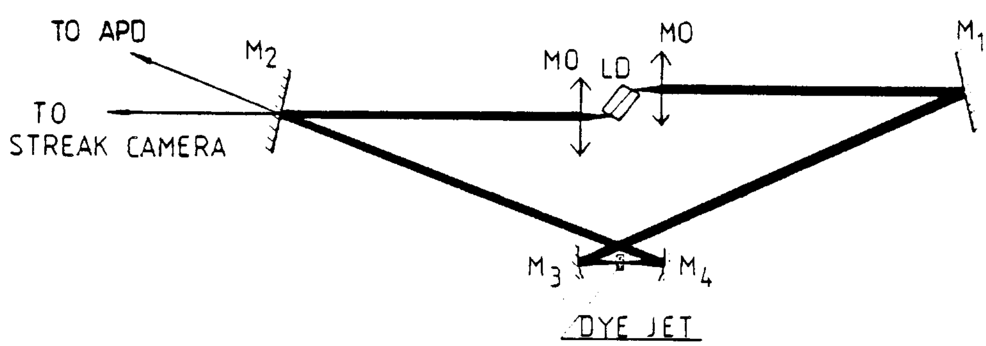

(b) CAVITY TYPE C4

Fig.(6-1) Two external cavity configurations of the mode-locked Brewster-angled diode lasers.

of the cavity length. In addition, the imbalance effect of the two "arms" of the linear cavity (which will be discussed later) to which the pulse duration was sensitive [5], would be built up causing the output pulses to become wider. Here the term "arm" refers to the optical length between the diode and either of the cavity reflectors. If the two arms are of equal length, the cavity is said to be balanced, otherwise unbalanced.

These shortcomings have been overcome in a practical manner for C3. The grating has been mounted in such a way that the laser beam intercepts the rotational axis of the grating along its ruled direction. For practical reasons, the rotational axis could not be set on the reflecting surface of the grating and since the laser beam had a finite size, some small perturbation was inevitable. However, the change in the cavity length during the course of tuning has been reduced to less than 10μm to which the arm imbalance effect was insensitive and the modulation frequency adjustment needed to compensate this length alteration was kept below the minimum allowable value of the radio frequency generator (which corresponded to a cavity variation of 15μm).

Mode-locking has also been achieved in a ring cavity (C4), as shown in Fig. (6-1b). In this configuration, the imbalance effect of the two arms was excluded [5] and colliding pulse mode-locking would be expected [10, 11].

Extra manoeuvrability was gained in C4 which allowed an active/passive hybrid mode-locking operation. At present, the shortest pulses were obtained in this configuration. Further modification might be made to this cavity in order to accommodate an intracavity frequency-tuning element. Attempts were also made to find an appropriate saturable absorber which might shorten the pulse duration from the mode-locked Brewster-angled diode lasers.

6.2.2. Diagnostic systems

Besides the diagnostic system used in Chapter 5 (which consisted of a pellicle, a photodiode and an oscilloscope), another two systems have been constructed to monitor the pulse duration and profile from the mode-locked Brewster-angled diode lasers.

One was composed of a silicon avalanche photodiode (BPW28) and a sampling oscilloscope (Tektronix 561B oscilloscope). This detector had a time resolution of about 250ps, and facilitated both the alignment procedure of the laser and the identification of the appropriate modulation frequency. About 30% of the laser output, divided by a beam splitter, was focused onto the window of the avalanche photodiode. The output signal from this photodiode was then fed into the sampling oscilloscope for continuous monitoring purposes. The other diagnostic system comprised a Synchroscan streak camera which was lens coupled to an optical multichannel analyser. (A detailed description of this system has been given in Chapter 2).

The injection system of the Brewster-angled diode has been shown in Chapter 4, Fig (4-8). Usually, the Brewster-angled diode was biased with a dc current of 70 to 90% of the threshold current. This value was similar to that used by Olsson et al [5]. Since the experimental observations did not show any systematic change in the pulse duration with the bias dc current within the range tested (from 0.6 to 1.2 I_{th}), there was no point in applying the higher dc bias which would reduce the lifetime of the diode. The bias of $0.7I_{th}$ was set up to avoid reverse bias on the laser diode.

The RF sinusoidal signal was generated by a frequency synthesiser (RACAL 9081). The frequency could be tuned manually at 10KHz intervals and 2.5KHz steps with the aid of the toggle switch which gave an accuracy of 1.6×10^{-5} to the relative change of the modulation frequency for the generally selected setting of 160MHz; in other words an ability of monitoring the variation of the cavity length by 15μm for a cavity length of 93cm.

6.3. Mode-Locking Results

After the system had been aligned with the aid of the pellicle-photodiode-oscilloscope diagnostic system under dc injection conditions, the dc current was reduced to 70% to 90% of the threshold value. Then a sinusoidal current signal whose frequency was twice the mode spacing of the external cavity for C2 or C3 (three times this spacing for C4), was superimposed onto the dc injection. The modulation frequency was scanned around twice the mode frequency spacing of the external cavity (pre-estimated using the measured cavity length) until the maximum output was obtained. It was observed that the optimum modulation frequency (referred to here as "the optimum frequency") which corresponds to the shortest pulse was very near the frequency at which the laser produced maximum output power [15] (referred to as "the maximum output frequency"). Observations showed that the difference between them was less than 0.2 MHz, although it changed a little from diode to diode.

The mode-locking frequency was also checked by comparing the output powers available with and without one of the reflectors of the resonator. When the modulation frequency was near the maximum output frequency (< 1.0MHz), removal of the reflectors would quench laser action. When the modulation frequency was far from the maximum output frequency (>1.2MH$_z$), misalignment of one reflector would reduce the output power of the system by no more than 20%. After the maximum output frequency was found, the sampling oscilloscope was put into operation and detector limited pulse durations were displayed on the scope, as shown in Fig. (6-2).

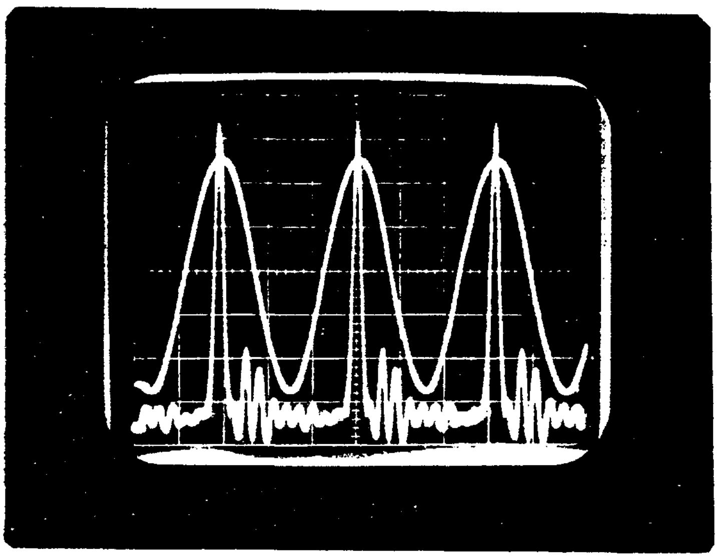

Fig. (6-2). Sampling oscilloscope display of resolution limited pulses from a mode-locked Brewster-angled diode laser, together with the modulation signals. Horizontal scale is 1ns/div.

For some quantitative studies of the pulses a Synchroscan streak camera was used. About 70% of the output power from the mode-locked Brewster-angled diode laser was sent into an otpical delay line, as shown in Fig.(6-3), in which each pulse was divided into two equal intensity components by a 50/50 beam splitter. These two subpulses were then reflected back from two 100% reflection mirrors, one of which was moveable (M_1). The preset time difference

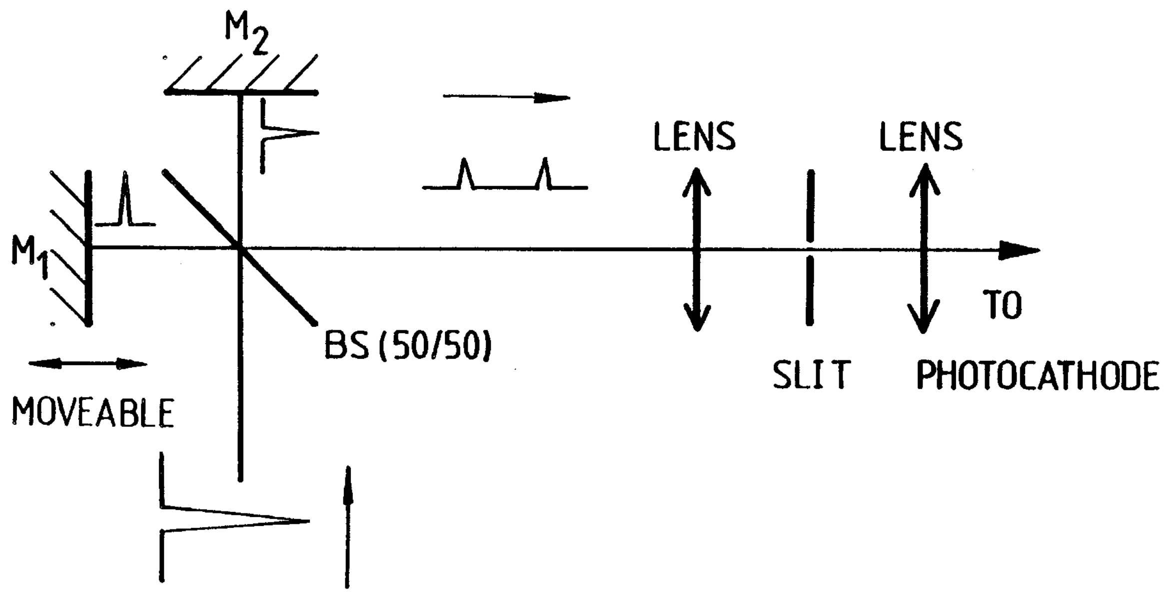

Fig. (6-3) An optical delay line in which a laser pulse is divided into two subpulses with equal intensities and calibrated separation.

thus introduced was used for calibration of the streak. The streak intensity profiles were recorded and displayed by an optical multichannel analyser (B & M, OSA 500/WP1) which was lens coupled (f/1.5 80mm lens) to the streak tube screen.

With the Synchroscan streak camera/optical multichannel analyser system, pulses of 9ps have been recorded, as shown in Fig. (6-4). In this diagram, the preset time difference between the arrival times of the subpulses at the photocathode was 60ps. After deconvolution of the time resolution of the detection system, via the Gaussian approximation [12], the pulses were established to be less than 7ps in duration. From Fig. (6-4), it can be seen that the output pulses from the mode-locked Brewster-angled diode laser were free from the effects of the internal resonator, which was defined by the two parallel cleaved facets of the diode chip. Such effects have always been observed from any of the mode-locked injection lasers using AR coated zero degree diodes as the gain media, and manifested themselves as a train of pulses being evenly separated by the round-trip time of the diode (about 12ps for GaAlAs diode of length of 500μm).

The time-averaged spectrum taken while the short pulses were recorded is given in Fig.(6-5). It can be seen that the output spectral width (∿0.5nm) from the mode-locked Brewster-angled diode laser was about ten times greater than

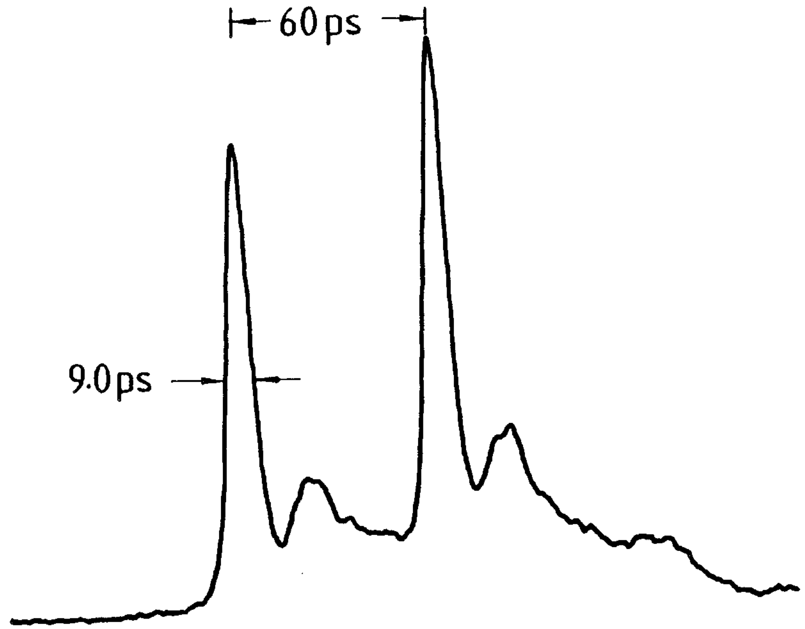

Fig.(6–4) Intensity profile of streak images (FWHM ~9ps) of pulses from an actively mode-locked Brewster-angled diode laser.

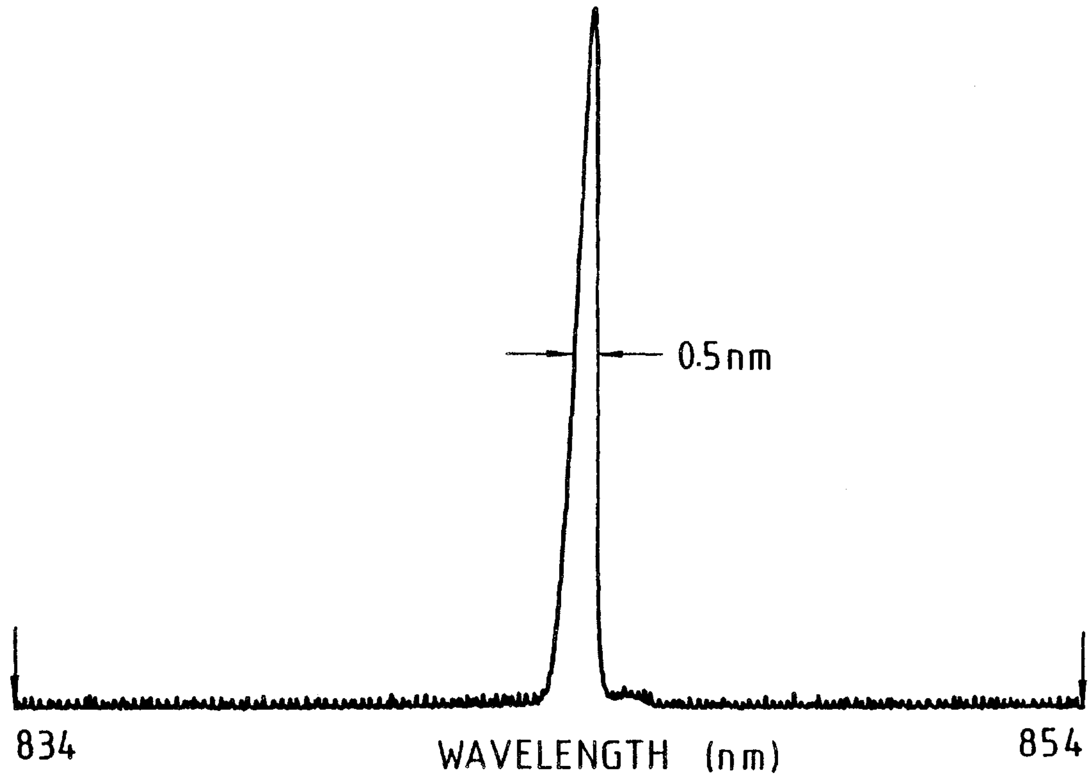

Fig. (6-5) Time — averaged spectrum of an actively mode-locked Brewster-angled diode laser.

that from the diode in dc operation (∿0.05nm). This phenomenon has been reported [2] for the conventional zero degree diode lasers.

Ikegami [17] has observed an increasing number of the oscillating longitudinal modes when the diode laser was modulated at a high pulse rate. Lin et al [18] have also stated that under the fast excitation conditions in semiconductor diode lasers, the number of the axial modes was larger than that of the CW case, causing spectral envelope broadening. They have also observed a transient shift of the spectral gain peak towards a longer wavelength during the optical pulse on the picosecond time scale.

In the mode-locked Brewster-angled diode laser, the situation should be different understandably, because there were only external cavity modes oscillating. Before the pulse arrived at the active medium, the injection carrier density has been established at a high level due to pumping and the separation between the two quasi-Fermi levels was accordingly large due to the filling-in of the bands with injection carriers [20]. When the pulse passed through the active medium, the carrier density would be drastically reduced due to the depletion effect of the carriers by the strong field. Considering that the intraband relaxation time of the free carriers is $\sim 10^{-13}$s [21], which is much shorter than the pulse width ∿7ps and the transit time (∿6ps) of the pulse through the gain medium, then the separation between the two quasi-Fermi levels would be continuously diminished as the pulse was sweeping across the active region. As a result, the peak wavelength of the medium gain would sweep from shorter wavelength to longer wavelength when the pulse was travelling in the active medium.

The shift of the peak wavelength due to the depletion effect could be estimated as follows. According to reference 22, the wavelength of the gain peak (λ_p) changed with the electron density (N) at a rate of

$$\Delta\lambda_p/\Delta N = -0.62 \times 10^{-17} \text{nm/cm}^3 \qquad (6\text{-}1)$$

Before the pulse reached the amplifying material, the system could be regarded as a spontaneous emission device and the carrier density was approximated by

$$N \sim \tau I/(e.dlw) \qquad (6\text{-}2)$$

where τ is the lifetime of the injection carrier (see Chapter 3, equation (3-11)). The difference between equations (3-11) and (6-2) is that "$\tau_r\eta$" and "J" in the former have been replaced by "τ" and "I/(lw)", respectively. From equation (6-2) it can be deduced that

$$\Delta N \sim [\tau/(edlw)]\Delta I \qquad (6\text{-}3)$$

Suppose the carrier density was equivalent to that created by a dc current which was $\sim$25mA higher than the threshold current I_{th} before the pulse arrived at the gain medium. Assuming that after the pulse has passed through this active region, the carrier density would be reduced to a level just below the threshold value, in this case, ΔI should be $\sim$25mA in equation (6-3). Using the following experimental parameters, $\tau \sim 10^{-9}$s [20], d=0.2μm, l=500μm, w=18μm, it is estimated using equation (6-3) that

$$\Delta N \sim 8.7 \times 10^{16} cm^{-3} \quad (6\text{-}4)$$

Substituting equation (6-4) into equation (6-1), it follows that $\Delta\lambda_p \sim 0.54$nm which is in agreement with the experimental value of the spectral width from the actively mode-locked Brewster-angled diode laser.

Without the frequency-tuning element, the laser was automatically oscillating close to the peak wavelength of the gain line if the losses were the same for each mode. The output spectrum would be the integrated effect of each "individual" wavelength oscillating at different instants while the strong field was passing through the active medium. The time-averaged spectrum of the mode-locked Brewster-angled diode laser should be wider and the width would be dependent on the reduction of the separation between the two quasi-Fermi levels. If there is a frequency-tuning element inside the cavity, the sweeping nature of the gain curve should not be altered. The tuning element only imposes a loss discrimination on different wavelengths. The lasing wavelength selected by the tuning element should also be swept along the wavelength axis and this results in a wider output spectrum. This can be understood from equation (2-33) given in Chapter 2. Under dc conditions, however, the separation between the two quasi-Fermi levels was almost fixed because of the restriction of the injection carrier density to the threshold value [19], and the output spectral width would be much narrower than that obtained under mode-locking conditions.

6.4. Modulation Frequency Mismatch

The term "mismatch" usually refers to the frequency difference between the modulation frequency f_m and the mode spacing f_c of the external cavity. No effective method has been found to measure the cavity mode spacing (or rather the optical length of the cavity) with an accuracy $\sim 10^{-5}$ [23], which should not be larger than the ratio of frequency change to which the pulse formation is sensitive to the modulation frequency. Consequently the term "the optimum modulation frequency", f_o, which was identified as the frequency at which the shortest pulse was obtained for a sequence of experimental measurements, has been adopted in this work and this mismatch is written as

$$\Delta f = f_m - f_o \qquad (6\text{-}5)$$

Much attention has recently been drawn to the mismatch effect on the pulse durations and profiles of synchronously pumped mode-locked lasers [15, 24 - 29]. It has been shown that the pulse duration varied asymmetrically with Δf in that the pulse broadening process has a smaller rate for positive mismatch than for the negative case. This asymmetric feature has also been observed in the actively mode-locked Brewster-angled diode lasers with the aid of the Synchroscan streak camera. The main characteristics of the measurements of the mismatch effect were as follows. Firstly, the observations were made by directly changing the modulation frequency instead of altering the "slave" laser cavity length as reported by other researchers for synchronously pumped lasers. Secondly, monitoring of the pulse profile was achieved by a real-time detection system, which made it possible to unambiguously trace the detailed evolution of the pulse profiles.

It can be seen in Fig. (6-4), that there is a small subpulse accompanying the main pulse. By blocking one arm of the optical delay line during the experiment, the attendant pulse has been identified as being at the trailing part of the main pulse. This phenomenon was recognizable in the earlier papers [30,31]. In reference 26, it can be seen that the optimum modulation frequency for the synchronously pumped dye laser was different from the frequency at which the accompanying pulse appeared by an amount $|\Delta f|/f_m=2x10^{-6}$.

Attempts have been made to eliminate this subpulse by varying the modulation frequency and the trade-off turns out to be the pulse duration (this will be discussed later). Moreover, in the cavity configuration C4, the inclusion of a saturable absorber dye jet was investigated in an effort to reduce this effect. Unfortunately, the pulse duration was not reduced, possibly because the dye (IR140) used could not recover its absorption fast enough after being saturated by the main pulse and it was therefore impossible to suppress the trailing component of the pulse.

The variation of pulse duration with frequency mismatch Δf has also been traced. The evolution of the pulse profiles recorded with the Synchroscan streak camera is shown in Fig. (6-6(1) and (2)). In Fig.(6-6(1)), the mismatch quantity Δf is varied in steps of 7.5 KHz, while in Fig. (6-6(2)) Δf is changed by 30KHz for each step. It can be seen from Fig. (6-6(1)) that when Δf was increased by 7.5KHz, the attendant pulse almost disappeared and the pulse duration was gradually increased with increasing positive mismatch. The pulse formation was frustrated when Δf was equal to -7.5 KHz (or $\Delta f/f_m = -1.6\times10^{-5}$). Dependence of the pulse duration on modulation frequency mismatch has also been plotted, as shown in Fig.(6-7 a and b). From this diagram, it can be clearly seen that the variation of the pulse width with mismatch was markedly asymmetric about the optimum modulation frequency (which corresponded to $\Delta f=0$).

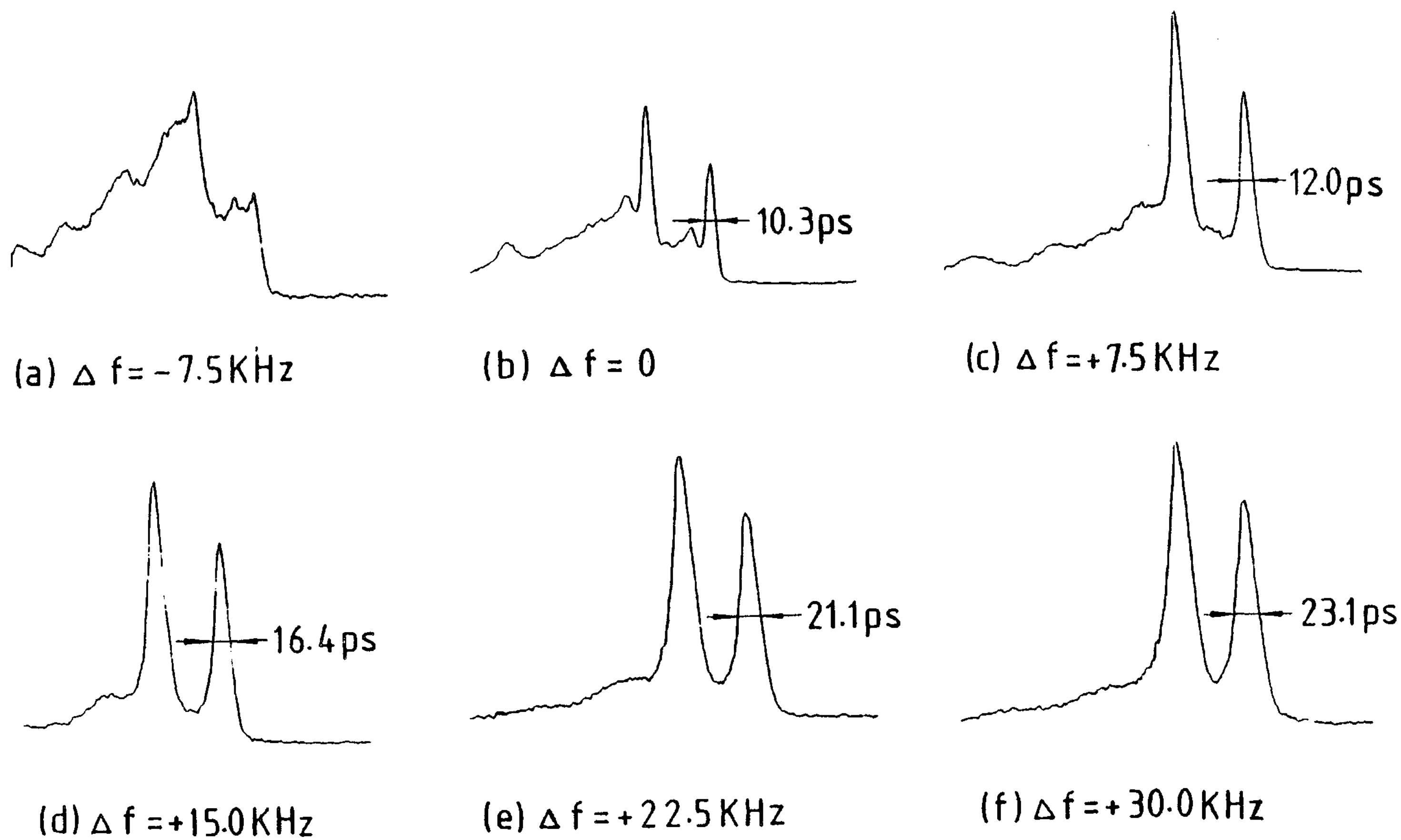

(1)

Fig. (6−6) Variation of pulse profile and duration with the modulation frequency mismatch (the optimum modulation frequency was ~483.1500MHz).

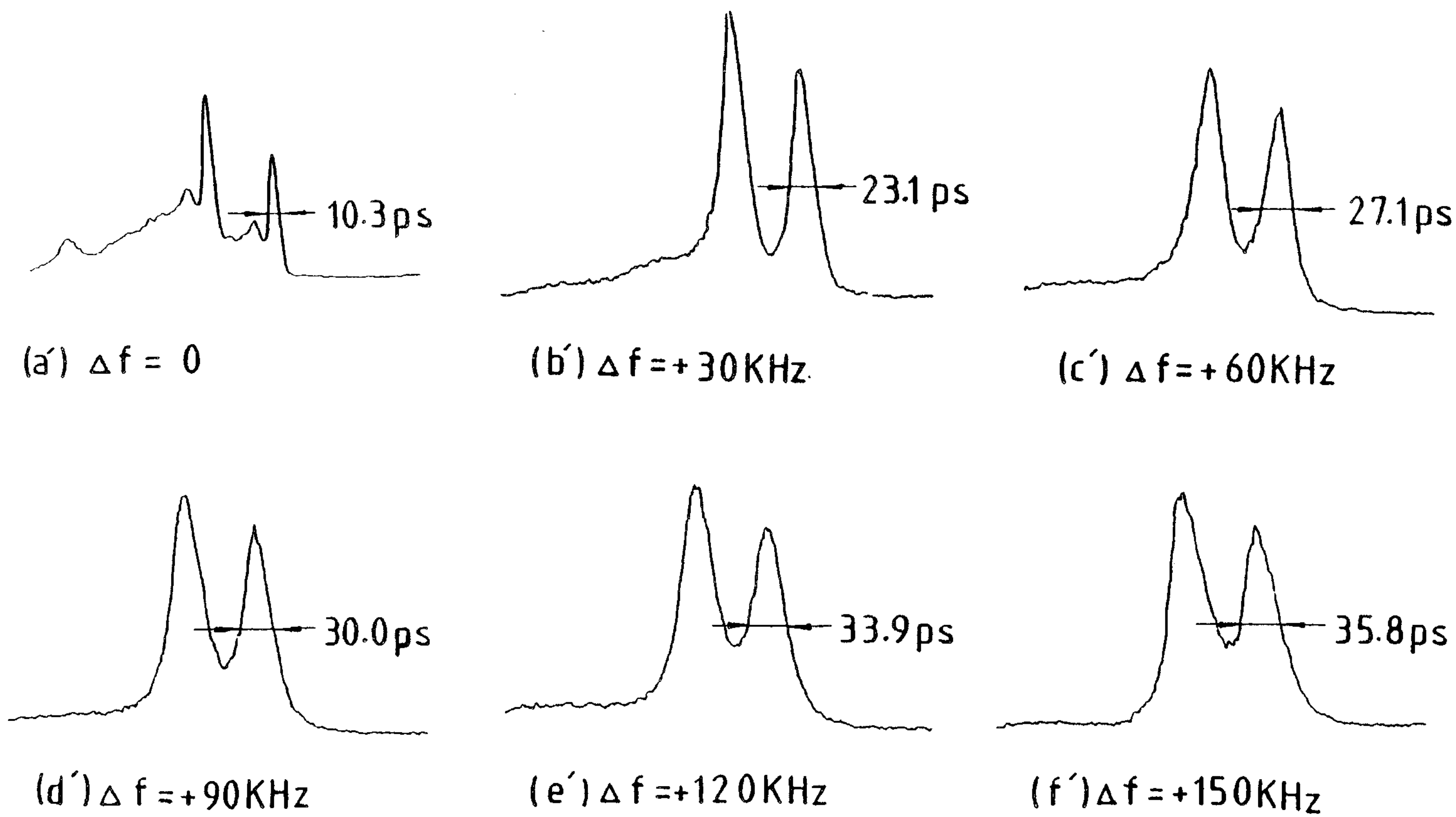
10.3ps
(a′) Δf = 0
23.1ps
(b′) Δf = +30KHz
27.1ps
(c′) Δf = +60KHz
30.0ps
(d′) Δf = +90KHz
33.9ps
(e′) Δf = +120KHz
35.8ps
(f′) Δf = +150KHz

(2)

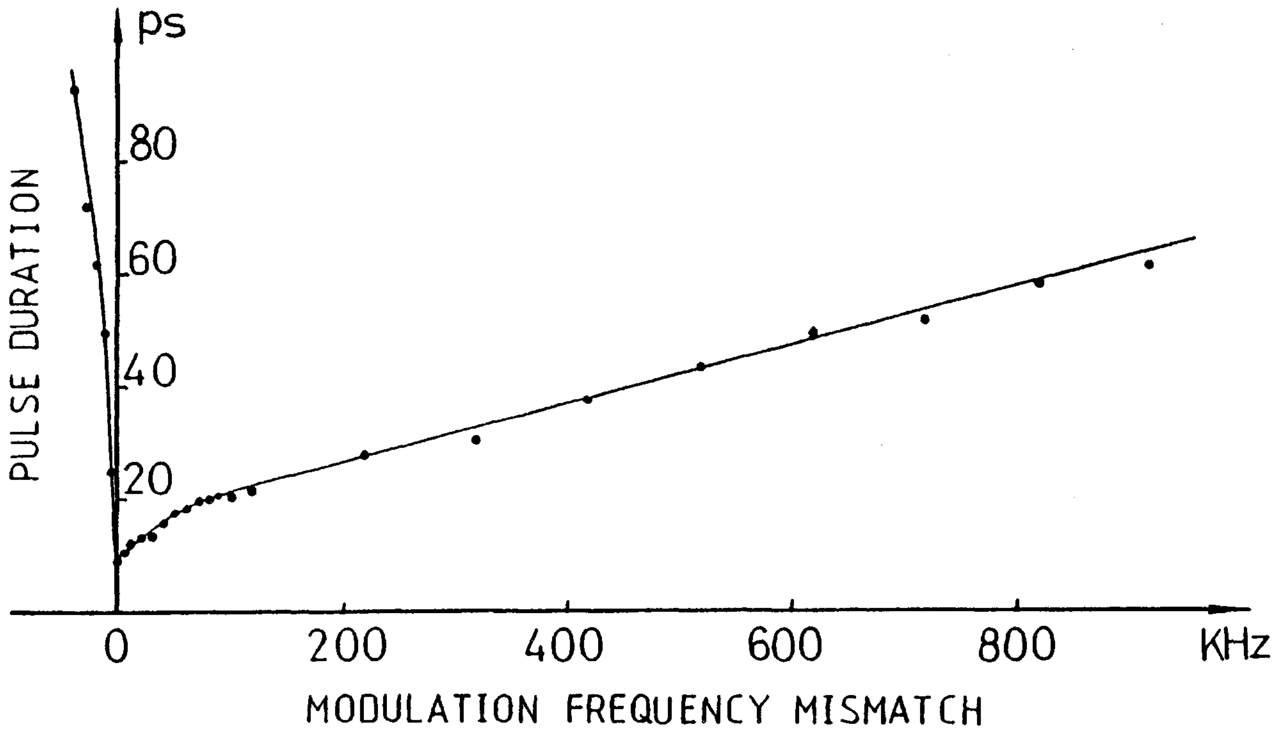

(a)

Fig. (6-7) Dependence of pulse duration on modulation frequency mismatch for two different diodes.

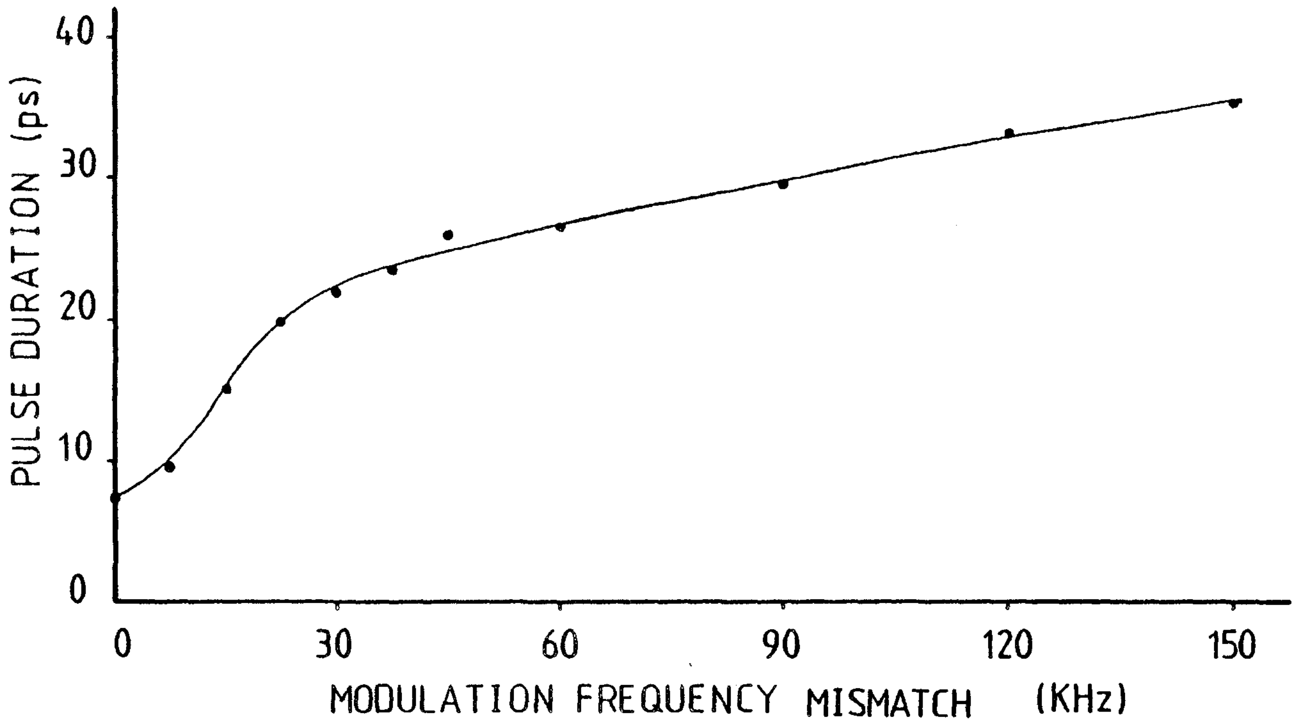

PULSE DURATION (ps)
40
30
20
10
0
0
30
60
90
120
150
MODULATION FREQUENCY MISMATCH (KHz)

(b)

The difference between (a) and (b) of Fig. (6-7) could possibly be due to slight variations between diodes, because several other diodes tested had different rates at which the pulses became wider at either direction of Δf although the highly asymmetric feature was maintained for all samples.

The following simple explanation to the modulation frequency mismatch effect on the pulse duration and profile is advanced. In order to simplify the discussion, a schematic of the time variation of the medium gain, g, due to the pump and the passage of the laser pulse can be drawn (see Fig. (6-8)), according to the physical analysis of the process [15]. Also the evolution of the small signal gain g_s in the absence of the laser pulse is indicated by the dashed line in the same diagram. The time at which the peak of the small signal gain was expected in the absence of the laser pulse is designated as t_O. Symbols t_{po}, t_{pn}, t_{pp} denote the arival time of the peaks of the laser pulses at the gain medium under the optimum modulation frequency, negative mismatch and positive mismatch conditions, respectively. The pulse duration is labelled by τ_p. Fig.(6-8a) shows that the pulse arrives at the active region at the optimum time, for which the time difference between t_{po} and t_O is denoted by Δt_o (ie, $\Delta t_o = t_O - t_{po}$) and results in the shortest pulse. Fig. (6-8b) depicts the case where the modulation frequency is smaller than the optimum

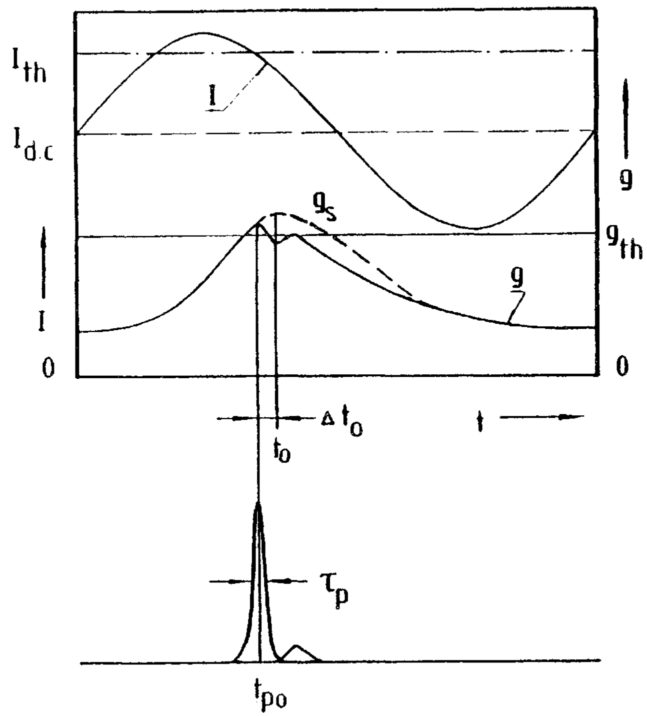

(a)

(a) Optimum modulation frequency condition.

Fig. (6-8) Schematic of the pulse evolution at different modulation frequencies.

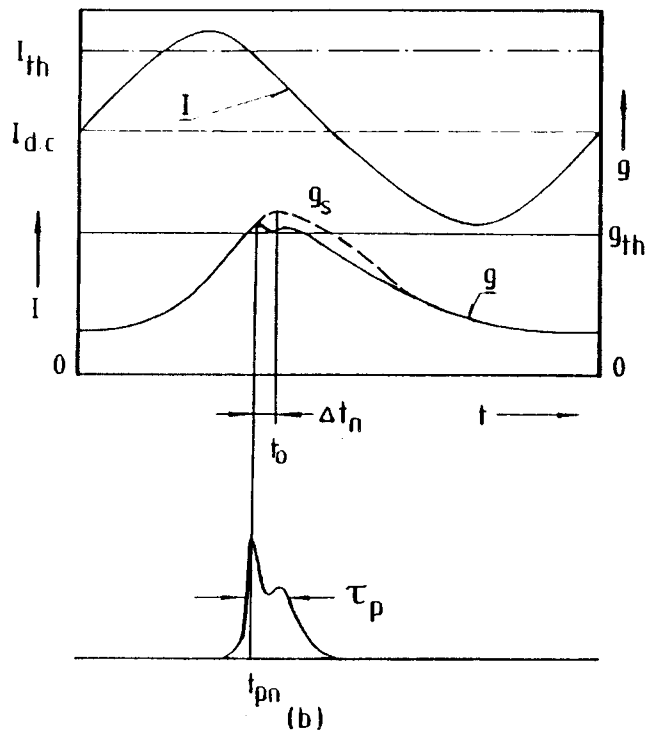

(b) Negative mismatch condition.

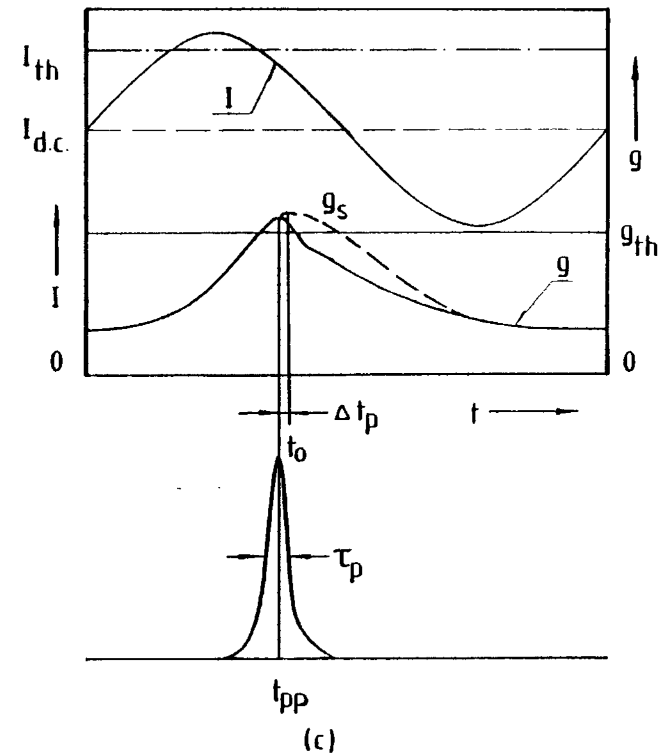

(c) Positive mismatch condition.

frequency, (ie, negative Δf) and the laser pulse, therefore, reaches the gain medium at an earlier time than the optimum time. In other words, the time gap between the arrival time and that at which the gain peak is due, $\Delta t_n \equiv t_O - t_{pn} > \Delta t_O$, and the output pulse becomes wider and is followed by a noticeable accompanying pulse. In (c) of Fig. (6-8), the positive mismatch situation (positive Δf) is illustrated. Because the modulation frequency is larger than the optimum frequency, the laser pulse approaches the amplifying medium at a time slightly later than the optimum time (ie, $\Delta t_p \equiv t_O - t_{pp} < \Delta t_O$) and becomes slightly wider in width but larger in amplitude.

When the system was operating at the optimum modulation frequency, the laser pulse energy and its timing with respect to the pumping peak should be such that the gain remained below threshold for a certain period after the depletion due to the laser pulse. The peak of the laser pulse should then pass through the gain medium slightly delayed from the point in time at which the gain first reached threshold [15]. Also, the laser pulse should arrive at the gain medium earlier than the time when the peak of the small signal gain was due to appear. These ensured that the leading part of the pulse was effectively suppressed. After the pulse has passed through the active region, the medium gain is substantially depleted and remains below threshold for a period. If the pump was still hard enough, the medium gain could reach the threshold once more, and the attendant pulse would appear in the trailing part of the output pulse as shown in Fig. (6-8a).

In the negative mismatch situation the laser pulse would enter the gain medium at a time (t_{pn}) slightly earlier than t_{po}. (Note that if $-\Delta f$ was too large, so that the pulse peak should arrive at the diode before the time when the small signal gain first established threshold, then the "pulse" would be attenuated while the trailing part be amplified, and pulse formation is completely frustrated. The case is beyond the scope of this discussion). The medium gain could not be exploited effectively because the depletion of the gain was dependent not only upon the photon number in the pulse but also on the time difference between t_o and the arrival time of the pulse peak. (Maximum depletion of the medium gain should be achieved when the pulse peak and the peak of the small signal gain overlapped temporally with each other if the photon number in the input pulse was constant). After the pulse has passed through the active region, the medium gain is only partly depleted and might still remain above threshold or might be reduced below the threshold but could recover quickly. As a result, any trailing pulse is subject to undesirable amplification. In the case that the gain was reduced below threshold but recovered quickly, this subpulse would be distinguishable from the main pulse, as shown in

Fig. (6-8b); otherwise, the main pulse would be merged with its trailing component and the output "compound" pulse would be very broad, as shown in Fig. (6-6(1)a). Depending on the degree of gain depletion in the medium induced by the input pulse (which was partly dependent on the strength of pump), the time for the medium to surmount the threshold again varied and the gap between the main pulse and its "tail" shifted accordingly, and the intensity and width of the trailing pulse also changed.

In the positive mismatch case the pulse should arrive at the diode at a time t_{pp}, for which $t_O - t_{pp} \equiv \Delta t_p < \Delta t_o$. At an earlier instance, ie, when $\Delta t_p > 0$, the pulse should be approaching the peak of the small signal gain. The results were as follows. Firstly, more medium gain would be depleted because the pulse peak was nearer to the peak of the small signal gain. This in turn leads to an increase in the photon number contained in the output pulse. Secondly, because the depletion effect became stronger as Δt_p became smaller, the time interval for the gain to return above threshold level became longer or even impossible if the remaining pump was not strong enough while the depletion effect was very effective. As a result, the time gap between the main pulse and the attendant pulse became progressively wider, and eventually the small pulse disappeared, as shown in Fig.(6-6(1))b to f. Thirdly, the major setback in this regime was that the leading part of the pulse would experience enough gain and be amplified undesirably, leading to the gradual increase of the pulse duration. At later phases of positive mismatch when Δt_p became negative, (or in other words when the pulse peak arrived at the amplifying medium after the peak of the small signal gain had been passed) the leading part of the pulse would be amplified considerably. This could result in a small peak in front of the main pulse and thus leave behind a limited gain from which the input pulse peak could benefit. Output of double pulses could not be ruled out, at least the width of the output pulse was large.

Finally, it should be pointed out that in this model, the optical pulse inside the cavity did not appear to travel at the speed of light. Only when the cavity mode spacing was precisely equal to the modulation frequency did the pulse appear to travel at the speed of light. When these two quantities are not identical to each other, the gain medium has the effect of "pulling" or "pushing" the pulse, depending on whether or not the modulation frequency is larger than the cavity mode spacing, and the pulse experiences the "re-shaping" process whenever it passes through the active medium. As a result, the repetition rate of the output pulse was kept the same as the modulation frequency. This viewpoint has been proven experimentally with the aid of the Synchroscan streak camera. In second-harmonic generation or two-photon-fluorescence method, the diagnostic system is not sensitive to the pulse period from the laser generator. In this work, however, the frequency of the deflection voltage was selected by the synthesizer which was independent of the mode spacing of the resonator. If the repetition rate of the pulse had been decided by the mode spacing of the laser cavity, then for a difference of 10^{-5} between the modulation frequency and the cavity mode separation there would have been a 2π phase shift between the pulses and the voltage on the deflection plates within every 10^5 cycles. As a result, the photo-electrons created by these 10^5 pulses would have been streaked to different places of the phosphor, and there would not have been any observable pulse displayed on the screen.

6.5. System Stability

The stability of the mode-locked Brewster-angled diode laser has been investigated. Pulses were recorded every thirty minutes with the Synchroscan streak camera and the results, presented in Fig. (6-9), showed that within three hours, the duration of the output pulse changed by less than 5% from the initial value. From Fig.(6-9), it can be seen that the pulse durations systematically broadened so this precluded stochastic fluctuations, at least those fast events with fluctuation times less than 1 hour. Such irreversible movements that could have happened to the

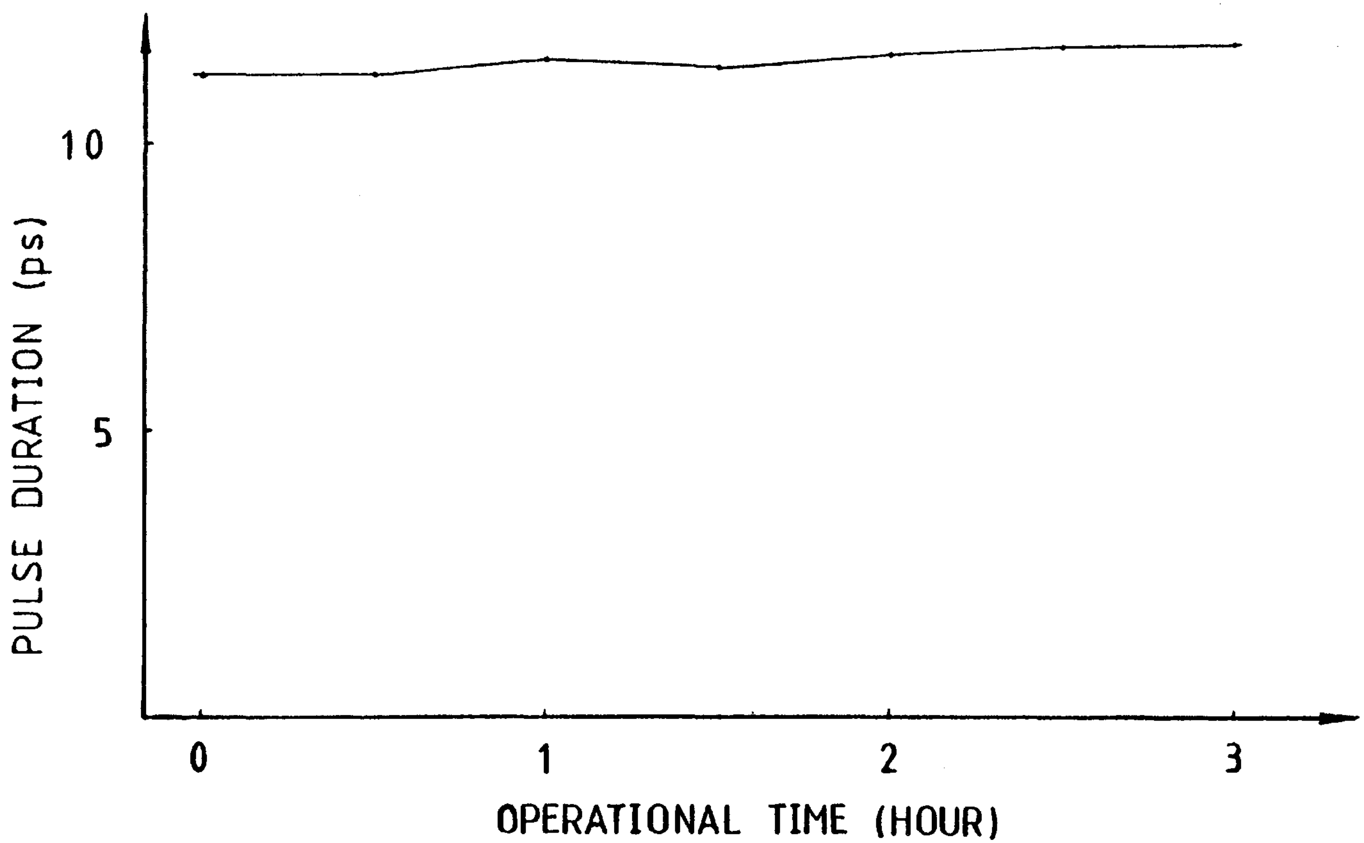

Fig.(6-9) Time stability of the pulse duration of an actively mode-locked Brewster-angled diode laser.

system include mechanical "relaxations" in optical mounts of the laser cavity. One possible solution to this could be to construct an external cavity using the optical fibres, where the fibres could be attached to the diode using a suitable epoxy having a matching refractive index.

6.6. Frequency-tuning methods for the mode-locked Brewster-angled diode lasers

Mode-locking and frequency-tuning techniques have been combined in experimental external cavity Brewster-angled diode lasers. In principle, there should not be much difference in the tuning range and the pulse duration between lasers using different intracavity frequency-tuning elements, such as the Fabry-Perot etalon or the diffraction grating. In practice, however, the results presented in this section were obtained for cavity configuration C3 for the reason given in Section 6.2.1. The pulse durations at different wavelengths could, therefore, be compared with each other at the same modulation frequency.

The effect of arm imbalance has been observed in the actively mode-locked Brewster-angled diode laser operating in C3. It was desirable that the diode be positioned in the middle of the cavity. Olsson et al [5] have reported that the linear cavity (similar to C2 without the etalon) was sensitive to small fluctuations of the cavity length when the two arms were of equal length. With the diode in the middle of the cavity and the system modulated at twice the cavity mode spacing, the two pulses circulating inside the cavity could meet at the diode and experience gain. Under these conditions, pulse shortening can be enhanced by a standing wave set up in the active medium due to the counterpropagating pulses. This would deplete the gain with greater effect than that due to a single unidirectional pulse as reported by May et al [26] for their synchronously pumped ring cavity CW dye laser.

Experimental observations indicated that there existed an optimum position for the moveable output mirror, as shown in Fig. (6-10). Under this condition the laser produced the shortest pulses. For a distinct cavity length different from this, the modulation frequency could be adjusted to secure the best pulsewidths but they were longer than this optimum value. It is therefore concluded that this implies that a proper balance may have been achieved between the two arms of the cavity. The experimental results have also shown that the pulse duration was not sensitive to the one-arm-variation within $\sim 50\mu m$ if the appropriate modulation frequency was used. This was probably because the temporal difference between the arrival times of the two counterpropagating pulses at the gain medium was much less than the transit time of the pulse through the diode chip ($\sim$6ps), and in practical terms, these

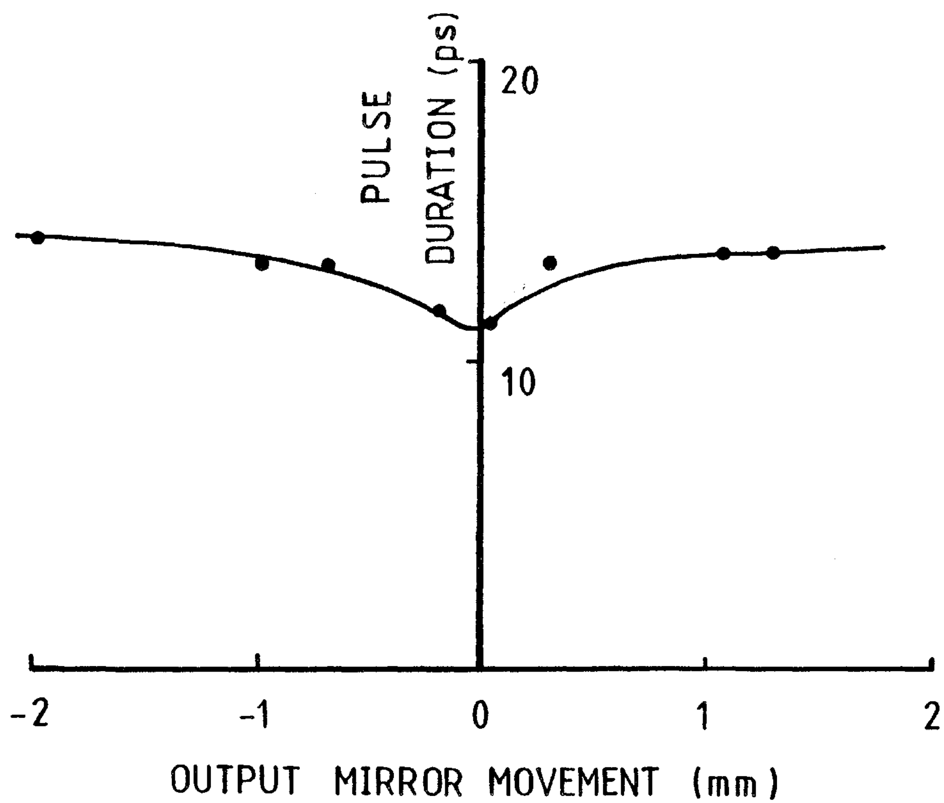

Fig.(6-10) Pulse duration changes with one-arm-shift of the cavity from the optimum length.

two pulses could still be regarded as arriving simultaneously at the gain medium. When the diode was positioned away from the cavity centre (by >100μm) the two pulses reflected back from the end reflectors could no longer be considered as reaching the gain medium simultaneously, so the greater gain depletion effect due to the standing wave built up in the active region by the counterpropagating pulses would be attenuated, and longer pulse durations are to be expected. If the diode was 750μm away from the cavity centre, then one pulse would approach the diode when the other had just left it, and there would be no standing wave effects in the diode. In this case, any enhanced gain depletion effects vanish, and the pulse which arrives first experiences different gain from the later one. Within one round-trip each pulse would meet the active medium at a non-optimum time at least once. This should further weaken the narrowing effect of the gain depletion on the pulse duration, and result in even wider pulses. Unfortunately, this was not experimentally checked in detail.

The experimental set-up for the frequency-tunable mode locked Brewster-angled diode laser was similar to that shown in Fig.(6-1a). The only difference was that after the system had been aligned, the avalanche photodiode was removed and the ∿30% output was focused onto the input slit of the monochromator. In this arrangement, both the output pulse duration and wavelength could be monitored simultaneously. In Fig.(6-11), pulse duration as a function of the lasing wavelength is shown. It can be seen that pulses of duration less than 20ps are produced over a 14nm tuning range. It can also be seen from this diagram that there is a "minimum" on the tuning curve but it could not be determined whether this minimum was due to the alignment of the laser or if it was linked to the wavelength characteristic of the gain peak.

In cavity C3, the tuning movement could alter the cavity length by only very small amount (less than 10μm) which in turn induced modulation frequency mismatch that could not even be compensated by the radio frequency generator (minimum adjustability corresponded to a variation of cavity length of ∿15μm). This effect would introduce an asymmetric feature to the tuning curve around the minimum. In this case, the arm imbalance effect was negligible because it was not sensitive to a 10μm cavity length shift.

Another possibility might be related to the medium gain which was wavelength dependent. The procedure of alignment had a consistent tendency of selecting the wavelength near the gain peak as the initial lasing wavelength. The experimental measurements had always started when the short pulses were observed. As a result, the wider pulses would always appear at wavelengths slightly removed from the peak wavelength of the medium gain.

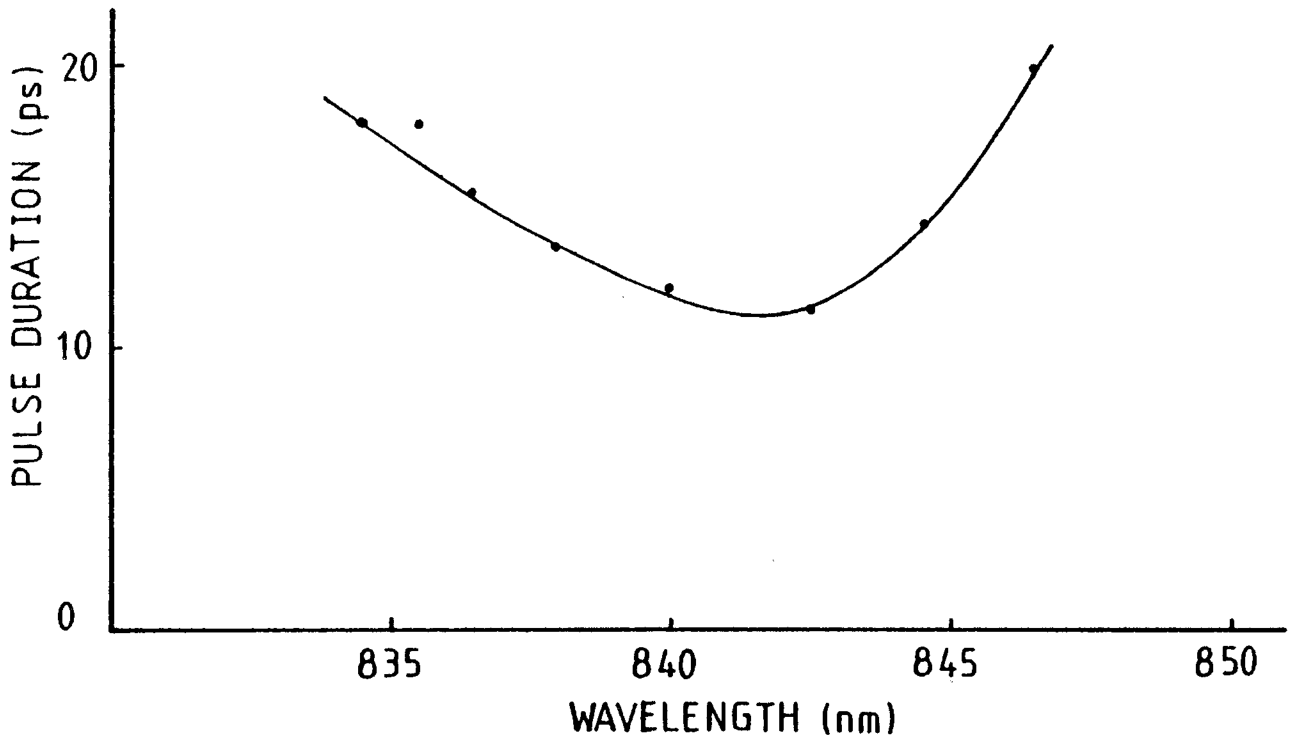

Fig. (6-11) Pulse duration as a function of lasing wavelength.

Lundquist et al [32] have reported that the minimum achievable pulse duration seemed to be dependent on the position of the emission line relative to the gain curve, and within a 20nm tuning range the pulse width had changed from 30ps to 50ps. This tendency is substantiated by the observations made in this work. Considering the slightly asymmetric feature of the tuning curve in Fig. (6-11), it seemed more likely that both factors may have been interactively involved.

Tuning spectra from a mode-locked Brewster-angled diode laser in a C3 cavity are shown in Fig. (6-12). Picosecond pulses of duration τ_p less than 20ps have been obtained over a spectral range of 14nm (which was almost the same as the tunability under the dc operation conditions).

6.7. Conclusions

In this chapter, actively mode-locked frequency-tunable Brewster-angled diode lasers have been described. Pulse durations and profiles have been recorded with the Synchroscan streak camera while the wavelengths were monitored by a photomultiplier with an S20 photocathode. Mode-locking experiments have been carried out in cavity types C2, C3 and C4. To date, the shortest pulse widths obtained were 9ps, and when the instrumental resolution limit of $\sim$7ps is deconvolved from this recorded

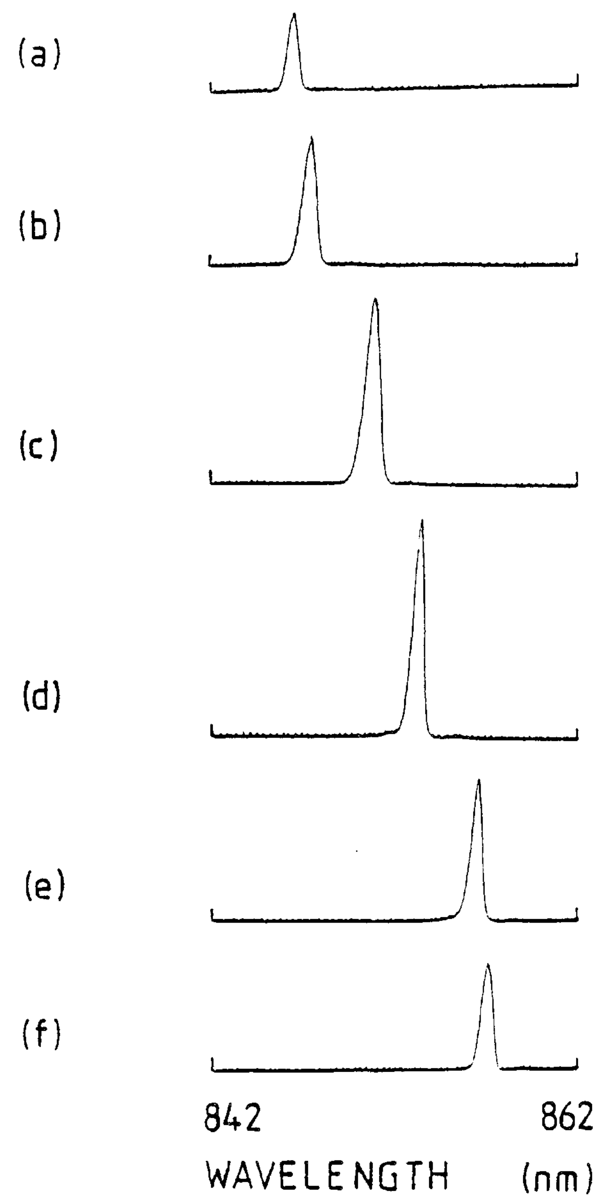

Fig. (6-12) Time-averaged output spectra from a frequency-tunable mode-locked Brewster-angled diode laser.

duration it may be concluded that pulsewidths less than 7ps have been generated from the actively mode-locked Brewster-angled diode lasers. It follows therefore that in the future a diagnostic system with better time resolution, for example, a Photochron IIA Synchroscan streak camera [13,14] which had a resolution of 1ps when used in conjunction with a passively mode-locked CW ring dye laser, is needed to obtain the more detailed information of the mode-locked Brewster-angled diode laser.

The spectral broadening under the mode-locking conditions has been observed. The origin of the spectral broadening has been attributed to the sweeping of the medium gain line from the shorter wavelength side to the longer side while the strong optical field propagated through the active region. This sweeping was due to the continuous reduction of the separation of the two quasi-Fermi levels arising from the depletion of the injection carriers when the pulse was interacting with the gain medium.

The effect of modulation frequency mismatch on the pulse duration and profile have been investigated by directly altering the modulation frequency. The experimental data have shown that the pulse broadening process with the mismatch was highly asymmetric about the optimum modulation frequency, with the pulse being broadened at a much higher rate for negative frequency mismatch than for the positive. An explanation has been given to account for this effect and experimental confirmations are discussed.

Experimental observations also indicated that the pulse duration was affected by the imbalance effect between the two arms of the linear cavity within which the diode was located. The ring cavity configuration has provided a simple solution to this problem.

Mode-locked pulses of less than 20ps have been tuned with an intracavity tuning element over a spectral range of 14nm which was about the same as that achieved under the dc operation conditions. These results indicated that the actively mode-locked, frequency-tunable Brewster-angled diode laser could operate at the time multiplexing and/or the frequency multiplexing regimes and would offer a potential capacity of very high bit rate for optical fibre communications [32].

References

[1] E. Mohn, Second Intern. Symposium on GaAs and related compounds, 101 (1968).

[2] P-T Ho et al, Appl.Phys.Lett., Vol.33, 241 (1978).

[3] M. B. Holbrook, W. E. Sleat, D. J. Bradley, Ibid, Vol. 37, 59 (1980).

[4] E. P. Ippen, D. J. Eittenberger, Ibid, Vol. 37, 267 (1980).

[5] A. Olsson, C. L. Tang, IEEE J. Quantum Electron., Vol. QE-17, 1977 (1981).

[6] J. P. van der Ziel, R. M. Mikulyak, J.Appl.Phys., Vol. 51, 3033 (1981).

[7] S. Akiba, G. E. Williams, H. A. Haus, Electron.Lett., Vol. 17, 527 (1981).

[8] R. S. Tucker, G. Eisenstein, I. P. Kaminov, Ibid, 552 (1983).

[9] J. P. van der Ziel et al, Appl.Phys.Lett., Vol. 39, 525 (1981).

[10] R. L. Fork, B. I. Greene, C. V. Shank, Ibid, Vol. 38, 671 (1981).

[11] P. G. May, W. Sibbett, J. R. Taylor, Appl.Phys., Vol.26B, 179 (1981).

[12] D. J. Bradley, "Methods of Generation", Ultra Short Light Pulses, Topics in Applied Physics, Vol. 18, (1977).

[13] M. D. Dawson, W. Sibbett, J. Vukusic, Appl.Phys.Lett., Vol. 43, 226 (1983).

[14] W. Sibbett et al, Proc. XV Int.Conf. High Speed Photography 1982, San Diego.

[15] C. P. Ausschnitt, R. K. Jain, J. P. Heritage, IEEE J. Quantum Electron., Vol. QE-15, 912 (1979).

[16] W. Sibbett, Ph.D. Thesis, Queen's University, Belfast, (1973).

[17] T. Ikegami, 1st European Conf. on Opt. Fibre Commun., 111 (1975).

[18] C. Lin, T. P. Lee, C. A. Burrus, Appl.Phys.Lett., Vol. 42, 141 (1983).

[19] K. Kishino, S. Aoki, Y. Suematsu, IEEE J. Quantum Electron., Vol. QE-18, 343 (1982).

[20] H. Kressel, J. K. Butler, "Semiconductor Lasers and Heterojunction LEDs", Academic Press, (1977).

[21] Y. Nishimura, Jpn.J.Appl.Phys., Vol. 13, 109 (1974).

[22] K. Stubkjaer et al, Ibid, Vol.20, 1499 (1981).

[23] M. B. Holbrook, Ph.D. Thesis, Univ. of London, (1980).

[24] A. Scavennec, Opt.Commun. Vol. 17, 14 (1976).

[25] D. M. Kim et al, Ibid, Vol. 27, 123 (1978).

[26] P. G. May et al, Opt. Commun., Vol. 42, 285 (1982).

[27] J. C. Goodwin, B. K. Garide, IEEE J. Quantum Electron., Vol. QE-19, 1069 (1983).

[28] J. AuYeung, Ibid, Vol. QE-17, 398 (1981).

[29] J. Chen, W. Sibbett, J. I. Vukusic, Opt.Commun., Vol. 48, 427 (1984).

[30] T. Kobayashi et al, J. Opt.Soc. America, Vol. 70, 667 (1980), Vol. 43, 715 (1983).

[31] J. Chen, W. Sibbett, J. I. Vukusic, Electron.Lett., Vol. 18, 426 (1982).

[32] S. Lundquist, T. Anderson, S. T. Eng, Appl.Phys.Lett., Vol. 43, 715 (1983).

Chapter 7

BREWSTER-ANGLED DIODE AMPLIFIERS

7.1. Introduction

Optical amplifiers, with dimensions compatible to optical fibres and elements of integrated optics can be made from semiconductor materials which have very high gain coefficients. Yamamoto et al [1,2] investigated the performance of an ordinary GaAlAs semiconductor diode, biased just below its threshold, as an amplifier. They found that the minimum detectable power (giving a 10^{-9} error probability) of a photodiode located after the amplifier was reduced by 15-20 dB compared to a direct photodiode detection system, and by 3-4 dB compared to a low-noise avalanche photodiode detection system. Meanwhile, Yamamoto [2] has outlined the possibility of introducing more than thirty amplifiers at λ=850nm and data rates B=100Mbit/s between two electronically regenerating repeaters. It was pointed out that if the semiconductor laser amplifier at λ=1.5μm exhibited a performance similar to the AlGaAs amplifier with a signal gain of 25dB and an input saturation power of -35dBm, the maximum number of repeaters became more than 70 at B=100Mbit/s [2]. This indicates that the loss problem would no longer be the major obstacle for a long distance optical fibre communication system if one considers that the fibre loss has been reduced to 0.2dB/Km [3].

The use of semiconductor diodes as laser amplifiers dates back to the early years of semiconductor laser research. In 1963, Coupland et al investigated the amplification action of an AR coated GaAs diode which had had a threshold current of about 5A before coating and showed no laser action at currents up to 30A after coating [4]. Adopting the following definition for the system gain,

$$\text{system gain} = \frac{\text{(total light reaching detector)} - \text{(amplifier self emission)}}{\text{(light reaching detector when amplifier is bypassed)}} \qquad (7-1)$$

they obtained a system gain of 2 at a current of 22A. Shortly afterwards, Crowe et al [5] reported experimental results for a diode amplifier. The gain medium used was also an AR coated diode which, they claimed, did not reach threshold with bias currents up to ten times the uncoated diode threshold current. The system gain was measured by first removing the amplifier from the field of view of the microscope objective and measuring the oscillator intensity; then the amplifier was brought back into alignment with the oscillator and the total output from the amplifier was measured. They claimed that gains of 1000 had been obtained in their experiments.

In 1968, Kosonocky and Cornely [6] presented experimental results of the characteristics of GaAs diode amplifiers closely coupled to diode oscillators. The separation between the oscillators and the amplifiers ranged from 0.2 to 2.0μm; the other sides of the amplifiers were lapped at angles of 10-15 degrees to the waveguide direction. They reported that the measured signal gain was a decaying function of the input power and approached a value of 2 to 4 for large input signals.

Recently, Kobayashi and Kimura [7], and Yamamoto et al [2] investigated the Fabry-Perot type semiconductor diode amplifiers biased below threshold. These amplifiers provided a gain coefficient of $36cm^{-1}$, and could be operated in a "multiple-pass" mode in order to obtain higher system gain. This type of amplifier suffered from several major setbacks which would greatly limit its usefulness.

Firstly, because the amplifier should not operate in the oscillating mode, the bias current was, therefore, set below the threshold of the diode. The upper limit of the gain coefficient was, thus, set up by the diode threshold rather than the material damage threshold.

Secondly, the operating conditions had to be controlled very accurately. In reference 8, Marcuse pointed out that the amplifier must remain carefully tuned to the input siganl (from the oscillator or the previous amplifier), and its current must be highly stable to prevent gain fluctuation and lasing. Longitudinal-mode wavelength matching between the oscillator and the amplifier was very critical. From Reference 2, it can be found that for an input signal of 100Mbit/s, amplifier current deviation of 0.5mA from the value satisfying the resonant condition, would increase the error probability from 10^{-9} to 10^{-5}. Kabayashi et al [2] have measured that a wavelength shift of 0.013nm from the peak wavelength of the gain would result in a reduction of 3dB in the gain. A temperature variation of 0.16K in the amplifier active region could induce this wavelength shift [2]. This would impose an enormous difficulty on the amplifier operation if the oscillator is to be operating in the frequency multiplexing regime. In particular, the critical control of the operating temperature of the amplifier would make it difficult to use these amplifiers in field application. On the other hand, because the wavelength matching between the oscillator and the amplifier is crucial, the spectral width of the input signal is confined. If a bandwidth of 0.013nm is taken as a limiting figure for the input signal, then the duration of the input pulse must be longer than 75ps for a Gaussian pulse at λ=850nm, otherwise distortion of the pulse shape is likely to arise. Attempts of increasing the bit rate in a time multiplexing regime could therefore be frustrated.

It seems that the Brewster-angled diode amplifier is an appropriate alternative with which to tackle the problems mentioned above. The bias current of the amplifier can be substantially higher than the usual threshold level for a zero degree diode and is ultimately limited by the damage threshold of the material. Moreover, the wavelength match between the oscillator and the amplifier is no longer critical provided the wavelength of the oscillator is encompassed by the bandwidth of the gain curve of the amplifier (14nm for the Brewster-angled diode used in this work). In this chapter, experimental results using the Brewster-angled diode as an amplifier will be presented.

7.2. Experimental Arrangement for the Brewster-Angled Diode Amplifiers

The Brewster-angled diode has been employed to amplify the output from the laser of the same material. The experimental set-up is shown in Fig. (7-1). The details of the external cavity diode laser have already been presented in Chapter 5, Section 5.3. The input beam from the oscillator was focused into the active region of the amplifier diode through a 20X microscope objective (MO). The output of the amplifier was collimated by another identical microscope objective and directed into the detection head of the optical power meter (OPM). Sometimes, the optical power meter was not in place, in which case the amplifier output was partly collected by a photodiode (PD2), used to align the system, and the remainder ($\sim$70%) was fed into a monochromator. The output power of the oscillator

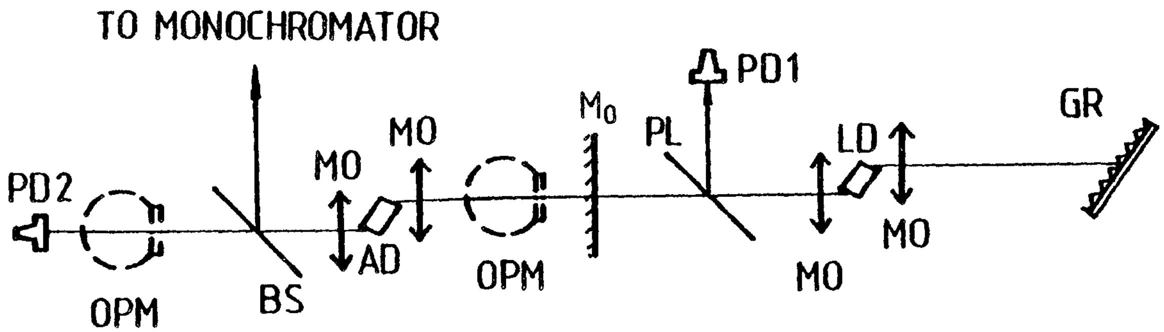

Fig. (7-1) Experimental set-up of the Brewster-angled diode laser and amplifier.

was measured by positioning the detector head of the optical power meter in front of the input microscope objective of the amplifier. There was no optical isolation between the laser and the amplifier. The experimental results showed that the amplifier had no observable effect on the output spectrum of the oscillator and little effect ($\sim 5\%$) on the output power measured by photodiode PD1. Both the microscope objectives and the amplifier diode mount were controlled by x-y-z translation stages, and piezoelectric devices have been used to adjust the movements of the input microscope objective.

(It is appropriate to point out that throughout the rest of this chapter, subscripts "L" and "A" will be used to refer to laser and amplifier parameters, respectively).

7.3. Characteristics of Brewster-angled diode amplifiers

After the system was aligned, the output power of the amplifier (P_A) as a function of the bias curent (I_A) was recorded with the output power of the oscillator (P_L) as a defining parameter (see Fig. (7-2)). Similarly, another curve Fig. (7-3) was obtained by fixing the injection current of the amplifier while changing the output power of the laser (via the bias current of the laser). From this diagram, it is clearly seen that the output power of the amplifier increases with the input power. In Figs. (7-2) and (7-3), it is also apparent that when the injection

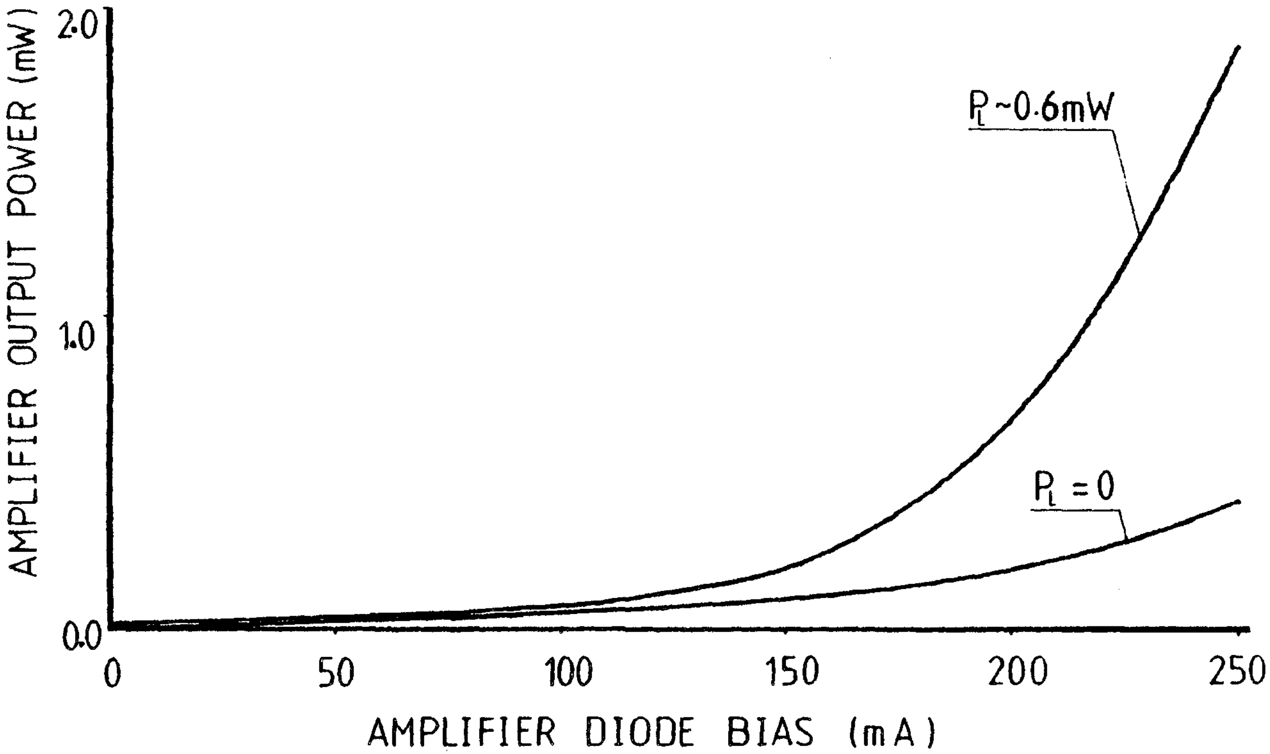

Fig. (7-2) Output power of the Brewster-angled diode amplifier as a function of the bias dc current.

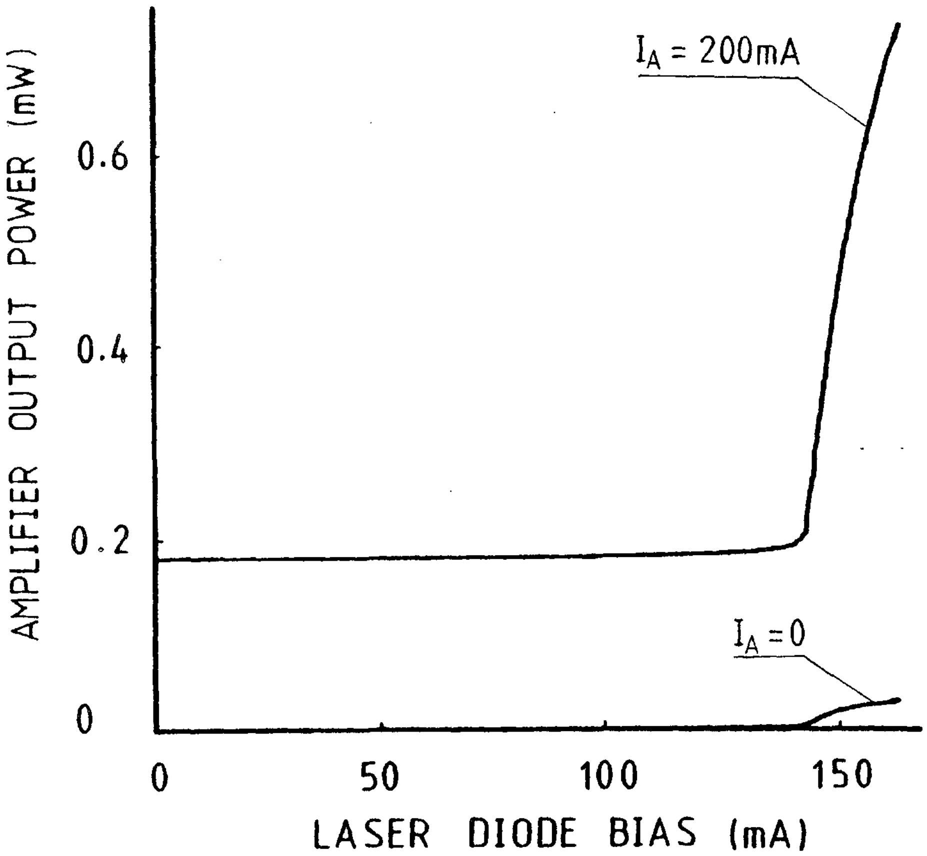

Fig. (7-3) Variation of the output power of a Brewster-angled diode amplifier as a function of input laser power (via laser bias current).

current of the amplifer is zero, there is still some light from the oscillator passing through the amplifier and reaching the detector. In the latter case, P_A at I_L=0 represents the spontaneous emission power of the amplifier diode.

The far field patterns of the Brewster-angled diode amplifier have been taken through an infra-red image converter under the conditions $P_L \neq 0$ and $P_L = 0$, and are shown in Fig. (7-4a and b) respectively. When the input power to the amplifier was zero, the output pattern of the amplifier was, in fact, the spontaneous emission of the Brewster-angled diode collimated by the microscope objective. When the laser output was fed into the amplifier, a very bright area could be seen on the far field pattern of the amplifier output. This area is believed to be due to the amplified input signal. The complex fine structures of these patterns arising from the combination of such effects as the refraction near the Brewster angle of the material, the diffraction associated with the dimensions of the light source, the distortion due to the microscope objective and the waveguide effect of the heterostructure, are now the subject of further studies, which hopefully will reveal the nature of these fine substructures in the far field patterns [9].

Amplifying action has also been confirmed by the output spectrum of the amplifier. In Fig.(7-5), the output

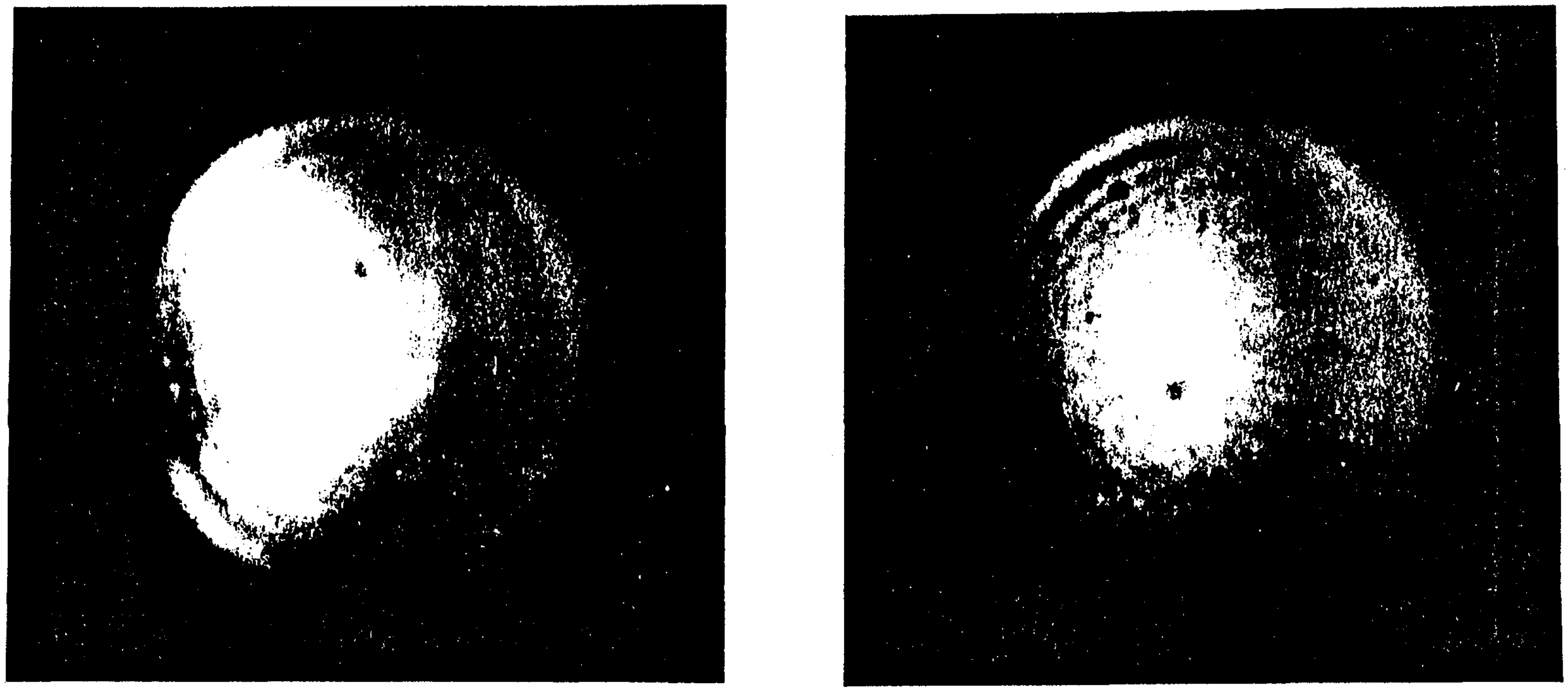

(a) (b)

Fig. (7-4) Far field patterns of the Brewster-angled diode amplifier biased at ~250 mA, (a) with, and (b) without the input signal.

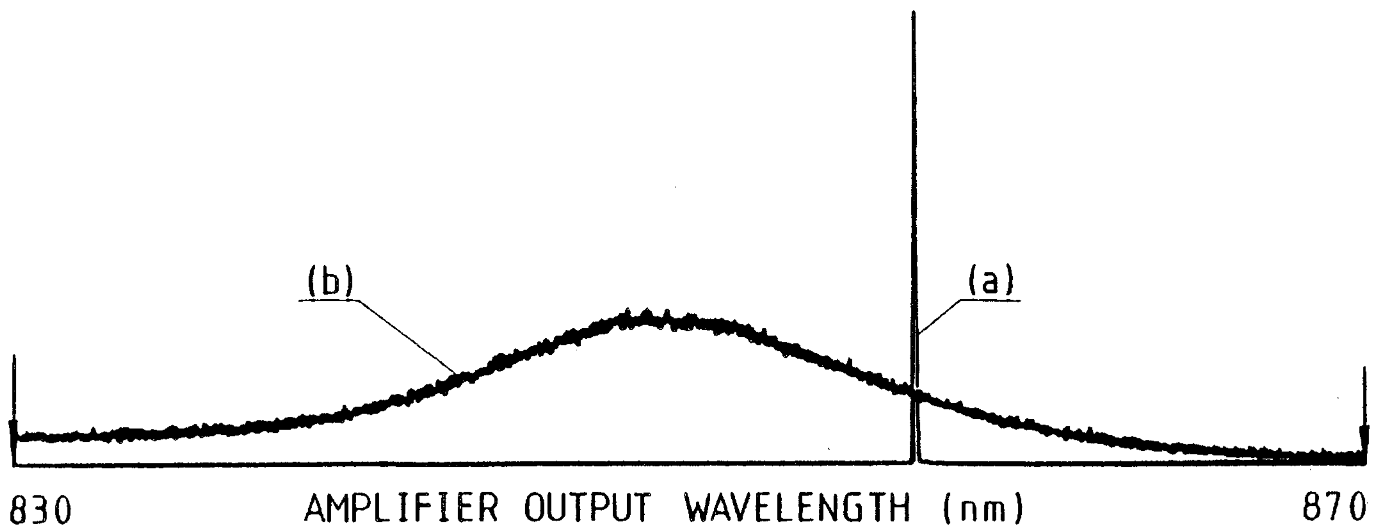

Fig. (7-5) Output spectra from a Brewster-angled diode amplifier biased at I_A ~200mA; (a) with and (b) without an input signal.

spectra of the amlifier at I_A=200mA are shown (a) with and (b) without an input signal (the vertical scale of (a) is 100 times larger than that of (b)).

In Fig.(7-6), the output spectra of a Brewster-angled diode amplifier are displayed for three different bias levels: (a) I_A=200mA, (b) I_A=100mA and (c) I_A=0 with the input power remaining unchanged. The vertical scales of the three spectra are as indicated on the diagram. This figure shows that the amplified signal power increases with the bias current of the amplifier.

The output spectra of the Brewster-angled diode amplifier have also been recorded for different input powers (see Fig. (7-7)). Here, it should be pointed out that the input power of 600μW marked in Fig.(7-7) was the laser output power measured by an optical power meter, other values were controlled by the calibrated density filters. Nevertheless, as pointed out by Kosonocky et al[6], the power actually coupled into the amplifier should be proportional to the laser output and was, therefore, used as the input parameter of the amplifier which corresponded to "perfect" coupling conditions (or a coupling coefficient of unity). The spectrum represented by Fig.(7-7a) is a characteristic feature of the diode amplifier. For the Brewster-angled diode laser, the contrast between the narrow peak of the lasing line and the broad background due to the spontaneous emission was much higher (at least a thousand

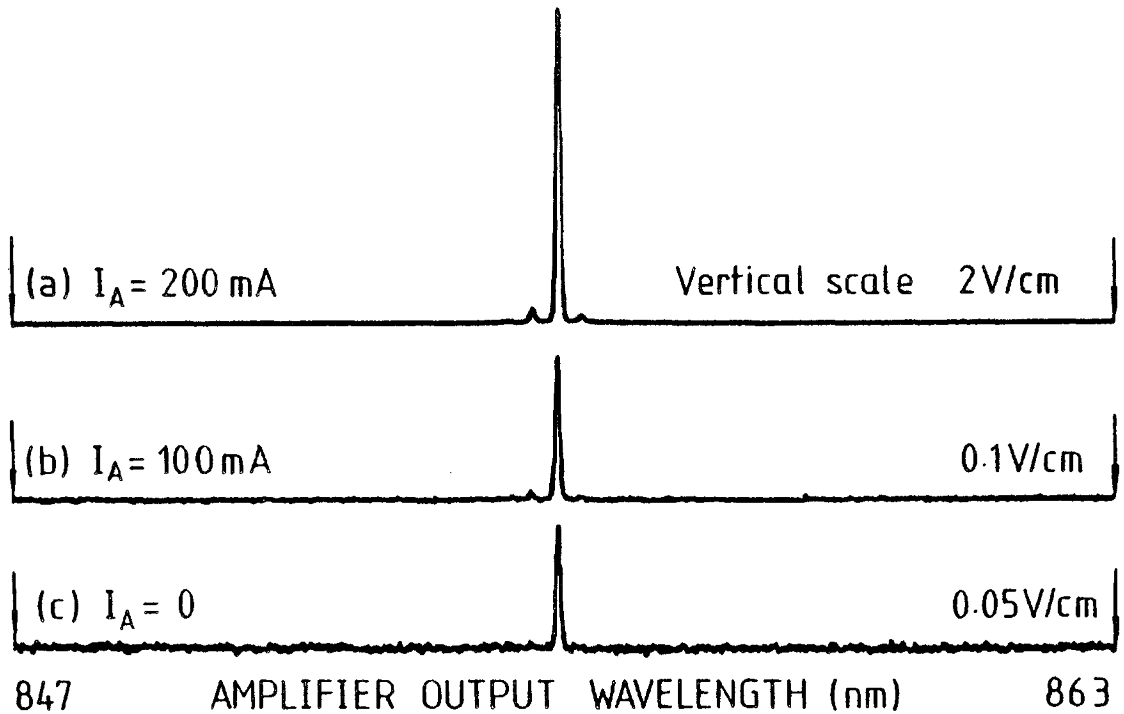

Fig. (7-6) Output spectra of a Brewster-angled diode amplifier at bias currents (a) $I_A \sim 200mA$ (b) $\sim 100mA$ and (c) 0.

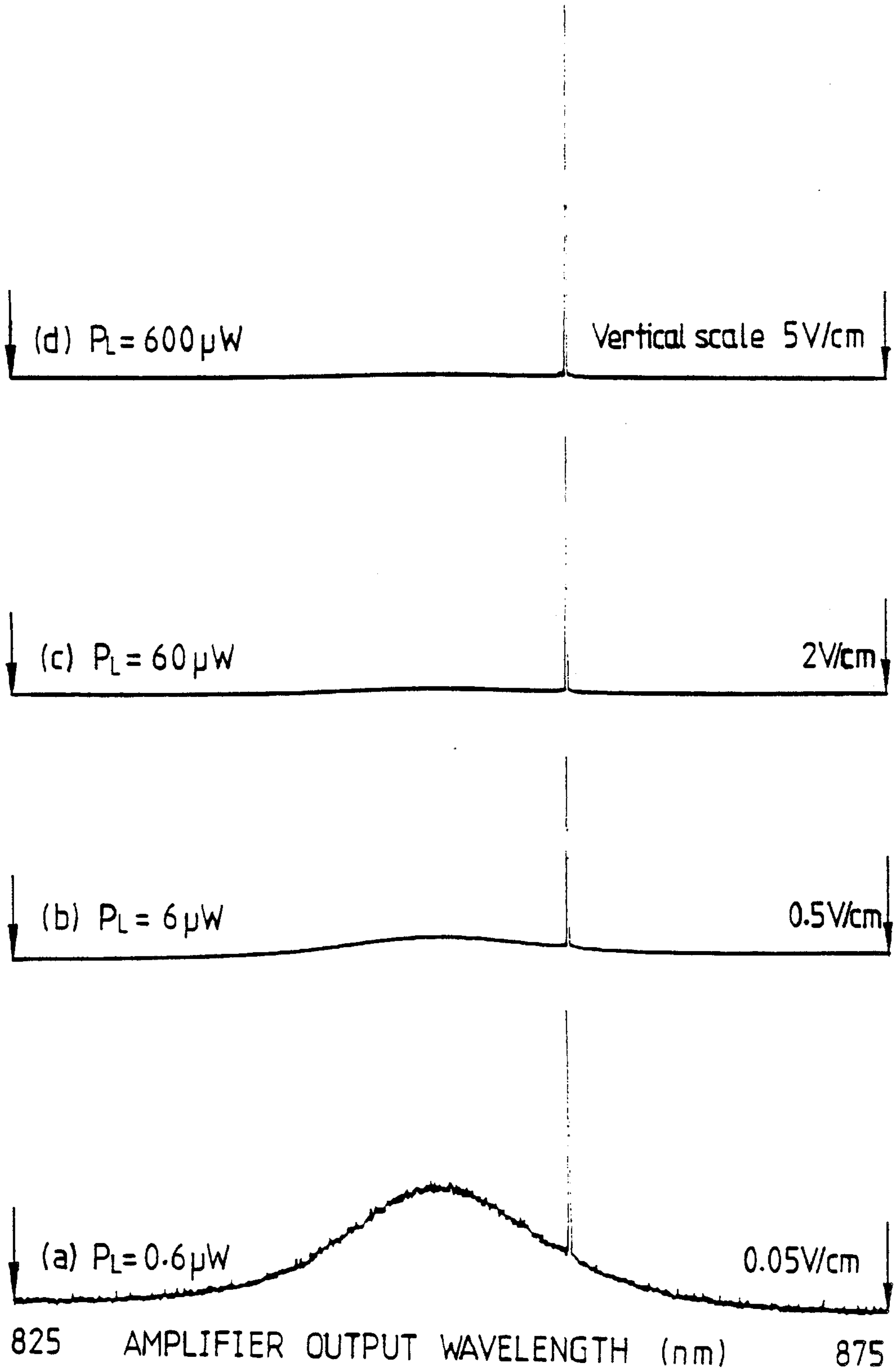

Fig.(7-7) Output spectra of a Brewster-angled diode amplifier for different input powers (I_A ~200mA).

times) than that between the narrow peak and the peak of the spontaneous emission shown in Fig. (7-7a).

In order to observe the variation of the spontaneous power from the amplifier, the vertical scale of the recording system was deliberately kept unchanged at different input levels. The results are shown in Fig.(7-8) for laser powers of (a) P_L=0, (b) P_L=6μw and (c) P_L=600μw, respectively, while the bias current of the amplifier remained constant at 200mA. Comparing these curves, it can be concluded that there was no observable change in the recorded background, although the output of the amplifier at the input wavelength varied with the input power level. These observations therefore justify the numerator of equation (7-1) for the input power used in this work.

Meanwhile, the effect of the spontaneous emission of the amplifier on the operation of the oscillator has also been investigated because there was no optical isolation device between them. In Fig.(7-9), output spectra of the Brewster-angled dioe laser are shown for amplifier bias currents of I_A=0 and 250mA respectively. These curves show no observable effect of the amplifier on the output spectrum of the laser. The total output power from the oscillator, monitored through the pellicle/photodiode PD1 system, has however been observed to have increased slightly (∿5%). This might have been due to part of the spontaneous emission from the amplifier passing through the output mirror of the

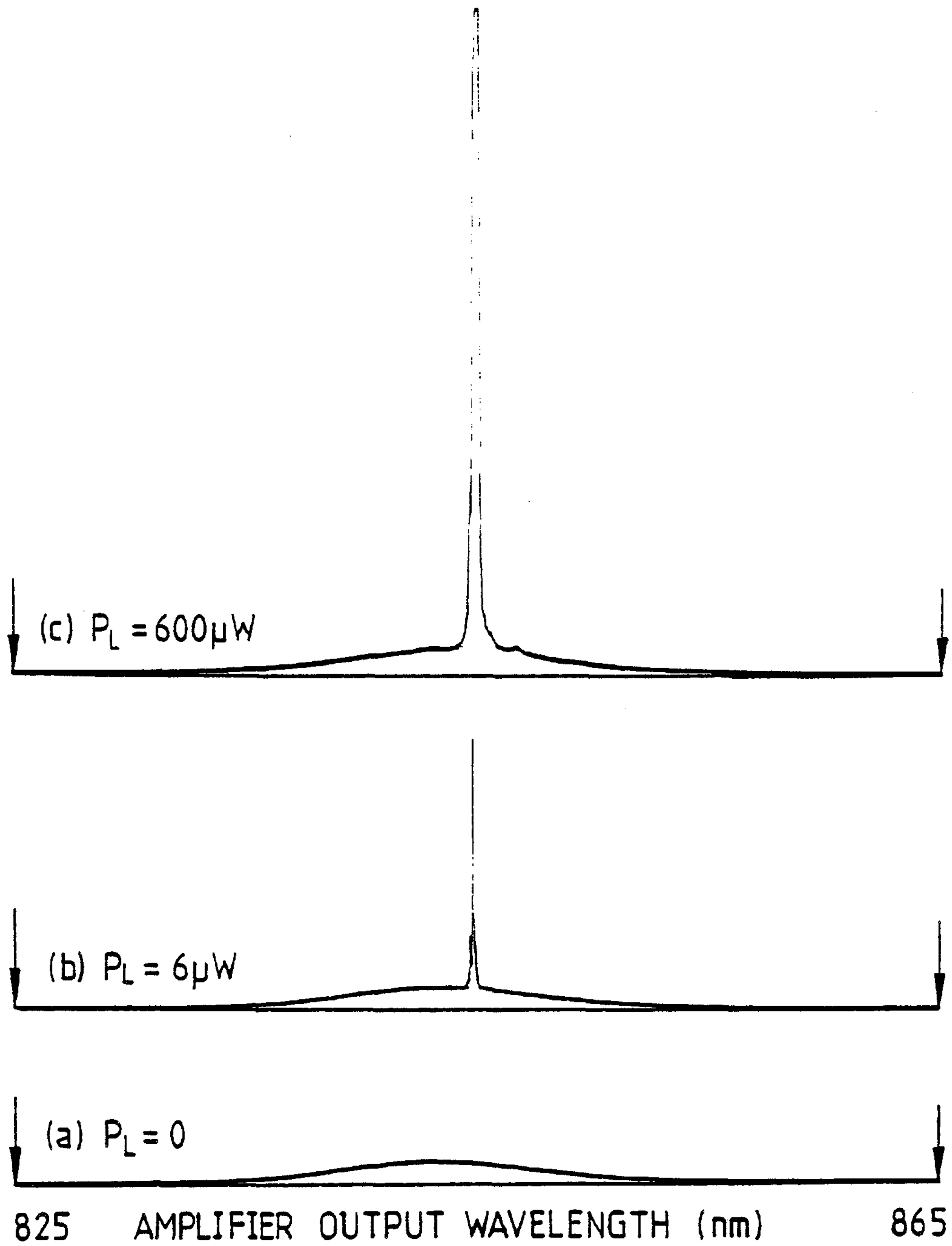

Fig. (7–8) Backgrounds of the output spectra of a Brewster-angled diode amplifier at different input powers ($I_A \sim 200$ mA).

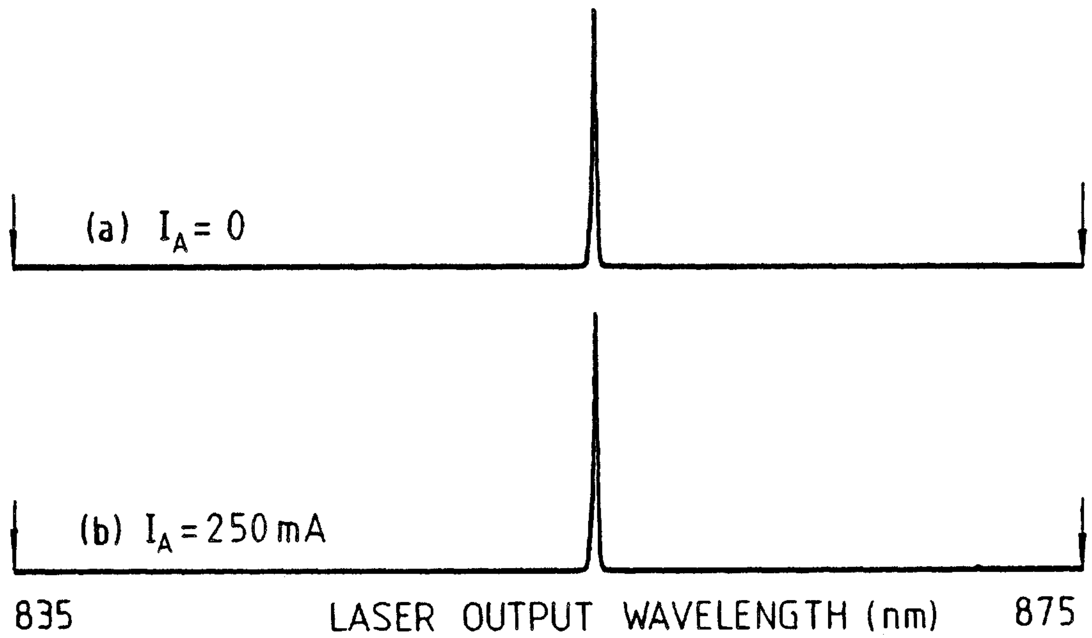

Fig. (7–9) Output spectra of a Brewster-angled diode laser for amplifier currents $I_A = 0$, and ~ 250mA .

oscillator (M_o), entering the laser diode and finally, after being amplified by the oscillator diode, striking the detection system. Because the light from the amplifier is distributed within a spectral width of 14nm, it follows that only a very small contribution to the stimulated output would be involved, and this increment in the total output power could only be registered by the photodiode PD1 which indiscriminately accepted all the incident photons. Moreover, the experimental arrangement afforded some isolation from the amplifier to the laser, so this would reduce the effect of the amplifier on the oscillator. This isolation arose from the lack of parallelism between the axes of the laser and the amplifier, which as already reported [5] is not critical to the operation of the amplifier.

7.4. System Gain

At present, it is difficult to determine the actual gain of the diode amplifier, because of the fact that the coupling coefficient (defined as the ratio of the light coupled into the active region of the amplifier diode to the incident power) cannot be readily established. A method has been designed to measure the gain of the multiple-pass Fabry-Perot type diode amplifier [2,7], but unfortunately this cannot be applied to the single-pass amplifier used in this work. With reference to Kosonocky [6] and Coupland

[4], the gain of the amplifier used in this work is defined as

$$G(P_L, I_A) = \frac{P_A(P_L, I_A) - P_A(O, I_A)}{KP_L} \qquad (7\text{-}2)$$

where P_L is the power measured at the entrance of the input microscope objective; $P_A(P_L, I_A)$ is the amplifier output at current I_A when the power incident onto the front of the microscope objective is P_L; $P_A(O, I_A)$ is the spontaneous emission of the amplifier biased at current I_A; K is the coupling coefficient, and $G(P_L, I_A)$ is the gain of the amplifier at current I_A and input power P_L. In the following discussion, the frequently used term "system gain" is obtained by letting K=1 in equation (7-2).

In fact, the coupling coefficient K can be regarded as the product of two factors x^2 and y, where x represents the transmissivity of the microscope objective and y denotes the ratio of the light coupled into the active region of the amplifier diode to that transmitted through the input microscope objective. The value for x has been measured to be ∿75%, and y was estimated as follows. The average threshold for the zero degree diode (with identical dimensions and fabricated by the same manufacturer) could be inferred from reference 10 to be 141mA, while that of the Brewster-angled diode laser was experimentally measured to be 155mA (see Chapter 4). In the former case, the equivalent loss coefficient attributed to the transmissivity of the diode facets could be estimated as $23cm^{-1}$ (for a facet reflectivity of 0.32). For the external cavity (C2) laser incorporating the Brewster-angled diode, extra losses were due to the transmissivity of the output mirror ($R\sim75\%$), the transmissivity of the microscope objectives ($x\sim0.75$), the coupling coefficient from the microscope objective to the active region of the diode (y), the reflection loss of the pellicle ($r<8\%$), coupling loss from the diode to the microscope objective (α_1), and the absorption of the atmosphere within the cavity (α_2). The last two items contributed very small losses to the system, and could therefore be omitted. According to reference 11, the medium gain coefficient g satisfies

$$g = A(J-J_t) \qquad (7-3)$$

where J is the injection current density, J_t is a constant at which the gain coefficient becomes positive, and the constant A is equal to $0.045cm^{-1}/(A.cm^{-2}.\mu m^{-1})$. Using the current I as the variable, equation (7-3) becomes

$$g = A(I-I_t)/(sd) \qquad (7-4)$$

where s is the area of the diode stripe, and d is the thickness of the active region. Substituting the experimental parameters of $s=9x10^{-5}cm^2$, $d=0.2\mu m$ into this equation, it can be deduced that

$$g = 2.5\ (I-I_t) \qquad (7-5)$$

where g is in cm^{-1} and I in mA. The extra gain coefficient needed for the Brewster-angled diode laser operating in the external cavity C2 could be estimated to be

$$\alpha_{extra} = 2.5 \times (155-141) = 35cm^{-1} \qquad (7\text{-}6)$$

It was therefore concluded that the external cavity system would have a loss coefficient $\sim 58cm^{-1}$ which accounted for the various losses of the laser (excluding the free carrier absorption, scattering losses of the active medium, which would be the same for both a zero degree diode and a Brewster-angled diode). By considering the light in the external cavity during one round-trip, it can be seen that

$$-\frac{1}{2l}\{\ln R + 4\ln x + 2\ln(1-r) + 2\ln y\} \sim 58cm^{-1} \qquad (7\text{-}7)$$

where l is the length of the diode (500μm). Using the experimental parameters, it was estimated that y ranged from 11.3% (for r=0) to 12.3% (for r=8%). These values are in good agreement with the figure 13.3% reported by Kobayashi et al [7].

In Fig. (7-10), the system gain (using equation (7-2) with K=1) is plotted against the bias current I_A of the amplifier for the laser output P_L=0.6mW. Taking X=0.75 and y=0.12, the gain of the diode amplifier at I_A=300mA is more than 50. This figure is much smaller than the so-called small signal gain G_s which is supposed to be equal to $\exp(g_o l)$, where g_o is the peak gain coefficient of the

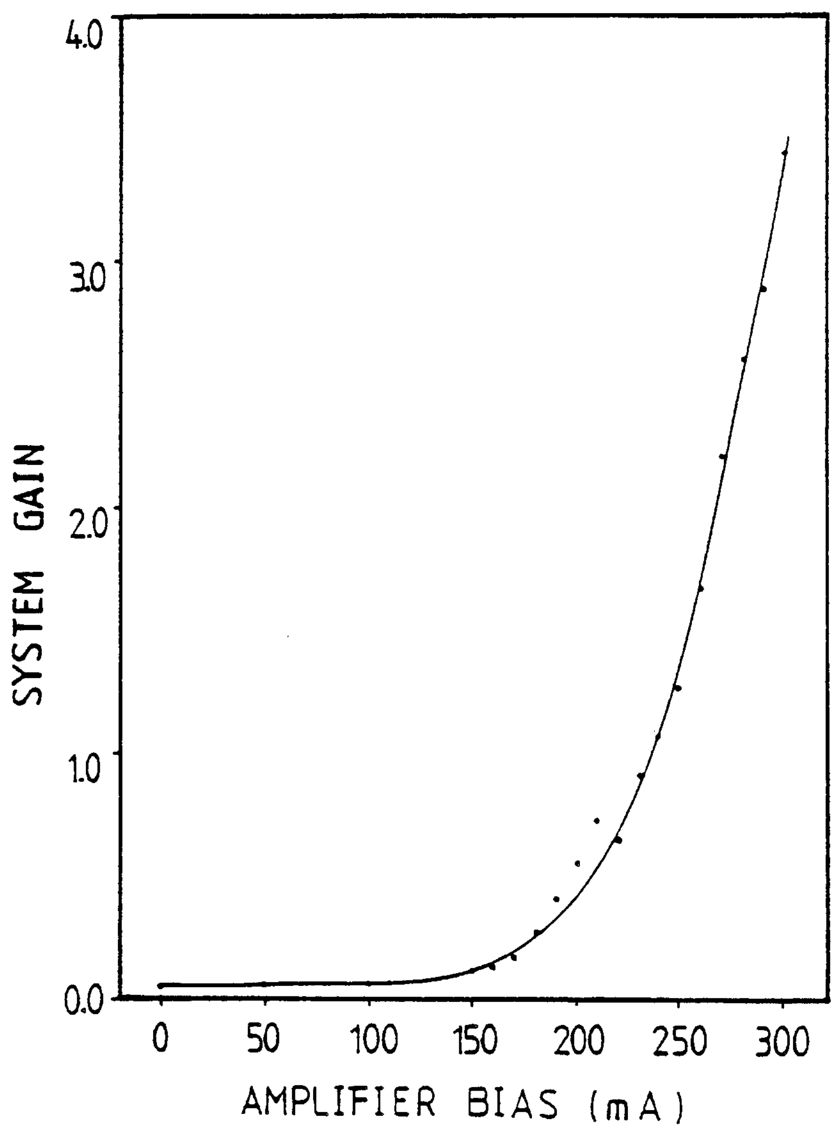

Fig. (7–10) System gain of the amplifier as a function of amplifier bias current.

active medium. One likely reason is that the carrier density, in the presence of gain depletion by the input signal, could not be maintained as high as for the case of small signal operation. This can be understood from the rate equation for carrier density N [12],

$$dN/dt = I/(eV) - N/\tau - B(N-N_o)S \qquad (7-8)$$

where I is the injection current, V is the volume of the active region, τ is the lifetime of the injection carrier, S is the photon density, and B and N_o are constants. The small signal gain was obtained by letting S=0, in this case the carrier density would be at a high level ($\bar{N}$). When the third term on the right hand side of equation (7-8) was taken into consideration, the carrier density N would be smaller than $\bar{N}$. If S is very large the situation would be similar to a laser, and the gain coefficient would be maintained at a very low level (in a laser, it is maintained at the threshold level). Another reason was that when the signal was travelling in the active region, it became stronger and stronger with increasing distance from the input facet. The saturation effect would thus become increasingly stronger, with the direct consequence that the amplifying action would become less and less effective. As a result, the observed gain would be much smaller than the small signal gain.

The system gain of the Brewster-angled diode amplifier at I_A=200mA has also been measured for different input powers, and this is presented in Fig.(7-11). Here, the laser output power was 0.75mW, while the laser input power to the amplifier was controlled with calibrated neutral density filters; the system gain was calculated from equation (7-2) with K=1. From this diagram, it can be seen that the system gain increases with the reduction of the input power as expected. At a lower input level, the carrier density should be kept at a higher level than that at a higher input, therefore the gain should be larger for the former case. Also, the saturation should be less prominant for a smaller input power, resulting in a higher gain.

The measurement was limited by the accuracy of the detection system. when the input power in front of the microscope objective was reduced to ∿75μW, the power difference between the outputs of the amplifier with and without the input became comparable to the spontaneous emission power of the amplifier. Afterwards, the "signal power" becomes smaller than the "noise power" if the spontaneous emission was regarded as the noise. Using a narrow band filter (∿5nm at the laser wavelength), the noise power could be reduced by more than half, and the results for an input level of -20dB was considered reliable. At -30dB input level, the amplitude of the amplified signal became comparable to the peak of the spontaneous emission

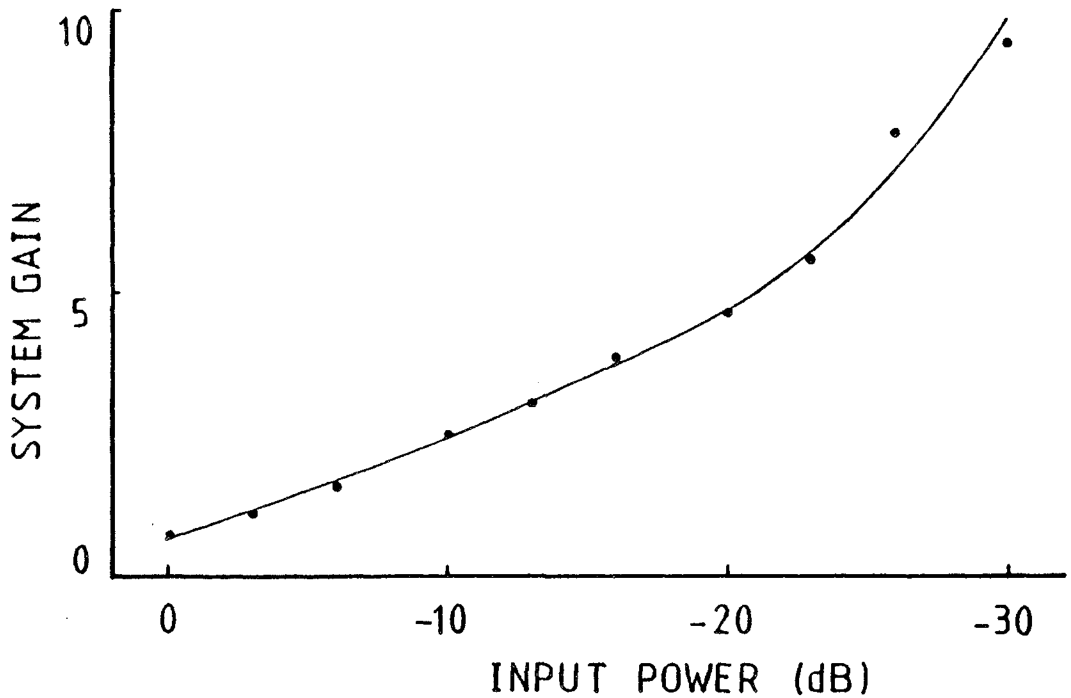

Fig. (7-11) System gain (at $I_A \sim 200mA$) as a function of the input power.

(see fig. (7-7)). Kobayashi et al [7] have carried out their experiment at an input power of -60dBm and claimed that the small signal gain has been obtained. From Fig. (7-11), with the coupling coefficient taken into consideration, it can be seen that an amplifier gain of about 140 has been achieved for the input power of ∿67nW at a bias current of 200mA.

In the pulsed input case (pulse repetition rate ∿320MHz), a system gain ∿20 has been observed for an average input power (incident on the microscope objective) ∿5μW, at a bias current of 250mA. These experimental observations were made with the avalanche photodiode/sampling oscilloscope combination. The input power of the amplifier was measured on the scope by removing the amplifier diode and aligning the optical system. The amplifier was then positioned and aligned, and the output of the amplifier was displayed on the scope. Taking the coupling coefficient from the microscope objective to the amplifier diode to be 12%, the actual gain of the diode amplifier at 250mA was ∿167. Again, this figure was much less than the theoretical limit. For a bias current of 250mA, there were $\tau(I-I_t)/e$ carriers avilable. If $(I-I_t)$ ∿125mA, the available number of carriers would be ∿7.8×10^8. Neglecting the spontaneous loss and the increment due to the pumping while the pulse was travelling in the active region, a "total" depletion of these carriers would generate an energy

$\sim 1.8 \times 10^{-10}$J at λ=850nm. If the depletion process was completed within the pulse duration, say 30ps, then the output power would be $\sim$6W. For an input pulse of about 4.5mW (peak power), the gain might be greater than one thousand. In practice, it was very difficult to harness all the carriers stored in the active region unless the input power was much larger than the saturation power of the medium. In this case, however, there could not have been much gain and the active medium only served as a transparent material. In this work, it has been observed that for an average input power (at the input microscope objective) $\sim$0.5mW, the system gain was $\sim$4, while for $\sim 5\mu$W the gain was observed to be $\sim$20. This showed the tendency of less gain for larger input.

7.5. Conclusions

In this chapter, preliminary experiments have been carried out with Brewster-angled diode amplifiers. It has been shown that this type of amplifier possesses the ability of amplifying any signal falling within its spectral bandwidth. Another merit of the Brewster-angled diode amplifier is that its bias current is limited by the operational temperature or the damage threshold of the material, therefore it can provide much greater small signal gain than a zero degree diode amplifier whose bias current is strictly confined below threshold.

It has been deduced that the gain of the amplifier was $\sim$140 for a CW input power $\sim$67nW at a bias level of 200mA, where the coupling coefficient from the microscope objective to the diode was estimated to be 12%. For the pulsed input signal (repetition frequency $\sim$320MHz), an amplifier gain of $\sim$167 has been observed for an average input power of 5μW (at the input microscope objective) at a bias level of 250mA, and this gain reduced to $\sim$33 for an average input of 500μW. It seemed that this type of amplifier might sustain a repetition rate of a pulse input somewhat higher than that used in this work ($\sim$320MHz) because the injection carriers seemed to be far from being "completely" depleted during the passage of the pulse through the active medium. In fact, if some method might be designed to couple more than one signal into the amplifier diode, several signals would be amplified simultaneously.

References

[1] Y. Yamamoto, H. Tsuchiya, Electron.Lett., Vol. 16, 233 (1980).

[2] Y. Yamamoto, IEEE J. Quantum Electron., Vol. QE-16, 1047 (1980).

[3] T. Miya et al, Electron.Lett., Vol. 15, 106 (1979).

[4] M. J. Coupland, K. G. Hambleton, C. Hilsum, Phys.Lett., Vol. 7, 231 (1963).

[5] J. W. Crowe, R. M. Craig, Jr., Appl.Phys.Lett., Vol. 4, 57 (1964).

[6] W. F. Kosonocky, R. H. Cornely, IEEE J. Quantum Electron., Vol. QE-4, 125 (1968).

[7] S. Kobayashi, T. Kimura, Electron.Lett., Vol. 16, 230 (1980).

[8] D. Marcuse, IEEE J. Quantum Electron., Vol. QE-19, 63 (1983).

[9] D. W. Crust, Private communication.

[10] G. J. Aspin, J. E. Carroll, R. G. Plumb, Appl.Phys.Lett., Vol. 39, 860 (1981).

[11] G. H. B. Thompson, "Physics of Semiconductor Laser Devices", John Wiley and Sons, (1980).

[12] H. Kressel, J. K. Butler, "Semiconductor Lasers and Heterojunction LEDs", Academic Press, (1977).

Chapter 8

GENERAL CONCLUSION

An actively mode-locked frequency-tunable injection laser using a Brewster-angled GaAlAs diode as the gain medium operating in external cavity configurations has been constructed and investigated. The shortest pulses achieved were less than 7ps and a tunability $\sim$14nm has been obtained. With the aid of a repetitively-operating (Synchroscan) streak camera, both the pulse duration and profile have been monitored while changing the modulation frequencies in order to provide a better understanding of the evolution of the short optical pulses from this actively mode-locked regime. Part of the initial work was devoted to the development of a specialised type of diode mount with appropriate compatibility with the geometry of the Brewster-angled diode.

The pulse duration for the actively mode-locked laser system has been refined to the stage that a better diagnostic system is now required. This requirement could be fulfilled with a Photochron IIA Synchroscan streak camera, which demonstrated a resolution of lps when used in conjunction with a passively mode-locked CW ring dye laser. This could render the potential to refine the system further and thus the opportunity of studying the evolution of the pulses from actively mode-locked injection lasers in a more detailed fashion.

A rigid and compact structure employing optical fibres as the external cavity could be developed which could give the laser system more flexibilities, better stability and would consequently represent a further step towards the practical application of the system. The same idea could also be applied to couple a diode amplifier to the laser oscillator in order to achieve long distance optical communication. This laser or laser/amplifier system could be operated in frequency multiplexing and/or time multiplexing regime(s) and hence substantially increase the bit rates of the transmission lines.

Meanwhile the duration of the pulses could be further reduced in the ring cavity configuration which could make use of the "colliding pulse" effect and provide the chance of inserting saturable absorbers into the cavity. The key point would be in the identification of a suitable and durable saturable absorber with an appropriate absorption spectrum which could recover quickly enough so that the trailing part of the mode-locked pulse could be cut off in a desirable way.

Mode-locking and frequency-tuning techniques described in this work could also be extended to an InGaAsP/InP Brewster-angled diode laser. Coherent radiations of ps durations with more desirable wavelengths for the fibre-optic telecommunication systems may be expected from this extension.

Preliminary studies of the GaAlAs Brewster-angled diode amplifier have revealed some promising properties of this type of amplifier. The diode gain has been estimated at more than one hundred for both continuous and pulsed inputs. Further studies could be carried out which may perhaps provide useful information about the semiconductor material such as the detailed gain broadening mechanism and saturation features of the medium gain, and may display some characteristics of the interaction between the light and the semiconductor. Such developments are expected to lead to interesting new applications in which both linear and nonlinear optics will be exploited.

ACKNOWLEDGEMENTS

I am indebted to Dr. W. Sibbett for his excellent supervision throughout the course of this work and his deep insight into the problems involved.

I am grateful to Dr. J. I. Vukusic for his consistent encouragement and indispensable help, in collaboration with whom most of the research was carried out.

I would like to thank all members of the Photonics Group at Imperial College for practical assistance and advice. In particular, I would gratefully acknowledge the help of Dr. M. R. Baggs and Mr. D. W. Crust.

Thanks are also due to all the technical staff of the Optics Section, and especially to Mr. T. Bates and Mr. R. S. Morrison for making the diode mounts used in this work.

I would also like to thank Miss A. Begg for typing this thesis.

I wish to express my thanks to the Standard Telecommunication Laboratories, U.K., for providing the Brewster-angled diode employed in this research.

Financial support from the Chinese government is also gratefully acknowledged.

TUNABLE MODE-LOCKED SEMICONDUCTOR LASERS INCORPORATING BREWSTER-ANGLED DIODES

J. CHEN *, W. SIBBETT and J.I. VUKUSIC
Optics Section, Blackett Laboratory, Imperial College, London SW7 2BZ, UK

Received 31 May 1983
Revised manuscript received 19 September 1983

A Brewster-angled GaAlAs semiconductor diode laser has been actively mode-locked in external cavity configurations to provide tunability over 15 nm and pulse durations ~9.5 ps. High stability of spectral output and pulse duration has been observed.

Semiconductor lasers provide a wide variety of compositional tuning, and for a selected composition, some temperature [1] tuning can be applied. These lasers, unfortunately, do not possess sufficient phase coherence to be used in high performance coherent optical fibre communication systems and when operated with RF injection currents, do not produce pulses short enough to be used at ultrahigh bit rates. To produce high phase coherence, external line narrowing has to be used, either by external cavity feedback using a spectral narrowing element [2,3] or by HeNe laser injection locking which restricts the wavelength selection [4]. By this means, it has been possible to use semiconductor lasers in high performance optical fibre systems at bit rates of a few 100 M bits/s [5]. However, much higher bit rates could be achieved in optical fibre communication network by utilizing picosecond optical pulses.

The successful operation of an actively mode-locked GaAlAs laser [6] stimulated a great deal of research aimed at generating picosecond optical pulses in semiconductor diode laser devices. Conventional mode-locking techniques [7], or excitation of semiconductor laser diodes by short electrical pulses [8], have been applied and optical pumping to achieve gain switching [9] or control losses [10] has also been used. Although the active volume of semiconductor lasers is very small with the consequence that they produce relatively low peak powers (~1 W), these powers are more than adequate for optical fibre communication purposes [11]. In addition, picosecond pulses produced by semiconductor lasers at very high bit rates, are an ideal source for potential optical computing methods which have prospects for greatly increased computing speeds.

Broadband tunability of semiconductor lasers was achieved by optical pumping of narrow GaAs whiskers [12] to create a superdense electron–hole plasma within a wedged optical cavity of 1 μm length. By pumping the GaAs with a 0.9 ps optical pulse, a 3–8 ps pulse of tunable infrared radiation was produced. Tang et al. [13] have obtained a CW semiconductor laser tuning by using electro-optic tuning in an external cavity where the intracavity side of the diode surfaces was AR coated to reduce subcavity effects. In our work we have used oxide insulated GaAlAs stripe geometry diodes supplied by the Standard Telecommunication Laboratories, UK [14]. These diodes which were 500 μm long, had a 15 μm wide stripe tilted at 15.5° from the crystal axis, which is approximately Brewster angle for GaAs. Tilted stripes were obtained by the method similar to that described in ref. [15]. Thus the semiconductor laser diode having frustrated feedback was transformed into a gain medium only, such

* Permanent address: Physics Department, Sichuan University, Chandu, China.

0.030-4018/84/$ 03.00 © Elsevier Science Publishers B.V. (North-Holland Publishing Division)

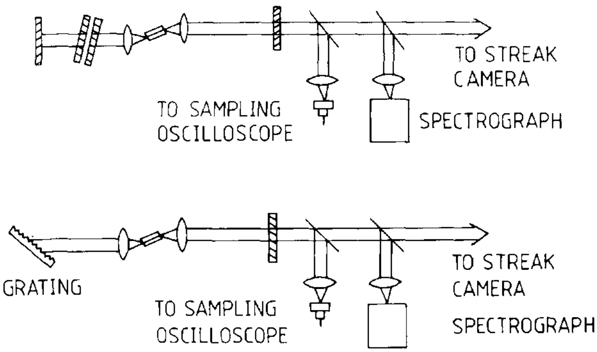

Fig. 1. Resonator configurations incorporating Brewster-angled diode.

that no evidence of lasing was observed even under the extreme condition of injection currents of 2.5 times the threshold current (140 mA) for zero-degree laser diodes cut from the same crystal wafer. Spectral output of such a Brewster-angled diode, instead of being narrower at higher driving currents, as is the case with zero-degree diodes, remained very wide (about 14 nm FWHM) at these high current levels. The diode was mounted onto a specially designed copper heat sink in such a way that X40 microscope objectives could be optically coupled to both facets of the diode.

When placed inside the resonator configuration shown in fig. 1, the laser threshold current was less than 150 mA for 100% and 90% reflectivity mirrors and two X20 microscope objectives with 0.5 NA (fig. 2). This low threshold, compared to our previous results [16], was attributed to the use of an improved version of the copper mount which was designed to minimise the diode temperature excursions.

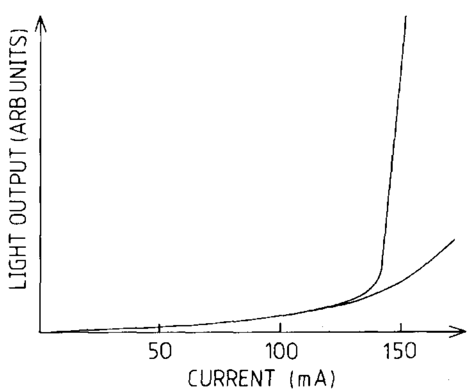

Fig. 2. Light outout versus current characteristics for aligned and misaligned resonator.

The two types of external laser cavities which were investigated are illustrated schematically in fig. 1. One had a 100% reflectivity mirror with an intracavity Fabry-Perot etalon and in the other, these two components were replaced by a diffraction grating. This grating was mounted in such a way that the cavity length did not change with the rotation of the grating and so when measuring pulse durations at different wavelengths, it was preferred to use the grating as the tuning element. In contrast, when the Fabry-Perot etalon was rotated to affect wavelength tuning, the length of the external cavity was altered and therefore optimisation of cavity length with applied RF current modulation had to be undertaken after each tuning step. When due account was taken of this factor, similar results were obtained for both configurations at preselected wavelengths but data presented here are restricted to the performance of the more convenient "grating" cavity.

The tuning range was 15 nm and the tuning curve appeared to have a weak spectral amplitude modulation as illustrated in fig. 3. Observations of the luminescence of the Brewster-angled laser diode without any

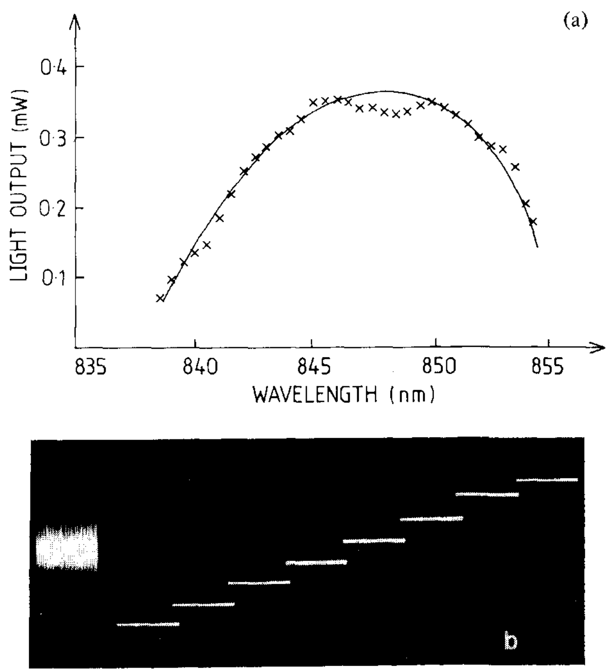

Fig. 3. Variation of light output with wavelengths for tuned semiconductor lasers.

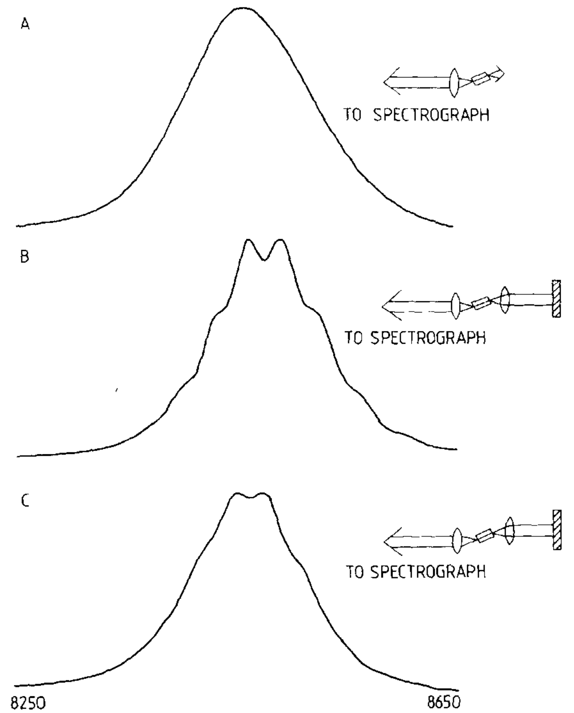

Fig. 4. Luminescence spectrum from: (a) Brewster-angled diode; (b) diode with feedback from one side only (slightly defocused) and (c) diode with optimised focusing of feedback.

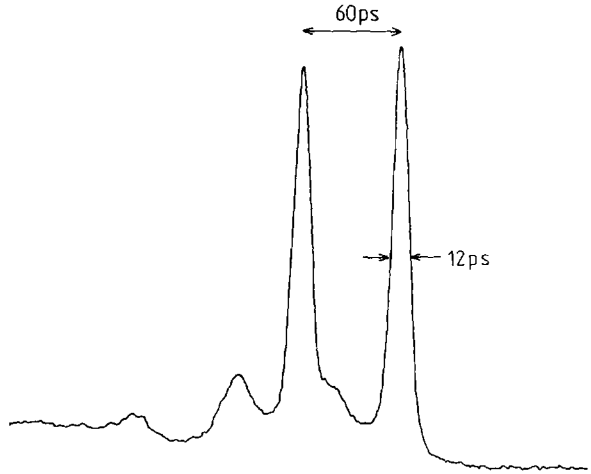

Fig. 5. Intensity profiles of streak images showing calibrated delay of 60 ps and recorded pulse duration of 12 ps. Deconvolution of synchroscan streak camera resolution gives actual laser pulse duration of 9.5 ps.

optical feedback were also made and no spectral amplitude variation was apparent (fig. 4a). When feedback was introduced on one side only, spectral amplitude variation was observed with maxima separated by approximately 3 nm. It was further noticed that if the feedback onto the diode facet was slightly defocused, the amplitude variation was more pronounced as indicated in fig. 4b. This is believed to be due to the interference of the light passing through the active medium with that passing through the cladding. The features of this interference suggest that the difference of refractive index between the active and cladding layers is 0.48 for the particular composition of our diode. For optimised focusing onto the diode facet the spectral amplitude variation almost disappeared and the luminescence curve was smooth (fig. 4c). When the luminescence spectrum of the diode was compared with the tuning range of the laser, it was noticeable that the laser could be tuned more readily to the longer wavelengths.

The laser was mode-locked in a similar way to that described earlier [16]. The laser cavity was arranged with the semiconductor gain medium in the centre of the linear cavity and for mode-locking the RF injection current modulation was applied at 326.0870 MHz which corresponded to twice the external cavity frequency. The laser pulse durations were measured using a Photochron I synchroscan streak camera [17] operating (without any intensification) at half the laser pulse repetition frequency to give a temporal resolution of 7 ps. For recording purposes, the streak camera was lens-coupled to an optical analyser (B & M, OSA 1). The shortest pulses obtained, with the cavity incorporating the grating, had durations of 9.5 ps (fig. 5). (This is the deconvolved pulse width when the camera resolution is taken into consideration.) In fig. 6 the dependence of pulse duration on modulation frequency is indicated and it can be seen that a reduction of as little as 10 kHz (0.003%) gives rise to an increased pulse duration 25 ps. However, it is also evident that an increase in the modulation frequency changes the pulse duration at a much slower rate. This is qualitatively equivalent to the observations reported for cavity-length detuning effects in synchronously pumped CW dye lasers [18–21]. This observed asymmetry in the variation of pulse duration with modulation frequency can be explained by considering the arrival of the pulse at a semiconduc-

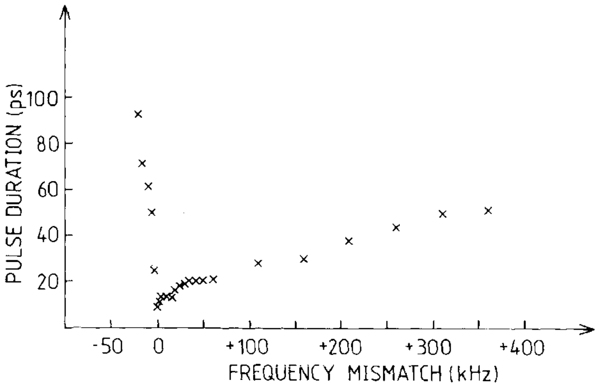

Fig. 6. Dependence of pulse duration on modulation frequency mismatch.

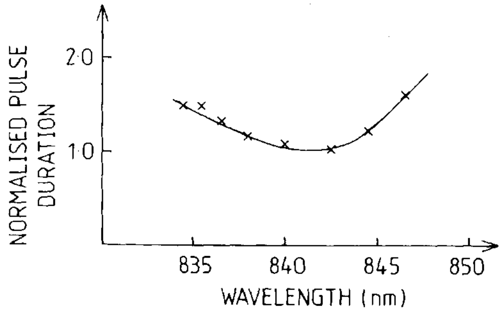

Fig. 7. Pulse duration as a function of lasing wavelength for "grating" cavity.

tor medium with respect to the provision of gain by the injected RF current. On varying the modulation frequency, the laser pulse will either arrive before or after the gain "synchronisation" instant of a preceding cycle and as a result the character of pulse evolution will change accordingly. When the modulation frequency is reduced, the laser pulse moves towards the initial instant where laser threshold occurs. The circulating pulse will experience less gain, and the system could generate subpulses because, as the main pulse moves forward experiencing less gain, the remaining inversion is capable of supporting one or more satellite pulses generated from noise accompanying the main pulse. In the Synchroscan camera the streak images of many pulses are accumulated and pulse substructure broadening effects are averaged within the instrumental temporal resolution of the camera.

If the modulating frequency is increased, the effect on lasing is not as strong. The initial mode locked pulse moves from its optimum position into a region of high and relatively slowly varying gain at later times and consequently the pulses will progressively broaden. The laser produced mode-locked pulses when tuned to any wavelength within the lasing spectral range (fig. 7) by simply rotating the grating, although there is an optimum wavelength, around the maximum gain of the laser, where the pulses are observed to be shortest.

The overall stability of the mode-locked laser output was monitored and recorded for an operational time of several hours. The wavelength fluctuations were observed to be less than 0.025 nm (spectrograph resolution limit) and the pulse durations varied by less than 10% in this period during which these measurements were taken.

The authors are indebted to R. Baulcombe of Standard Telephone Laboratories, Harlow, Essex, for supplying Brewster-angled diodes, and to T. Bates and R. Morrison for technical assistance.

Financial support from the UK Science and Engineering Research Council is gratefully acknowledged.

References

[1] J.C. Camparo and C.H. Volk, IEEE J. Quant. Electron. QE-18 (1982) 1990.
[2] M.W. Fleming and A. Mooradian, IEEE J. Quant. Electron. QE-17 (1981) 44.
[3] R. Wyatt and W.J. Devlin, Electron. Lett. 19 (1983) 110.
[4] R. Wyatt, D.W. Smith and K.H. Cameson, Electron. Lett. 18 (1982) 292.
[5] T.G. Hodgkinson, R. Wyatt and D.W. Smith, Electron. Lett. 18 (1982) 523.
[6] P.T. Ho, L.A. Glasser, E.P. Ippen and H.A. Haus, Appl. Phys. Lett. 33 (1978) 241.
[7] M.B. Holbrook, W.E. Sleat and D.J. Bradley, Appl. Phys. Lett. 37 (1980) 59.
[8] T. Kobayashi, A. Yoshikawa, A. Morimoto, Y. Aski and T. Sueta, Dig. Tech. Papers XI, IQEC, Boston, MA, 1980.
[9] C.B. Roxlo, D. Debelarr and M.M. Salour, Appl. Phys. Lett. 38 (1981) 507.
[10] C. Harder, J.S. Smith, K.Y. Lau and A. Yariv, Appl. Phys. Lett. 42 (1983) 772.
[11] T.G. Hodgkinson, R. Wyatt, D.J. Malyon, B.K. Nayar, R. Harmon and C.W. Smith, eighth ECOC, Cannes, France, Sept. 1982.
[12] T.C. Damen, M.A. Duguay and J. Shah, Appl. Phys. Lett. 39 (1981) 142.
[13] C.L. Tang, V.G. Kresmanls and J.M. Ballantyne, Appl. Phys. Lett. 30 (1977) 113.

[14] Standard Telecommunication Laboratories Ltd., London Road, Harlow, Essex, England CM17 9NA.
[15] R.W. Engelman and E. Bourkoff, eighth Intern. Symposium on GaAs and related compounds, Vienna, 1980 (Institute of Physics Conference Series, Bristol, 1981) p. 309.
[16] J. Chen, W. Sibbett and J.I. Vukusic, Electron. Lett. 18 (1982) 426.
[17] M.C. Adams, W. Sibbett and D.J. Bradley, Optics Comm. 26 (1978) 273.
[18] P.G. May, W. Sibbett, K. Smith, J.R. Taylor and J.P. Willson, Optics Comm. 42 (1982) 285.
[19] C.K. Chen, S.O. Sari and R.E. Foster, J. Appl. Phys. 47 (1976) 1139.
[20] A. Scavennec, Optics Comm. 17 (1976) 14.
[21] J.M. Catherall, Ph.D. Thesis (Imperial College, London, 1983).

MODE LOCKING OF BREWSTER-ANGLED SEMICONDUCTOR LASERS

Indexing terms: Lasers and applications, Semiconductor lasers

Brewster-angled semiconductor laser diodes have been actively mode locked in an external cavity to produce mode-locked pulses of 11 ps duration and 0·5 W peak power with no evidence of temporal or spectral substructure.

Introduction: Research on producing picosecond optical pulses by semiconductor lasers has advanced to the stage where they could be used in optical communications with high-density optical integration.

Direct modulation of semiconductor lasers has produced pulses as short as 28 ps using the gain switching method at a repetition frequency of 2·5 GHz.[1] Using a semiconductor laser coupled to an external resonator, much shorter pulses with high peak power could be produced if the reflection from diode facets could be eliminated. If diode facets are AR coated, even a small residual reflectivity causes diode mode structure and introduces additional temporal structure on the mode-locked pulses.

The first experiments on laser diodes coupled to external resonators were reported in 1964,[2] and the first mode-locked semiconductor laser coupled to an external resonator was demonstrated in 1978.[3] A number of authors have since reported mode locking of semiconductor lasers in an external cavity, either by AR coating one facet of the diode or both,[4–6] but all had pulses with temporal structure caused by the residual reflectivity of the diode facets. Using a DH laser with tilted stripe at an angle of 5° to the facets and AR coating the facets,[7] no temporal structure of the mode-locked 16 ps pulses was observed.

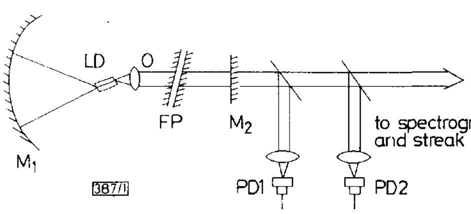

Fig. 1 *Experimental set-up for Brewster-angled semiconductor laser*
Cavity length $L = 52$ cm, microscope objective ×20, 0·5 NA, Fabry–Perot 10 μm gap and finnesse of 10
Output mirror $R = 70\%$

In our experiments, we used a GaAlAs DH laser-diode 500 μm- and 20 μm-wide oxide isolated strip at an angle of 15° to the facets. The diodes were mounted onto the brass heat sink of 480 μm diameter using indium as a solder. The experimental arrangement is shown in Fig. 1. The laser diode, on its heat sink, was positioned so that one of its facets was at the centre of a 5 cm radius of curvature semispherical mirror, so as to obtain maximum feedback. A ×20, 0·5 NA microscope objective collimated the laser-diode emission from the other facet. A broadband dielectric mirror $R = 70\%$ at 870 nm was used as the output coupler, and a 10 μm-gap Fabry–Perot etalon inserted in the cavity limited the laser spectral width to 0·45 nm.

Fig. 2*a* shows the laser output as a function of direct current for the condition of aligned and misaligned external cavity. For the aligned-cavity configuration, for most of the diodes, the direct threshold current was in the range of 170–210 mA. The direct current was reduced to 110 mA and an RF current was added at the external-resonator round-trip frequency of 285·2 MHz. The resulting dependence of the average laser output power on generated input RF power shown in Fig. 2*b* exhibits a much sharper threshold than the corresponding DC bias characteristic in Fig. 2*a*. The temporal and spectral features were investigated for the mode-locked Brewster-angled laser system.

The laser pulse duration was measured with an S20 Photochron 1 streak camera,[8] operated without any additional intensification at half the laser pulse repetition frequency (i.e. 142·6 MHz) to give a temporal resolution of 7 ps. For recording purposes, the streak camera was lens coupled to an optical spectral analyser (B & M, OSA 1). The shortest laser pulses were obtained for a direct current of 110 mA and an RF power of 0·9 W and the corresponding intensity profile reproduced in Fig. 3.

The calibration optical delay was 60 ps, and the recorded pulses had a duration (FWHM) of 13 ps, such that, when the instrumental function was deconvolved for the measurement, the actual laser pulse durations were 11 ps. The attendant background pulse energy that is evident in the result shown in Fig. 4 disappeared at higher radio frequencies (~ +10 kHz), but the resulting pulsewidths were increased by approximately 30% above the optimum value.

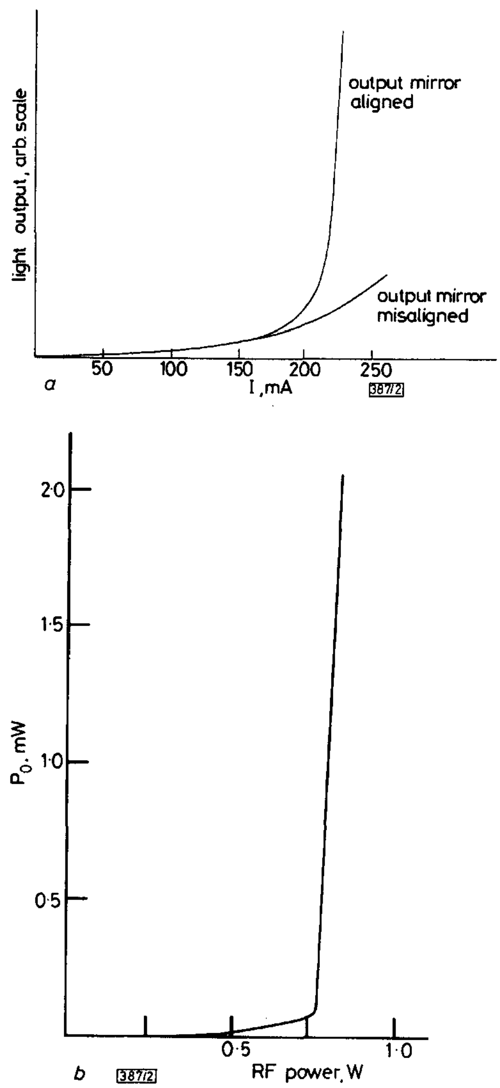

Fig. 2 *Light-output/current characteristics of Brewster-angled laser diode*
a DC biased only
b Direct current 110 mA

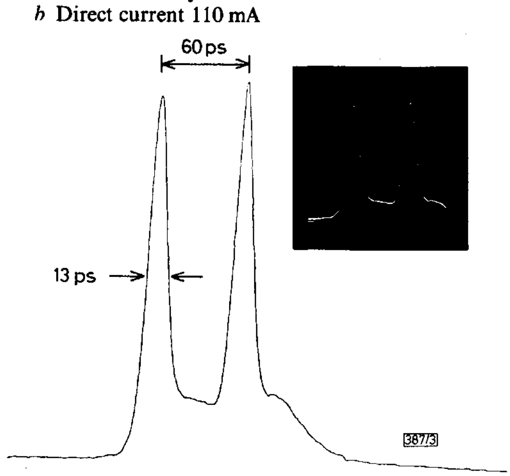

Fig. 3 *Pair of pulses (separated by 60 ps) generated by Michelson interferometer optical delay line, recorded by streak camera and optical spectrum analyser*

Spectral output from the laser was measured using a 1 m spectrograph with resolution of 0·025 nm with no evidence of subcavity resonances. Fig. 4*a* shows fluorescence from the diode if the cavity is misaligned, giving 14 nm FWHM centred at 865 nm. When the external resonator is aligned the spectral width is 0·45 nm and is centred at 870·7 nm, Fig. 4*b*.

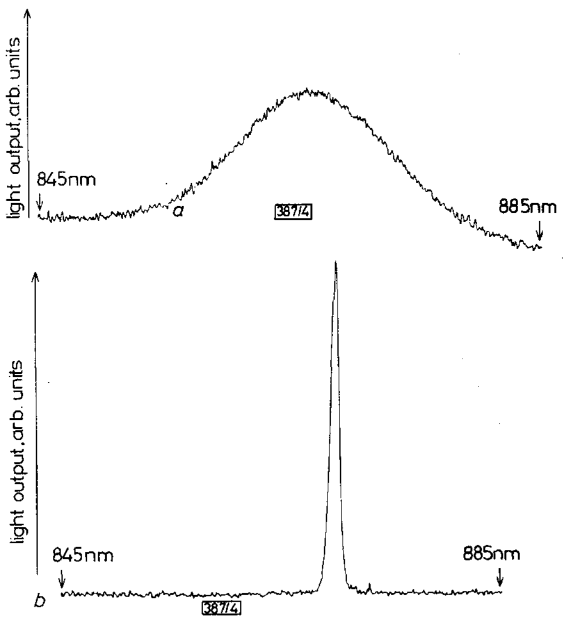

Fig. 4 *Spectral output from Brewster-angled laser diode*

a Cavity misaligned
b Cavity aligned

Conclusion: In this letter we have given an experimental study of mode locking using Brewster-angled-geometry semiconductor laser diodes. Subcavity effects formed by the cleaved facets have thus been eliminated without the necessity of additional AR coating. By introducing further refinements with current modulation circuitry and cavity configuration, it should be possible to demonstrate improved performance characteristics of this laser.

Acknowledgments: The authors are indebted to the Standard Telephone Laboratories, Harlow, Essex, for supplying Brewster-angled diodes, and to T. Bates and R. S. Morrison for technical assistance. Financial support from the UK Science & Engineering Council is gratefully acknowledged.

J. CHEN*
W. SIBBETT
J. I. VUKUSIC

Optics Section, Blackett Laboratory
Imperial College, London SW7 2AZ, England

7th April 1982

* Permanent address: Physics Department, Sichuan University, Chengdu, China

References

1 AUYEUNG, J.: 'Picosecond optical pulse generation at gigahertz rates by direct modulation of a semiconductor laser', *Appl. Phys. Lett.*, 1981, **38**

2 CROWE, J. W., and CRAIG, R. M., JUN.: 'GaAs laser linewidth measurements by heterodyne detection', *ibid.*, 1964, **5**

3 HO, P. T., GLASSER, L. A., IPPEN, E. P., and HAUS, H. A.: 'Picosecond pulse generation with cw GaAlAs laser diode', *ibid.*, 1978, **33**

4 VAN DER ZIEL, J. P., LOGAN, R. A., and MIKULYAK, R. M.: 'Generation of subpicosecond pulses from an actively mode-locked GaAs laser in an external ring cavity', *ibid.*, 1981, **39**

5 YOKOYAMA, H., ITO, H., and INABA, H.: 'Generation of subpicosecond coherent optical pulses by passive mode-locking of an AlGaAs diode laser', *ibid.*, 1982, **40**

6 VAN DER ZIEL, J. P., TSANG, W. T., LOGAN, R. A., MIKULYAK, R. M., and AUGUSTYNIAK, W. M.: 'Subpicosecond pulses from passively mode-locked GaAs buried optical guide semiconductor laser', *ibid.*, 1981, **39**

7 HOLBROOK, M. B., SLEAT, W. E., and BRADLEY, D. J.: 'Bandwidth-limited picosecond pulse generation in an actively mode-locked GaAlAs diode laser', *ibid.*, 1980, **37**

8 ADAMS, M. C., SIBBETT, W., and BRADLEY, D. J.: 'Linear picosecond electron optical chronoscopy at a repetition rate of 140 MHz', *Opt. Commun.*, 1978, **26**

0013-5194/82/100426-03$1.50/0